

Electronic Thesis and Dissertation Repository

---

5-19-2023 10:30 AM

## Geoelectrical Signatures of Acid-Generating Mine Waste Rock

Difan Su, *Western University*

Supervisor: Christopher Power, *The University of Western Ontario*

A thesis submitted in partial fulfillment of the requirements for the Master of Engineering Science degree in Civil and Environmental Engineering

© Difan Su 2023

Follow this and additional works at: <https://ir.lib.uwo.ca/etd>



Part of the [Civil Engineering Commons](#), [Environmental Engineering Commons](#), and the [Mining Engineering Commons](#)

---

### Recommended Citation

Su, Difan, "Geoelectrical Signatures of Acid-Generating Mine Waste Rock" (2023). *Electronic Thesis and Dissertation Repository*. 9300.

<https://ir.lib.uwo.ca/etd/9300>

This Dissertation/Thesis is brought to you for free and open access by Scholarship@Western. It has been accepted for inclusion in Electronic Thesis and Dissertation Repository by an authorized administrator of Scholarship@Western. For more information, please contact [wlsadmin@uwo.ca](mailto:wlsadmin@uwo.ca).

## ABSTRACT

Acid mine drainage (AMD) contamination associated with waste rock piles (WRPs) at mining sites is a global concern, and understanding the generation and release of AMD from these piles is highly desirable. Traditional WRP monitoring techniques involve the installation of monitoring wells and periodic core sampling; however, these approaches are invasive, expensive and can only provide data with limited spatial and temporal resolution. An attractive alternative is non-invasive geophysical techniques that can provide continuous information on subsurface features and processes. This thesis aims to investigate the feasibility of the spectral induced polarization (SIP) method for monitoring changes in mine waste rock characteristics. Waste rock samples were obtained from three WRPs in the Sydney Coalfield in Nova Scotia, Canada. The properties of the waste rock were extensively characterized before kinetic column leaching and humidity cell experiments were performed with simultaneous tracking by SIP. Results show that the waste rock contained very low sulfide concentrations with SIP unable to capture distinct mineralogy changes during oxidation of the sulfides. However, SIP was extremely effective in monitoring the changes in the waste rock porewater characteristics associated with metal leaching and AMD flushing. Overall, this thesis improves our understanding of the capability of SIP to track changes in waste rock, while also introducing a robust approach for future experiments on waste rock and SIP.

*Keywords:* Acid mine drainage; mine waste rock; hydrogeophysics; spectral induced polarization; contaminant monitoring; environmental site characterization

## SUMMARY FOR LAY AUDIENCE

Mining activities come with environmental consequences, including the production of unwanted waste rocks. These waste rocks are usually stored in stockpiles on the ground surface, known as waste rock piles (WRPs). Once exposed to water and air, these rocks can produce very acidic and polluted water known as acid mine drainage (AMD) that can pose a threat to the health of the environment. It is critical for environmental professionals to understand how these WRPs produce and release AMD. Usually, this understanding is obtained by drilling into the WRP to collect rock and water samples to be taken back to the laboratory for analysis. However, this is slow and expensive, and only helps us understand small parts of these very large WRPs. Geophysical techniques are available that can image the ground like an x-ray and may be able to help us monitor the waste rock. One such technique is called spectral induced polarization (SIP), which may have the ability to find changes in both the water between the rock and the rock itself but needs more research to be better understood. This thesis aims to address this by performing experiments in plastic laboratory columns where SIP is used to track waste rock that is changing as it is exposed to water and air. The results in this thesis suggest that SIP has potential to capture these changes, and with more research, it may ultimately help to understand how AMD is produced and then transported from WRPs over time.

## CO-AUTHORSHIP STATEMENT

This thesis is a result of the collaboration of Dr. Christopher Power and Difan Su and is written accordance to the guidelines specified by the Faculty of Graduate and Postdoctoral Studies at Western University. The candidate was responsible for the (i) design of the experimental methodology, (ii) collection and analysis of laboratory data, and (iii) drafting all chapters in this thesis. Dr. Christopher Power provided the initial motivation for this research, assisted with data analysis, and provided revisions for the improvement of this thesis.

The co-authorship breakdown of Chapter 3, which will be submitted for publication in the Journal of Environmental Management, is as follows:

*Authors:* Difan Su, Christopher Power

*Contributions:* Difan Su developed the experimental methodology, conducted experiments, collected data, performed data analysis, interpreted the results, and prepared drafts of each thesis chapter. Christopher Power provided the motivation for the study, funded the research, assisted with the experimental design, supervised data collection and analysis, provided insight in data interpretation, and reviewed the draft chapter of Chapter 3.

## ACKNOWLEDGEMENTS

I want to express my utmost gratitude to my supervisor, Dr. Christopher Power, for giving me the amazing opportunity to conduct research that has forever changed my life. I am incredibly grateful for your guidance and encouragement over the past two years. I appreciate every single opportunity you have given me and the trust you have always had in me.

I would also like to thank Dr. Clare Robinson and the entire RESTORE group for creating a warm and welcoming environment where I can learn from brilliant minds. I am especially grateful to my colleague Angelos Almpanis, who acted like a big brother and supported me throughout my entire research. I enjoyed the times we spent together in the lab and the beers we had together at Buffalo Wild Wings.

I want to give a special shoutout to Xiaomeng Li, who is a wonderful role model. She is always curious, brilliant, and inspiring, and I am thankful for her friendship and unconditional support, which helped me achieve what I never thought possible.

Lastly, I want to express my gratitude to my parents, Xiaoming Su and Hua Yan, for their endless love.

# TABLE OF CONTENTS

ABSTRACT.....	ii
SUMMARY FOR LAY AUDIENCE.....	iii
CO-AUTHORSHIP STATEMENT.....	iv
ACKNOWLEDGEMENTS.....	v
LIST OF TABLES.....	ix
LIST OF FIGURES.....	x
CHAPTER 1 - INTRODUCTION.....	1
1.1 RESEARCH BACKGROUND.....	1
1.2 RESEARCH OBJECTIVES.....	3
1.3 THESIS OUTLINE.....	4
1.4 REFERENCES.....	6
CHAPTER 2 - LITERATURE REVIEW.....	10
2.1 MINING AND WASTE ROCKS.....	10
2.1.1 The Mining Process and Mine Waste Production.....	10
2.1.2 Waste Rock, a Unique Class of Mine Waste.....	11
2.2 ACID MINE DRAINAGE.....	12
2.2.1 AMD Sources: Oxidation of Sulfide Minerals.....	12
2.2.2 Generation and Quality of AMD.....	15
2.2.2.1 Mineralogy.....	15
2.2.2.2 Microorganisms.....	15
2.2.2.3 pH.....	16
2.2.3 Environmental Impacts of AMD.....	17
2.2.4 Controlling AMD Release from WRPs.....	18
2.3 MINE WASTE CHARACTERIZATION METHODS.....	20
2.3.1 Chemical Properties: Static and Kinetic Tests.....	22
2.3.1.1 Static tests- acid base accounting & net acid generation.....	22
2.3.1.2 Kinetic test – column leaching.....	24
2.3.1.3 Kinetic test – humidity cell.....	25
2.3.2 Physical Properties: Grain Size and Mineralogy.....	27
2.3.2.1 Particle size measurements.....	27
2.3.2.2 Mineralogical methods.....	28
2.4 GEOELECTRICAL CHARACTERIZATION OF MINE WASTE.....	29
2.4.1 Introduction.....	29
2.4.2 Direct Current Resistivity.....	30
2.4.3 Induced Polarization.....	32

2.4.4	Spectral Induced Polarization .....	35
2.4.5	The Application of SIP in Mine Waste Characterization and Monitoring.....	38
2.5	RESEARCH SUMMARY AND GAPS.....	42
2.6	REFERENCES.....	43
CHAPTER 3 - GEOELECTRICAL SIGNATURES OF ACID-GENERATING MINE		
WASTE ROCK .....		
3.1	INTRODUCTION .....	52
3.2	MATERIALS AND METHODS.....	56
3.2.1	Waste Rock Samples .....	56
3.2.2	Waste Rock Characterization.....	57
3.2.2.1	<i>Sample preparation</i> .....	57
3.2.2.2	<i>Particle size distribution</i> .....	59
3.2.2.2	<i>Mineralogy</i> .....	59
3.2.2.3	<i>Acid base accounting</i> .....	59
3.2.3	SIP monitoring of waste rock kinetics.....	60
3.2.3.1	<i>Column leaching test</i> .....	60
3.2.3.2	<i>Humidity cell test</i> .....	64
3.3	RESULTS AND DISCUSSIONS.....	67
3.3.1	Mine Waste Characterization.....	67
3.3.1.1	<i>Particle size distribution</i> .....	67
3.3.1.2	<i>Mineralogy</i> .....	68
3.3.1.3	<i>Acid base accounting</i> .....	70
3.3.2	Kinetic Tests.....	72
3.3.2.1	<i>Column leaching test</i> .....	72
3.3.2.2	<i>Humidity cell test</i> .....	75
3.3.2.3	<i>Acid generation characteristics of the waste rock samples</i> .....	78
3.3.3	SIP Response of the Acid Generating Waste Rocks.....	79
3.3.3.1	<i>Real conductivity</i> .....	79
3.3.3.2	<i>Imaginary conductivity</i> .....	83
3.3	CONCLUSIONS .....	87
3.3	REFERENCES.....	89
CHAPTER 4 - CONCLUSION .....		
4.1	SUMMARY & CONCLUSIONS.....	100
4.2	LIMITATIONS .....	101
4.3	RECOMMENDATIONS .....	102
4.3	REFERENCES.....	104
APPENDICES.....		
List of Appendix Tables.....		
		107

List of Appendix Figures .....	108
Appendix A: Experiment Apparatus Photos .....	111
Appendix B: SIP Measurement Electrode Selection.....	114
Appendix C: Geometric Factors .....	117
Appendix D: Sample Preparation .....	127
Appendix E: XRD Test Results .....	130
Appendix F: SEM/EDX Results .....	133
Appendix G: Supplementary SIP Results.....	136
CURRICULUM VITAE.....	140

## LIST OF TABLES

<b>Table 2.1</b> Selected primary sulfide minerals found in mine wastes (modified from Hudson-Edwards et al., 2011).....	12
<b>Table 2.2</b> Summary of the various oxidation reactions for sulfide minerals (Dold, 2016)14	
<b>Table 2.3</b> Summary of the five categories of AMD characteristics (Kirby, 2014).....	16
<b>Table 3.1</b> Summary of all characterization tests performed on the waste rock samples	58
<b>Table 3.2</b> Summary of kinetic tests performed on waste rock samples .....	64
<b>Table 3.3</b> Mineralogy of the Lingan, Summit and Victoria Junction samples based on XRD results.....	69
<b>Table 3.4</b> Summary of acid base accounting test results for each pre- and post-experiment waste rock sample .....	71
<b>Table 3.5</b> Waste rock acid generation characteristics classification .....	79

## LIST OF FIGURES

<b>Figure 2.1</b> Five categories of acid mine drainage impacts (Acharya & Kharel, 2020)...	17
<b>Figure 2.2</b> Conceptual model of a WRP showing the various pathways .....	18
<b>Figure 2.3</b> Conceptual WRP showing unique pile construction to control water flow and prevent AMD (Dubuc et al., 2017) .....	19
<b>Figure 2.4</b> Overview of the various cover systems installed over WRPs (Argunham, 2014) .....	20
<b>Figure 2.5</b> Summary of the various mine waste characterization tests .....	21
<b>Figure 2.6</b> Hierarchy of mine waste characterization tests based on scale, complicity, and costs .....	21
<b>Figure 2.7</b> The categories of a sample resulting from ABA tests (Hajizaden & Li, 2016)	24
<b>Figure 2.8</b> Column leaching test set up example. a) Column cross-section; b) view of different sizes of columns (Erguler et al., 2014).....	25
<b>Figure 2.9</b> Humidity cell set up example: a) small cell, b) large cell, and c) humidifier (Hakkou, 2008).....	26
<b>Figure 2.10</b> Principle of resistivity measurement with a four-electrodes array (Knodel et al., 2007) .....	31
<b>Figure 2.11</b> TL-ERT monitoring of a tracer infiltration with surface and borehole electrodes. (i) Top panel shows the true spatial-temporal distribution of tracer concentration, (ii) medium panel presents the distribution of elec resistivity (Dimech et al., 2022).....	32
<b>Figure 2.12</b> Equilibrium ion distribution (left) and polarization following application of an electric field (right) (Slater & Lesmes, 2000) .....	33
<b>Figure 2.13</b> Measurement of time-domain induced polarization (Dusabemariya et al., 2020) .....	34
<b>Figure 2.14</b> Current and voltage waveforms in SIP measurements showing a phase difference (Joseph, 2016).....	35

**Figure 2.15** Mechanisms that generate the IP effect in the ground: (a) electrode chemical, (b) membrane and (c) Maxwell-Wagner polarization mechanisms. .... 37

**Figure 2.16** Time-lapse SIP response of pyrite-sand (py-sand) and pyrrhotite-sand (po-sand) mixtures during oxidation: a) phase shift, b) imaginary conductivity and c) real conductivity (Placencia-Gomez, 2015)..... 41

**Figure 3.1** Site map of the Sydney Coalfield and the location of Lingan, Summit, and Victoria Junction ..... 57

**Figure 3.2** Schematic of the apparatus for the column leaching experiment..... 61

**Figure 3.3** Illustration of the apparatus for the humidity cell during each stage of the experiment: (a) saturation and SIP measurement, (b) air displacement of porewater and effluent collection, (c) three days of dry air, and (d) three days of humid air. .... 67

**Figure 3.4** Particle size distribution curve for each of the prepared waste rock samples.68

**Figure 3.5** Classification of waste rock samples in terms of NNP and paste pH..... 71

**Figure 3.6** Temporal evolution of (a) modified acidity, (b) pH, (c) sulfate, and (d) EC of effluent leachate during the duration of the column leaching experiments..... 72

**Figure 3.7** Column leaching test selected dissolved metal evolution of a) Fe, b) Mn, c) Al, d) Zn, e) Ca, and f) Mg..... 75

**Figure 3.8** Humidity cell test, temporal evolution of (a) pH, (b) sulfate, and (c) EC in the effluent..... 77

**Figure 3.9** Humidity cell test selected dissolved metal evolution of a) Mg, b) Mn, c) Al, d) Fe, e) Ca, and f) Zn ..... 78

**Figure 3.10** Real conductivity for (a) Lingan, (b) Summit, and (c) Victoria Junction leaching columns. The EC of corresponding effluent (solid circles) is included on the secondary axes. Note that the real conductivity is shown from the A-B (diamonds) and B-C (plus sign) potential pairs..... 81

**Figure 3.11** Real conductivity (diamonds) for (a) Lingan, and (b) Summit humidity cells.

The EC of corresponding effluent (circles) is included on the secondary axes.....	83
<b>Figure 3.12</b> Imaginary conductivity and phase shift for (a) Lingan, (b) Summit, and (c) Victoria Junction humidity cells at selected PVs.....	84
<b>Figure 3.13</b> Imaginary conductivity and phase shift for (a) Lingan, and (b) Summit humidity cells at selected PVs .....	86

# CHAPTER 1 - INTRODUCTION

## 1.1 RESEARCH BACKGROUND

Mining plays an important role in the Canadian economy. In 2021, the Canadian minerals and metal sector contributed \$97 billion to the country's total GDP, which accounted for 4% of the overall Canadian GDP (Natural Resources Canada, 2023). Unfortunately, mining in Canada comes with environmental consequences. When valuable minerals are extracted, a significant amount of uneconomic mine waste is produced (e.g., tailings and waste rocks) (Bao et al., 2021). It was estimated that the Canadian mining industry produces mine waste volumes that are over 30 times larger than the total volumes of municipal and industrial wastes on a yearly basis (Mine Watch Canada, 2020).

The waste rocks, produced through the mineral extraction process, are typically deposited in large unsaturated piles, also known as waste rock piles (WRPs). These WRPs typically contain trace amounts of various oxidizable sulfide minerals, such as pyrite, pyrrhotite, and chalcopyrite (Dold, 2017). Once exposed to the atmosphere, these reactive sulfide minerals can become geochemically unstable and generate a toxic leachate known as acid mine drainage (AMD) that is characterized by low pH and high concentrations of sulfate and metal(loid)s (Amos, 2014). Water flowing through the WRPs can transport AMD and other dissolved substances out of the WRP and negatively impact the receiving environment and pose a significant threat to animals, plants, and human health (Chen et al., 2021; Bao et al., 2022). AMD is recognized as a long-standing challenge encountered by the global mining industry.

Impacts of AMD from WRPs can be minimized by several strategies, such as the prevention of AMD formation, migration control and effluent treatment (Kefeni et al., 2017). Examples of these strategies include the implementation of engineered cover systems over the WRP to isolate the mine waste and prevent AMD formation, and the use of constructed wetlands to

treat the discharged AMD in a relatively economic way (e.g., Hersey & Power, 2023; Pat-Espadas et al., 2018). Knowledge on the physical and geochemical characteristics of the stockpiled waste rock material is highly desirable for the successful design and implementation of these remediation strategies (MEND, 2004; MEND, 2012; Gusek & Wildeman, 1997; USEPA, 1983).

Traditional methods for monitoring the geochemical stability of WRPs include monitoring wells and core sampling (e.g., Bao et al., 2020; Ramasamy & Power 2019). Core samples can be extracted from WRPs to determine the chemical characteristics of the mine waste samples via a range of test methods, including the widely used static acid base accounting (ABA) test, and kinetic column and humidity cell experiments (Jacobs et al., 2013; Parbhakar-Fox & Lottermoser, 2015). Physical properties such as the particle size distribution and mineralogy of the waste materials can also be determined to supplement the geochemical characterization results (USEPA, 1994). Nevertheless, despite the range of tests available, these mine waste characterization methods are time consuming, expensive, and only provide sparsely distributed point information. These limitations are exasperated as mine WRPs are extremely large facilities (Dimech et al., 2022).

Geophysical techniques are becoming increasingly popular for characterizing and monitoring subsurface features and processes at geoenvironmental sites, where they can provide relatively fast, cost-effective, and continuous spatial and temporal information. Mine wastes and AMD plumes are known to be more electrically conductive relative to typical surrounding host materials, providing the motivation to employ geoelectrical methods such as direct current (DC) resistivity and induced polarization (IP) for monitoring WRP and AMD characteristics. DC and IP are widely used and highly complementary geophysical techniques for near-surface applications (Dimech et al., 2022). DC measures the distribution of electrical resistivity (or its reciprocal, conductivity) in the subsurface, which is influenced by porewater conductivity and mineral surface conductivity. IP measures the capacitive (chargeable) properties of within

subsurface materials and is commonly used to better understand the mineralogy in the subsurface (e.g., Power and Almpanis, 2022; Robinson et al., 2022).

IP in the frequency domain, known as spectral IP (SIP), measures the complex conductivity, which is expressed in terms of real conductivity (porewater and mineral surface) and imaginary conductivity (mineralogy) to reveal more detailed information about porous media (Joseph, 2016; Rubin & Hubbard, 2006). For WRP and AMD applications, the real conductivity should be sensitive to AMD-rich water that is normally more conductive due to elevated constituents such as metal(loid)s, while the imaginary component can be used to identify zones with sulfide minerals (do Nascimento et al., 2022). SIP has recently been ‘re-discovered’ for mine waste monitoring and characterization (Campbell & Horton, 2001; Placencia-Gomez, 2015; Gunther & Martin, 2016; Martin et al., 2020; Martine et al., 2021). However, while these studies have demonstrated the capability of SIP to detect sulfide-rich zones in mine waste storage facilities and predicted the SIP response of sulfide-containing mine waste under oxidation (e.g., Wong, 1971; Mahan et al., 1986; Campbell & Horton, 2001; Placencia-Gomez et al., 2013), the time-lapse SIP response of real waste rock has not been robustly investigated. No study has compared SIP response changes of multiple waste rock samples with detailed geochemical data supporting their results. Therefore, despite the potential of the SIP method, more knowledge on its performance for monitoring the kinetics of waste rock is needed.

The experiment was conducted using standardized tests, including leaching column and humidity cells, and simultaneous measurements of geochemistry and SIP were carried out. The results obtained from the SIP method were then compared to the geochemical evolution of the waste rock samples to validate its potential as a monitoring tool.

## 1.2 RESEARCH OBJECTIVES

The overall goal of this thesis is to evaluate the capability of the SIP technique for monitoring the changes associated with evolving waste material characteristics over time. To compete this

goal, three sub-objectives were addressed:

1. Understand the physical and chemical properties of real waste rock sample that were extracted from three different WRPs in the Sydney Coalfield in Nova Scotia, Canada. Traditional characterization methods were used such as sieve analysis (particle size distribution), x-ray diffraction tests (mineralogy), and modified ABA tests (paste pH, sulfur content, and acid generation characteristics).
2. Examine the geochemical behavior of the waste rock samples during exposure to oxidizing and leaching conditions. This was achieved by performing traditional kinetic experiments such as leaching column and humidity cell tests. The effluent collected from these tests were periodically analyzed for geochemical parameters such as pH, modified acidity, sulfate, EC, and dissolved concentrations of selected metals.
3. Assess the SIP response change associated with the evolving waste rock samples during the kinetic experiments. Validate the SIP responses with the measured physical/chemical properties of the samples and the geochemical behavior occurring during the experiments. Discuss the feasibility of the SIP method as a site tool for mapping waste rock characteristics.

### 1.3 THESIS OUTLINE

This thesis is written in an “Integrated Article” format, following specifications outlined by the School of Graduate and Postdoctoral Studies at Western University. Brief descriptions of the thesis chapters are presented as follows:

- Chapter 2: summarization of relevant literature. This literature involves mine waste production and the formation mechanisms of AMD. Traditional AMD prediction

methods such as static and kinetic tests are discussed, along with the general concepts of the geoelectrical methods including DC resistivity and IP.

- Chapter 3: presents the experimental methodology used for the initial selection and characterization of the waste rock samples, and simultaneously tracking their geochemical behavior and SIP response during kinetic experiments. This chapter also includes the results obtained from these experiments and is written in a manuscript format for the purpose of submitting to a peer-reviewed journal publication.
- Chapter 4: provides a summary of the research and the overall findings, along with implications and recommendations.
- Appendices: additional information and supplementary material that is referenced throughout the thesis to support the results presented.

## 1.4 REFERENCES

- Amos, R. T., Blowes, D. W., Bailey, B. L., Segó, D. C., Smith, L., & Ritchie, A. I. M. (2015). Waste-rock hydrogeology and geochemistry. *Applied Geochemistry*, *57*, 140–156. <https://doi.org/10.1016/j.apgeochem.2014.06.020>
- Bao, Z., Bain, J., Holland, S. P., Wilson, D., MacKenzie, P., Ptacek, C. J., & Blowes, D. W. (2020). Faro Waste Rock Project: Characterizing geochemical heterogeneity in sulfide- and carbonate-rich waste rock. *Applied Geochemistry*, *121*, 104691–. <https://doi.org/10.1016/j.apgeochem.2020.104691>
- Bao, Z., Bain, J., Holland, S. P., Wilson, D., Ptacek, C. J., & Blowes, D. W. (2022). Hydrogeochemical Response of a Variably Saturated Sulfide-Bearing Mine Waste-Rock Pile to Precipitation: A Field-Scale Study in the Discontinuous Permafrost Region of Northern Canada. *Water Resources Research*, *58*(1). <https://doi.org/10.1029/2021WR031082>
- Campbell, D. L., & Horton, R. J. (2001). Spectral induced polarization studies of mine waste piles in Colorado and New Mexico. *Symposium on the Application of Geophysics to Engineering and Environmental Problems 2001*. <https://doi.org/10.4133/1.2922850>
- Chen, G., Ye, Y., Yao, N., Hu, N., Zhang, J., & Huang, Y. (2021). A critical review of prevention, treatment, reuse, and resource recovery from acid mine drainage. *Journal of Cleaner Production*, *329*, 129666–. <https://doi.org/10.1016/j.jclepro.2021.129666>
- Dimech, A., Chouteau, M., Aubertin, M., Bussière, B., Martin, V., & Plante, B. (2019). Three-Dimensional Time-Lapse Geoelectrical Monitoring of Water Infiltration in an Experimental Mine Waste Rock Pile. *Vadose Zone Journal*, *18*(1), 1–19. <https://doi.org/10.2136/vzj2018.05.0098>

- Dold, B. (2017). Acid rock drainage prediction: A critical review. *Journal of Geochemical Exploration*, 172, 120–132. <https://doi.org/10.1016/j.gexplo.2016.09.014>
- Gusek, J., & Wildeman, T. (1997). Treatment of Acid Mine Drainage Part I [short course]. *4th International Conference on Acid Rock Drainage*. Vancouver, BC, Canada.
- Jacobs, J. A., Lehr, J. H., & Testa, S. M. (2013). *Acid mine drainage, rock drainage, and acid sulfate soils : causes, assessment, prediction, prevention, and remediation* (J. A. (James A. Jacobs, J. H. Lehr, & S. M. Testa, Eds.). Hoboken, New Jersey: John Wiley & Sons, Inc.
- Hersey, D., & Power, C. (2023). Assessing the importance of drainage layers over geomembrane liners within engineered cover systems: Seven years of field monitoring at three mine waste rock piles. *Geotextiles and Geomembranes*, 51(3), 381–389. <https://doi.org/10.1016/j.geotextmem.2023.01.002>
- Joseph, Sheen (2016): The Application of Spectral Induced Polarization to Determination of Hydraulic Conductivity. Open Access Te Herenga Waka-Victoria University of Wellington. Thesis. <https://doi.org/10.26686/wgtn.17013986.v1>
- Kefeni, K. K., Msagati, T. A. M., & Mamba, B. B. (2017). Acid mine drainage: Prevention, treatment options, and resource recovery: A review. *Journal of Cleaner Production*, 151, 475–493. <https://doi.org/10.1016/j.jclepro.2017.03.082>
- MEND (Mine Environment Neutral Drainage). (2004). Design, construction and performance monitoring of cover systems for waste rock and tailings: volume 1 – summary, Canadian Mine Environment Neutral Drainage Program, Project 2.21.4a, July 2004. <http://mend-nedem.org/wpcontent/uploads/2.21.4a-Cover-Design Manual.pdf>. Accessed 10 December 2022.
- MEND (Mine Environment Neutral Drainage). (2012). Cold regions cover system design technical guidance document. *Canadian Mine Environment Neutral Drainage Program*,

Project 1.61.5c, March 2012.

Mining Watch Canada. (2020). Mine Waste in Canada: A Growing Liability. Accessed 4 April 2022. Retrieved from <https://miningwatch.ca/blog/2020/10/5/mine-waste-canada-growing-liability>

do Nascimento, M. M. P. F., Moreira, C. A., Duz, B. G., & da Silveira, A. J. T. (2022). Geophysical Diagnosis of Diversion Channel Infiltration in a Uranium Waste Rock Pile. *Mine Water and the Environment*, 41(3), 704–720. <https://doi.org/10.1007/s10230-022-00878-3>

Natural Resources Canada (2023, April 12). *Minerals and the economy*. Natural Resources Canada. Retrieved April 25, 2023, from <https://natural-resources.canada.ca/our-natural-resources/minerals-mining/minerals-metals-facts/minerals-and-the-economy/20529>

Parbhakar-Fox, A., & Lottermoser, B. G. (2015). A critical review of acid rock drainage prediction methods and practices. *Minerals Engineering*, 82, 107–124. <https://doi.org/10.1016/j.mineng.2015.03.015>

Pat-Espadas, A., Loredó Portales, R., Amabilis-Sosa, L., Gómez, G., & Vidal, G. (2018). Review of Constructed Wetlands for Acid Mine Drainage Treatment. *Water (Basel)*, 10(11), 1685–. <https://doi.org/10.3390/w10111685>

Placencia-Gómez, E., Slater, L., Ntarlagiannis, D., & Binley, A. (2013). Laboratory SIP signatures associated with oxidation of disseminated metal sulfides. *Journal of Contaminant Hydrology*, 148, 25–38. <https://doi.org/10.1016/j.jconhyd.2013.02.007>

Power, C., & Almpanis, A. (2022). Improved imaging efficiency of large mine waste rock piles with integrated electrical and electromagnetic geophysical techniques. *Journal of Applied Geophysics*, 206, 104824–. <https://doi.org/10.1016/j.jappgeo.2022.104824>

- Ramasamy, M., & Power, C. (2019). Evolution of Acid Mine Drainage from a Coal Waste Rock Pile Reclaimed with a Simple Soil Cover. *Hydrology*, 6(4), 83–. <https://doi.org/10.3390/hydrology6040083>
- Robinson, K., Robinson, C. E., Roy, J. W., Vissers, M., Almpanis, A., Schneidewind, U., & Power, C. (2022). Improved interpretation of groundwater-surface water interactions along a stream reach using 3D high-resolution combined DC resistivity and induced polarization (DC-IP) geoelectrical imaging. *Journal of Hydrology (Amsterdam)*, 613, 128468–. <https://doi.org/10.1016/j.jhydrol.2022.128468>
- Rubin, Hubbard, S. S., & Hubbard, S. S. (Susan S. (2005). *Hydrogeophysics*.
- United States Environmental Protection Agency (USEPA), 1983. Neutralization of Acid Mine Drainage. Design Manual EPA-600/2-83-001. US EPA, Chicago, Illinois, USA.
- United States Environmental Protection Agency (USEPA), 1994. Acid Mine Drainage Prediction. Technical Documents EPA530-R-94-036. US EPA, Washington, DC, USA. 1-52.

## CHAPTER 2 - LITERATURE REVIEW

### 2.1 MINING AND WASTE ROCKS

#### 2.1.1 The Mining Process and Mine Waste Production

Mining is extremely important to the development of human society. Since the dawn of human civilization, minerals have been extracted to produce a wide range of goods, from tools to weapons, and buildings to computers. One of the most well-known and traditional reasons for mining has been to generate energy resources to supply power for society. More recently, specific minerals such as rare earth elements are being mined to support the ongoing advancement of smart technologies (Balaram, 2019).

Minerals and energy resources are mined using two main methods. The first method is open-pit mining, a surface mining technique that extracts minerals such as coal and low-grade ore deposits from an open pit in the ground. Overburden material is removed via blasting so that the ores buried underneath can be accessed (Cohen & Coelho, 2021). The second method is underground mining which aims to extract ore deposits located underneath thick layers of rocks and soils. In most underground mining operations, vertical and horizontal tunnels, also known as adits or shafts, are drilled to access the underground mine (Miranda, 2007). Other lesser used mining methods exist that target different resources and are applied under different environments. For example, *in situ* leach mining is primarily used for mining uranium, using chemical solutions to dissolve the uranium deposits so they can be pumped out for further processing (Mudd, 2001). For unconsolidated minerals mixed with sediments in river channels, the placer mining method can be used to sift out the valuable minerals from the sediments (Davey, 2022).

The use of economically valuable mineral and energy resources comes with an environmental cost. Enormous volumes of mine waste are produced from mining operations. It is estimated

that for each ton of base metal produced (copper, nickel, and zinc), 20 to 200 tonnes of solid waste can be generated (Mining Watch Canada, 2020). In 2008, the Canadian mining industry produced 473 million tonnes of mine waste (Statistics Canada, 2012). It was estimated that Canadian mine waste production is 30 times more than the volumes of municipal and industrial waste produced on a yearly basis (Mine Watch Canada, 2020).

### 2.1.2 Waste Rock, a Unique Class of Mine Waste

Mine wastes can be divided into two categories: (1) waste rock, and (2) tailings. Waste rock is the solid waste that is removed during the excavation process to provide access to the ore bodies, while tailings are the residual liquid waste recovered during the mineral extraction process by separation (MSPR, 2022). Different mining methods produce different amounts of mine waste. Based on the Canadian average, the proportions between waste rock and tailings produced from underground mining activities in terms of the total solid waste is 10% and 90%, respectively. In open-pit mining, the percentage of waste rock production increased to 65%. This increase is due to the significant amount of overburden removed during the excavation process (Aubertin, 2013).

Tailings and waste rocks are similar to some degree, though they do have behavioral differences. The most obvious difference is the geochemical and physical transport processes that occur within the mine waste storage facilities. Waste rocks are often placed on the ground surface as porous unsaturated piles, allowing interaction of the waste materials to atmospheric water and oxygen. On the other hand, mine tailings are stored at tailing ponds, where the ambient exposure of the settled waste materials is limited. The grain size of tailings is much finer than waste rock, resulting in higher exposed material surface area and increased geochemical reaction rates. Waste rock materials have a wider particle size range that can cause non-uniform hydrodynamic behavior (Vriens et al., 2020).

## 2.2 ACID MINE DRAINAGE

### 2.2.1 AMD Sources: Oxidation of Sulfide Minerals

The most serious and costly environmental problem associated with mine waste rock is the production of acid mine drainage (AMD) (Jamieson, 2015). AMD is a highly acidic leachate that is characterized by low pH, and elevated concentrations of sulfate and dissolved metals (Amos, 2014). AMD released from mine waste sites causes significant contamination to the receiving environment (Chen et al., 2021).

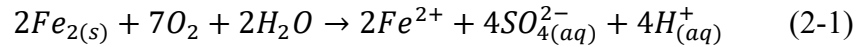
AMD is formed through the oxidation of sulfide minerals that are widely distributed in ore deposits and rocks (Vriens et al., 2020; Jacobs et al., 2013). Table 2.1 presents a list of different sulfide minerals found in mine wastes. Pyrite is the most abundant sulfide mineral in mine wastes (Vriens et al., 2020) and its oxidation is considered to be the most dominant reaction of AMD formation.

**Table 2.1** Selected primary sulfide minerals found in mine wastes (Hudson-Edwards et al., 2011)

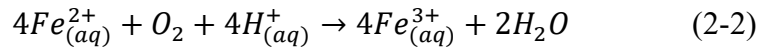
<b>Mineral</b>	<b>Formula</b>
Pyrite	FeS <sub>2</sub>
Marcasite	FeS <sub>2</sub>
Pyrrhotite	Fe <sub>(1-x)</sub> S
Chalcopyrite	CuFeS <sub>2</sub>
Bornite	Cu <sub>5</sub> FeS <sub>4</sub>
Sphalerite	(Zn,Fe)S
Pentlandite	(Fe,Ni) <sub>9</sub> S <sub>8</sub>
Enargite	Cu <sub>3</sub> AsS <sub>4</sub>
Galena	PbS
Cinnabar	HgS
Cobaltite	CoAsS
Stibnite	Sb <sub>2</sub> S <sub>3</sub>
Realgar	AsS
Orpiment	As <sub>2</sub> S <sub>3</sub>

The pyrite oxidation process has been extensively studied, with detailed reviews provided by Acharya & Kharel (2020), Akcil & Koldas (2006), and Jennings & Neuman (2008). The process can be summarized into the following reactions and can be applied to all geological settings including coal mines, hard rock mines, and acid surface soils (Jacobs et al., 2013).

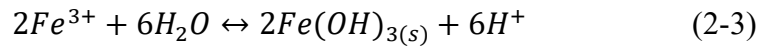
The first reaction demonstrates the oxidation of pyrite (FeS<sub>2</sub>) as it interacts with atmospheric water and oxygen to produce Fe<sup>2+</sup> (ferrous iron), sulfate (SO<sub>4</sub><sup>2-</sup>), and (H<sup>+</sup>) hydrogen ion. These hydrogen ions will further combine with sulfate to produce sulfuric acid (H<sub>2</sub>SO<sub>4</sub>).



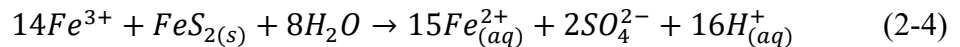
When pH > 4.0, the liberated Fe<sup>2+</sup> in the water will automatically oxidize into ferric iron (Fe<sup>3+</sup>). When pH < 4.0, the process can be catalyzed by bacterial activity. This is also known as a rate-limiting step in pyrite oxidation.



When pH > 3.0, the Fe<sup>3+</sup> produced in reaction (2-2) can be then hydrolyzed and precipitate out of the solution as ferric hydroxide (Fe(OH)<sub>3</sub>), a precipitate that gives AMD its reddish-to-yellow color.



The Fe<sup>3+</sup> that did not precipitate as Fe(OH)<sub>3</sub> can also react with FeS<sub>2</sub> to produce additional acidity.



It should be noted that each of these minerals has its own capability to react and produce AMD under different conditions, with various reactions presented in Table 2.2. Vriens et al. (2020)

further summarized and noted that the reactivity of the sulfide minerals is also different, where pyrrhotite is the most reactive, followed by galena, sphalerite, bornite, pentlandite, arsenopyrite, marcasite, pyrite, and chalcopyrite (Vriens et al., 2020).

**Table 2.2** Summary of the various oxidation reactions for sulfide minerals (Dold, 2016)

Sulfide mineral	Formula	Moles H <sup>+</sup>
Oxidation via oxygen + hydrolysis of Fe <sup>3+</sup>		
Pyrite (FeS <sub>2</sub> )	FeS <sub>2</sub> +3.75O <sub>2</sub> +3.5H <sub>2</sub> O=Fe(OH) <sub>3</sub> +SO <sub>4</sub> <sup>2-</sup> +4H <sup>+</sup>	4
Arsenopyrite (FeAsS)	FeAsS+2O <sub>2</sub> +3H <sub>2</sub> O=Fe(OH) <sub>3</sub> +SO <sub>4</sub> <sup>2-</sup> +HAsO <sub>4</sub> <sup>2-</sup> +3H <sup>+</sup>	3
Chalcopyrite (CuFeS <sub>2</sub> )	CuFeS <sub>2</sub> +4O <sub>2</sub> +3H <sub>2</sub> O=Cu <sup>2+</sup> +Fe(OH) <sub>3</sub> +2SO <sub>4</sub> <sup>2-</sup> +2H <sup>+</sup>	2
Pyrrhotite (Fe <sub>(1-x)</sub> S)	X=0.1:Fe <sub>(0.9)</sub> S+2.175O <sub>2</sub> +2.35H <sub>2</sub> O=0.9Fe(OH) <sub>3</sub> +SO <sub>4</sub> <sup>2-</sup> +2H <sup>+</sup>	2
Enargite (Cu <sub>3</sub> AsS <sub>4</sub> )	Cu <sub>3</sub> AsS <sub>4</sub> +8.75O <sub>2</sub> +2.5H <sub>2</sub> O=3Cu <sup>2+</sup> +HAsO <sub>4</sub> <sup>2-</sup> +4H <sup>+</sup>	4
Sphalerite (ZnS)	ZnS+2O <sub>2</sub> =Zn <sup>2+</sup> +SO <sub>4</sub> <sup>2-</sup>	0
Galena (PbS)	PbS+2O <sub>2</sub> =Zn <sup>2+</sup> +SO <sub>4</sub> <sup>2-</sup>	0
Covellite (CuS)	CuS+2O <sub>2</sub> =Zn <sup>2+</sup> +SO <sub>4</sub> <sup>2-</sup>	0
Oxidation via ferric iron		
Pyrite (FeS <sub>2</sub> )	FeS <sub>2</sub> +14Fe <sup>3+</sup> +8H <sub>2</sub> O=15Fe <sup>2+</sup> +2SO <sub>4</sub> <sup>2-</sup> +16H <sup>+</sup>	16/2 <sup>a</sup>
Arsenopyrite (FeAsS)	FeAsS+13Fe <sup>3+</sup> +8H <sub>2</sub> O=14Fe <sup>2+</sup> +SO <sub>4</sub> <sup>2-</sup> +HAsO <sub>4</sub> <sup>2-</sup> +15H <sup>+</sup>	15/2 <sup>a</sup>
Chalcopyrite (CuFeS <sub>2</sub> )	CuFeS <sub>2</sub> +16Fe <sup>3+</sup> +8H <sub>2</sub> O=Cu <sup>2+</sup> +17Fe <sup>2+</sup> +2SO <sub>4</sub> <sup>2-</sup> +16H <sup>+</sup>	16/0 <sup>a</sup>
Pyrrhotite (Fe <sub>(1-x)</sub> S)	x=0.1:Fe <sub>(0.9)</sub> S+7.8Fe <sup>3+</sup> +4H <sub>2</sub> O=8.7Fe <sup>2+</sup> +SO <sub>4</sub> <sup>2-</sup> +8H <sup>+</sup>	8/0.2 <sup>a</sup>
Enargite (Cu <sub>3</sub> AsS <sub>4</sub> )	Cu <sub>3</sub> AsS <sub>4</sub> +35Fe <sup>3+</sup> +20H <sub>2</sub> O=3Cu <sup>2+</sup> +HAsO <sub>4</sub> <sup>2-</sup> +35Fe <sup>2+</sup> +4SO <sub>4</sub> <sup>2-</sup> +39H <sup>+</sup>	39/4 <sup>a</sup>
Sphalerite (ZnS)	ZnS+8Fe <sup>3+</sup> +4H <sub>2</sub> O=8Fe <sup>2+</sup> +SO <sub>4</sub> <sup>2-</sup> +8H <sup>+</sup>	8/0 <sup>a</sup>
Galena (PbS)	PbS+8Fe <sup>3+</sup> +4H <sub>2</sub> O=8Fe <sup>2+</sup> +SO <sub>4</sub> <sup>2-</sup> +8H <sup>+</sup>	8/0 <sup>a</sup>
Covellite (CuS)	CuS+8Fe <sup>3+</sup> +4H <sub>2</sub> O=8Fe <sup>2+</sup> +SO <sub>4</sub> <sup>2-</sup> +8H <sup>+</sup>	8/0 <sup>a</sup>

## 2.2.2 Generation and Quality of AMD

The generation of AMD depends on many factors. One example can be the physical characteristics of the stockpile containing the waste rock, known as waste rock piles (WRPs). Waste rock with high permeability tends to have higher chemical reaction rates as the pore space between the rock species allows larger oxygen flow, thereby increasing the temperature within the WRP and creating convection in the structure to draw in more oxygen (Ackil & Koldas, 2006). Other factors include the sulfide mineral morphology, neutralizing mineral content, microorganisms, and pH.

### 2.2.2.1 Mineralogy

The formation of AMD is driven by the oxidation of sulfide minerals. Furthermore, the quality of the AMD can also vary based on the mineral's morphology. Caruccio et al. (1997) found that coarse-grained pyrite particles with non-framboidal structures are less reactive, meaning they decompose slower and produce less acidity than fine-grained pyrite with framboidal structures (Ackil & Koldas, 2006). Aside from sulfide minerals, WRPs also contain naturally occurring non-acid-generating minerals such as carbonates, hydroxides, and silicates (Dold, 2016). The dissolution of these minerals can consume the protons produced by the pyrite oxidation process and introduce alkalinity to the system (Langmuir, 1997). When there are sufficient non-acid-generating minerals in the system to buffer the acidities, neutral mine drainage (NMD) or metal leaching (ML) can be produced (Plante et al., 2010). This type of drainage is characterized by high hardness, metal(oid)s, and other contaminants that can be mobilized under non-acidic conditions (Virens et al., 2020).

### 2.2.2.2 Microorganisms

The chemical reaction rate of sulfide mineral oxidation can be significantly accelerated by bacteria such as thiobacillus and acidithobacillus species (Jennings & Neuman, 2008). The

oxidation of sulfide minerals with the presence of microbial activities can produce 1,000 times more acid drainage than chemical reactions alone (Adams et al., 2005). Bacteria can participate in the pyrite oxidation process by both contact and non-contact oxidation mechanisms. The contact oxidation mechanism involves the attachment of the cell or bacterium to the mineral surface to generate the oxidizing agent. Whereas in the non-contact mechanisms, bacteria are involved in the oxidation of  $Fe^{2+}$  to  $Fe^{3+}$  that can further oxidize the sulfide minerals, as shown previously in Equation (2-4) (Amos, 2014).

### 2.2.2.3 pH

Chemical factors such as pH level have the greatest impact on AMD (Acharya & Kharel, 2020). The characteristics of AMD are very different under different pH conditions and can be categorized into five types, which are summarized in Table 2.3. The pH of AMD is also negatively correlated with the amount of dissolved sulfides and metals present in the solution. It is found that drainage's electrical conductivity tends to increase along with its metal content (Equeenuddin et al., 2010).

**Table 2.3** Summary of the five categories of AMD characteristics (Kirby, 2014)

Type	Drainage Characteristic	Description
1	pH < 4.5	Higher levels of metal (iron, aluminum & manganese) and oxygen
2	pH > 6.0	Less acidic, Higher levels of dissolved solids, ferrous iron, and manganese
3	Alkaline	Moderate to high levels of dissolved solids, with low to moderate levels of iron and manganese
4	pH > 6.0	High level of suspended particulates
5	Neutralized	High total dissolved solids, and dissolved calcium and magnesium

### 2.2.3 Environmental Impacts of AMD

The impact of AMD is a global concern. The US EPA stated that the environmental risks due to AMD are second only to global warming and ozone depletion (Acharya & Kharel, 2020). The impact of AMD is very difficult to predict, and its assessment process is also difficult (Gray, 2017). It is different from site to site depending on its historical land use, climate, the scale of mining, and mine waste geochemistry. In general, AMD impacts can be divided into five categories: (1) chemical, (2) physical, (3) biological, (4) ecological, and (5) socioeconomic (Acharya & Kharel, 2020). These categories are summarized in Figure 2.1.

While the impact of AMD is multifold, its biological impact should be highlighted. The contamination of water bodies by AMD can result in the elimination of aquatic species, simplifying the food chain, and reducing ecological stability (Gray, 1996). Fish kills resulting from uncontrolled AMD release have been reported worldwide. Nordstrom and Alpers (1999) reported that over the past century, many millions of fish have been killed from mining activities in the U.S. (Jennings & Neuman, 2008).

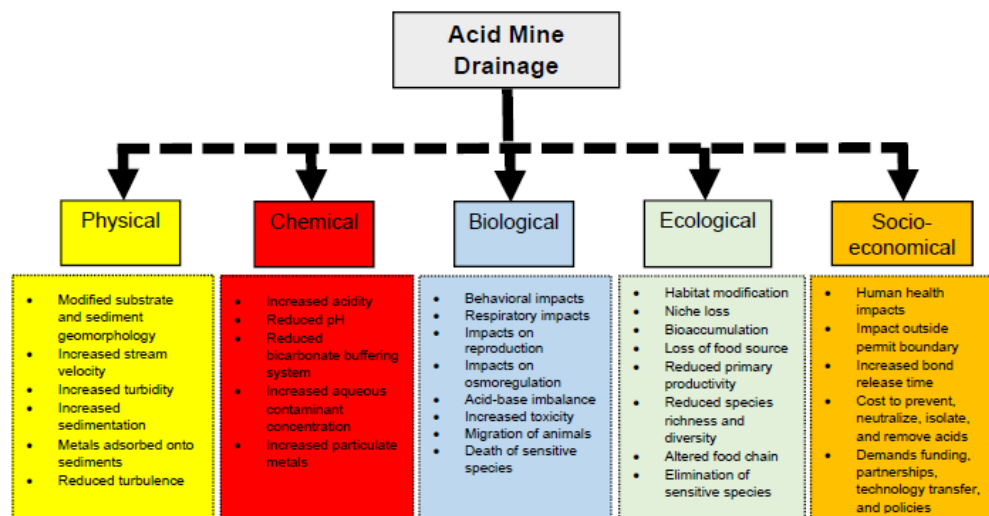


**Figure 2.1** Five categories of acid mine drainage impacts (Acharya & Kharel, 2020)

#### 2.2.4 Controlling AMD Release from WRPs

Waste rocks are often placed on the ground surface in stockpiles that can be enormous in size (e.g., at least 15 WRPs in Canada have a footprint that exceeds 10 km<sup>2</sup>) (Bussiere & Guittonny, 2022). These piles are porous and unsaturated. As the mine waste interacts with atmospheric oxygen and water, the sulfide minerals will proceed with the oxidation process and produce AMD. Waste rock acidity exists in two forms: stored acidity or potential acidity. Stored acidity is acidity that is available to be transported within the pile and is formed through the oxidation process of the sulfide minerals. Potential acidity first requires oxidation of sulfide minerals to generate additional stored acidity (Power et al., 2017).

AMD generally leaves WRPs via two pathways: surface runoff flow and basal/toe seepage. The surface runoff pathway involves precipitation that has interacted with the exposed waste rock and then travels from the WRP. Unsaturated flow occurs when precipitation infiltrates the waste rock providing the conditions for AMD generation (i.e., water and oxygen). This AMD water then infiltrates towards the base and/or toe of the pile before being released to surface water and/or groundwater receptors. Figure 2.2 presents a conceptual model of the various processes and pathways occurring in WRPs.

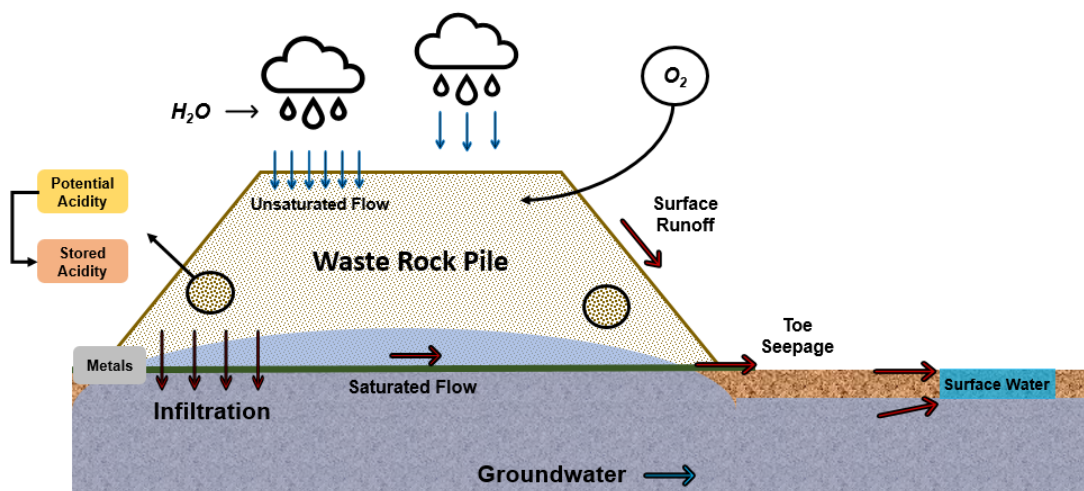


**Figure 2.2** Conceptual model of a WRP showing the various pathways

The impacts of AMD from WRPs can be minimized at three levels: (1) primary prevention of AMD process, (2) secondary control involving prevention of AMD migration, and (3) tertiary control or collection and treatment of effluents (Kefeni et al., 2017). The primary prevention of AMD process aims to minimize the influx of atmospheric oxygen and water percolation to the waste rock, which can be accomplished through two approaches. The first approach involves using unique pile construction sequences to control the flow within the pile, as shown in Figure 2.3. It relies on the capillary breaks developed between the fine and coarse materials. Fine grained layers are constructed with an angle towards the exterior of the pile so the water can be diverted before it can reach the pile core (Broda et al., 2014; Dubuc et al., 2017).

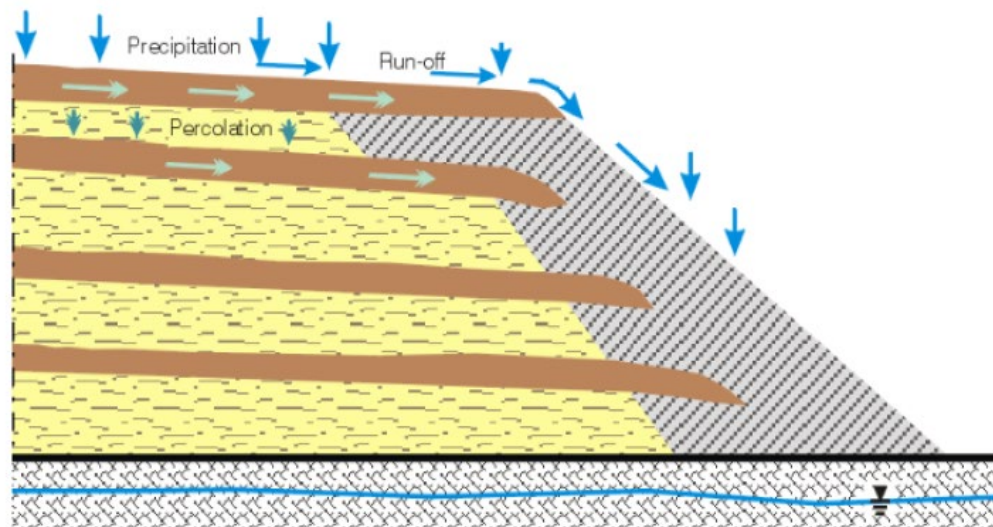


**Figure 2.3** Conceptual WRP showing unique pile construction to control water flow and prevent AMD (Dubuc et al., 2017)

The second approach involves the installation of cover systems to isolate the mine waste materials and limit the ingress of oxygen and water (Amos, 2014). Argunham (2014) categorized cover systems into two categories: (i) oxygen consuming covers, and (ii) oxygen diffusion covers. As shown in Figure 2.4, oxygen diffusion covers can be further categorized into dry covers and wet covers. The selection of a cover type is site-specific that depends on the local climate, as well as the characteristics of the mine waste (MEND, 2004).

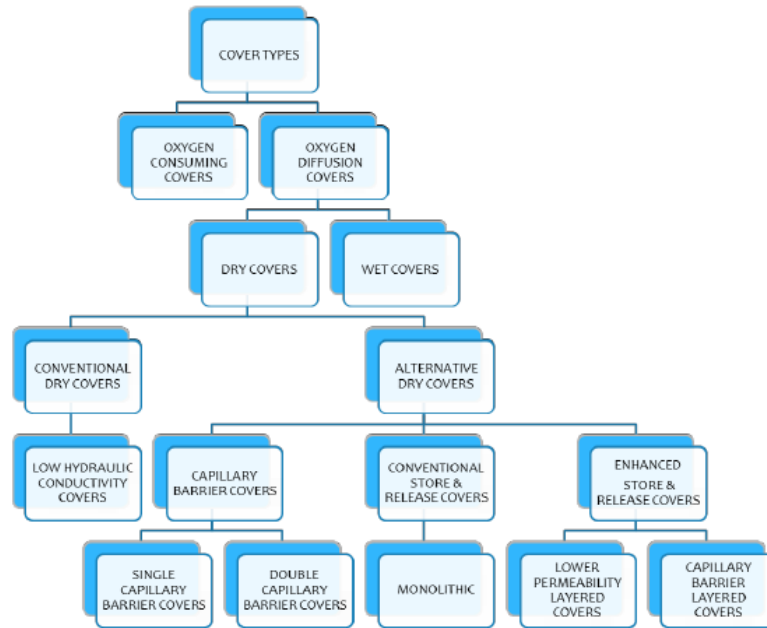


**Figure 2.4** Overview of the various cover systems installed over WRPs (Argunham, 2014)

Adequate sampling and analysis of the waste rock is crucial for both the design of the cover system and subsequent performance monitoring. The geochemical behavior of the WRP site can be assessed by porewater sampling from monitoring wells, surface water grab sampling, and coring of sediments and rocks. Waste rock is often cored from the WRP and taken for laboratory characterization to determine both the acidity already inside the rock (stored acidity) and the capacity of the rock to generate more (potential acidity).

### 2.3 MINE WASTE CHARACTERIZATION METHODS

Mine site regulators will only permit mining if a proper waste management plan has been developed (Parbhakar-Fox & Lottermoser, 2015). Mine wastes should be effectively characterized so that its future behavior, including AMD generation and risks, can be predicted, thereby assisting in the decision-making and development of appropriate plans for mine waste disposal and AMD prevention (Acharya & Kharel, 2020; MEND, 2008).

Mine waste characterization includes a range of tests that can determine the chemical and physical characteristics of the waste samples (Parbhakar-Fox & Lottermoser, 2015). These

tests are either field or laboratory-based and are summarized in Figure 2.5.

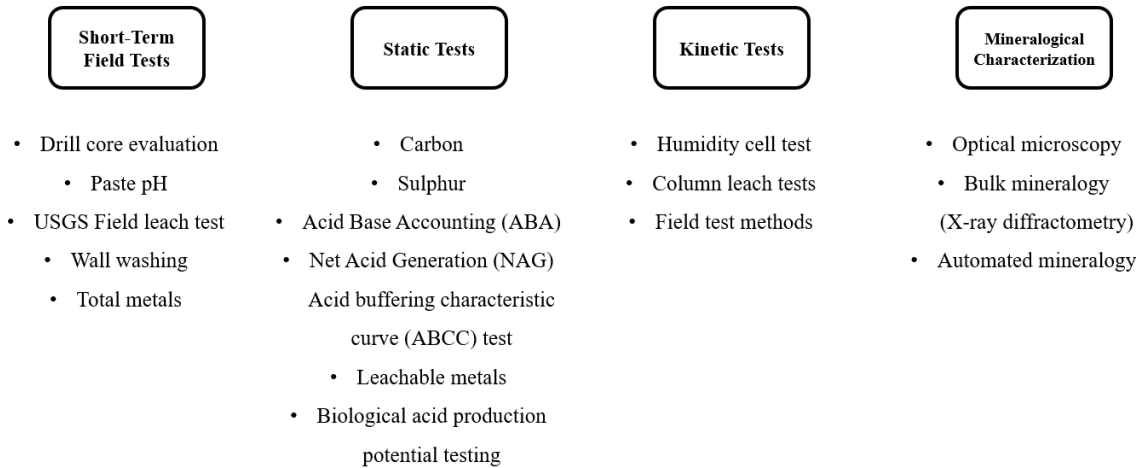


**Figure 2.5** Summary of the various mine waste characterization tests

Karlsson (2020) further divided these tests into different levels, where the scale, complexity, and cost of the tests increase from Level 1 to Level 4. A detailed hierarchy illustrating these levels is shown in Figure 2.6.

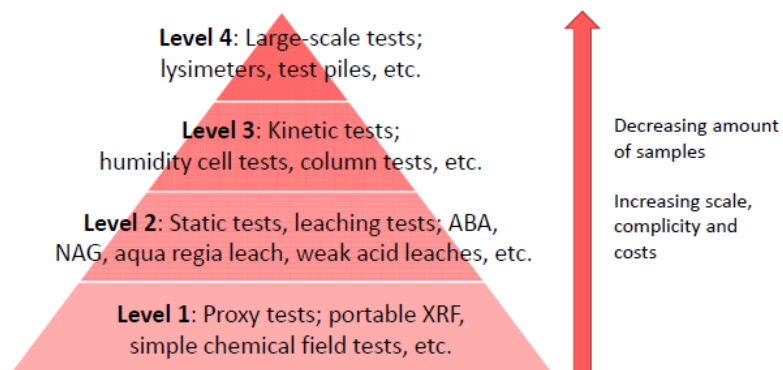


**Figure 2.6** Hierarchy of mine waste characterization tests based on scale, complicity, and costs

In this section, the most widely used laboratory methods will be discussed. Static and kinetic tests are commonly used for assessing the chemical properties of the mine waste rock, while grain size and mineralogical methods are used for determining the physical properties.

### 2.3.1 Chemical Properties: Static and Kinetic Tests

In the mining industry, static tests are widely applied to determine the sulfur content of a soil or rock sample, and estimate its level of acidity (Jacobs et al., 2013). The term ‘static’ is used because this type of test does not consider how fast the sample produces and consumes acidity (MEND, 2008; Jacobs et al., 2013). Although many protocols exist in the industry, the most known static test methods fall into two types: (1) acid base accounting (ABA), and (2) net acid generation (NAG) (Parbhakar-Fox & Lottermoser, 2015).

Kinetic tests are distinguished from static tests in their approach to define the acid generation characteristics of a sample. The term ‘kinetic’ is used because in kinetic tests, the acid generation characteristics of a sample are measured with respect to time (Jacobs et al., 2013). Kinetic tests can be used to assess the impact of different variables on the sample’s potential to generate acid. For example, the sample may be inoculated with bacteria, or the temperature of the sample environment is controlled during the test. Acid drainage control mechanisms, such as increasing alkalinity through the addition of lime, may also be examined using kinetic tests (USEPA, 1994). There are different types of kinetic tests to estimate the reaction rates and depletion time for various minerals, with the most common tests being column leaching tests and humidity cell tests (Benzaazoua et al., 2004).

#### 2.3.1.1 *Static tests- acid base accounting & net acid generation*

ABA is a widely used method that predicts the drainage quality by comparing the acid producing components to the acid consuming components of a sample (USEPA, 1994). The maximum acid generation potential (AGP) is controlled by the sulfide minerals in the sample and can be determined by multiplying the percent of the sulfide sulfur in a sample by a conversion factor (i.e.,  $AGP = 31.25 \times \text{wt\% Sulfide Sulfur}$ ). In contrast, the maximum acid neutralization potential (ANP) measures how much carbonate material is available in the sample to neutralize acid, and this can be determined by titration methods. The difference

between the AGP and ANP is known as the net neutralization potential (i.e.,  $NNP = ANP - AGP$ ) (US EPA, 1994).

The result of the ABA test can be used to divide the sample into categories (see Figure 2.7) that indicate whether the sample is: (i) potentially acid forming (PAF), (ii) non-acid forming (NAF), or (iii) uncertain (UC) types (Parbhakar-Fox & Lottermoser, 2015, Pearce et al., 2016). If the sample lies in the uncertain category, more acid potential generation testing is required (Jacobs et al., 2013).

The ABA test also has its limitations. For example, the AGP might be overestimated due to the presence of non-acid forming sulfur bearing phases, such as gypsum, epsomite, barite, etc. The ANP might be overestimated due to the presence of Fe carbonates, such as siderite. To overcome these limitations, the NAG test can be used as a supplement to obtain more reliable results. NAG tests predict AMD generation by reacting the sample with hydrogen peroxide. During the NAG test, acid generation and neutralization reactions can occur simultaneously, and the result represents the net amount of acid generated by the sample. The NAG test result can be used in conjunction with the ABA test result to determine whether a sample is acid forming or non-acid forming. Units for static test results are typically expressed in mass of calcium carbonate per 1000 metric tonnes of sample (MEND, 2008).

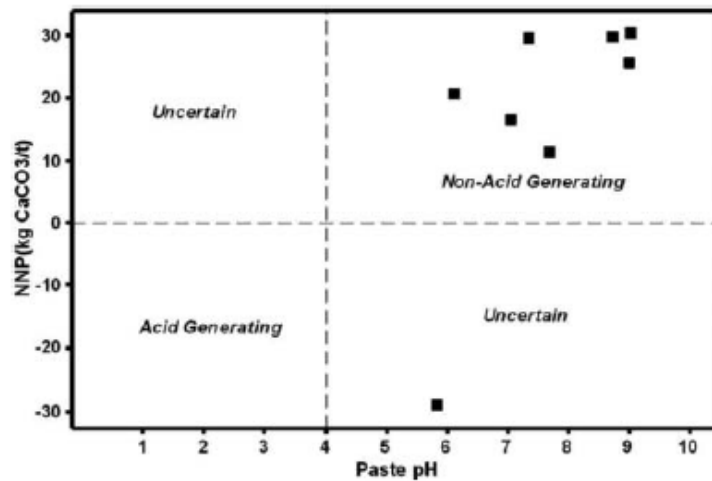


**Figure 2.7** The categories of a sample resulting from ABA tests (Hajizaden & Li, 2016)

### 2.3.1.2 Kinetic test – column leaching

In column tests, mine waste samples are stacked in cylinders and exposed to desired conditions (e.g., continuous water flushing, wetting/drying cycles), with the resulting leachate effluent collected at regular intervals for quality analysis. Column leaching tests can simulate the kinetic behavior of waste materials stored at ground surface (sub-aerial), and/or in tailing ponds (sub-aqueous) (Jacobs et al., 2013; Parbhakar-Fox & Lottermoser, 2015). There is no ‘standardized’ column test procedure, and they can be highly material or site specific (Jacobs et al., 2013; Parbhakar-Fox & Lottermoser, 2015). Column tests are highly flexible and designed and modified freely; for example, sample mass, water infiltration, and degree of oxidation in column tests can be freely controlled.

Column tests can be used to simulate a wide range of possible field conditions (Bradham & Caruccio, 1991). For the Mount Polly Mine Tailing Dam Failure project, the contractor conducted three column leaching tests to evaluate the effect of longer water flow paths, as longer flow paths were known to represent field conditions (SKR, 2015). Benzaazoua et al. (2001) and Kossoff et al. (2011) employed column tests to simulate field conditions for mine tailings, while Poaty et al. (2018) used column tests on a sample taken from Lac Tio Mine to

simulate the drainage quality behavior leaching from different waste rock configurations.

It is noted that column tests do have their disadvantages, which include the long test time required, the associated high cost, and the potential for channeling within the sample material (USEPA, 1994).

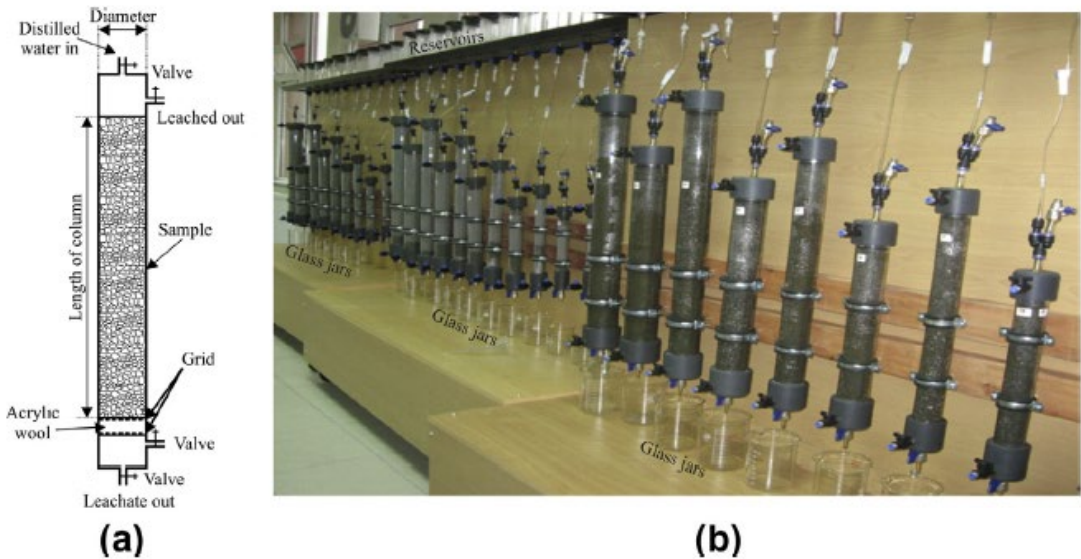


**Figure 2.8** Column leaching test set up example. a) Column cross-section; b) view of different sizes of columns (Erguler et al., 2014)

### 2.3.1.3 Kinetic test – humidity cell

Humidity cell tests are designed to investigate the weathering condition of mine waste materials, but with an accelerated oxidation rate. Acid generation and chemical release generally occur faster in humidity cell experiments (Parbhakar-Fox & Lottermoser, 2015).

While humidity cells previously varied ‘randomly’ in dimension, laboratories now adopt the American Society for Testing and Materials (ASTM) D5744-96 (Standard Test Method for Accelerated Weathering of Soil Materials Using a Modified Humidity Cell) for standardization. According to the ASTM specification, humidity cells should be 203 mm in height and 102 mm in diameter for coarse materials passing the 6.3 mm sieve, and 102 mm in height by 203 mm

in diameter for fine materials passing the 150-micron sieve (Jacobs et al., 2013).

The humidity cell test procedure involves exposing the sample material to a repeated 7-day cycle: three days of dry air, three days of humid air, and one day of water flushing/leaching, with the drainage water then analyzed for its geochemical characteristics. It is recommended that this 7-day cycle is repeated approximately 20 to 25 times. The drainage water parameters that are analyzed on a weekly basis (i.e., after the one day of water flushing) normally include pH, sulfate, and dissolved metals (Dold, 2016).

In comparison to some specially designed column leaching tests, the humidity cell method can only determine 'if' a mine waste sample will produce acidity, but not 'when' the original undisturbed material at the field site will produce acidity. The humidity cell is designed to accelerate the oxidation rate of the samples and reduce the length of the total experiment time, thereby likely resulting in higher acid and dissolved metals production. Thus, the leachate evolution measured during each cycle is expected to be overestimated compared to if it occurred in the field (Jacobs et al., 2013).

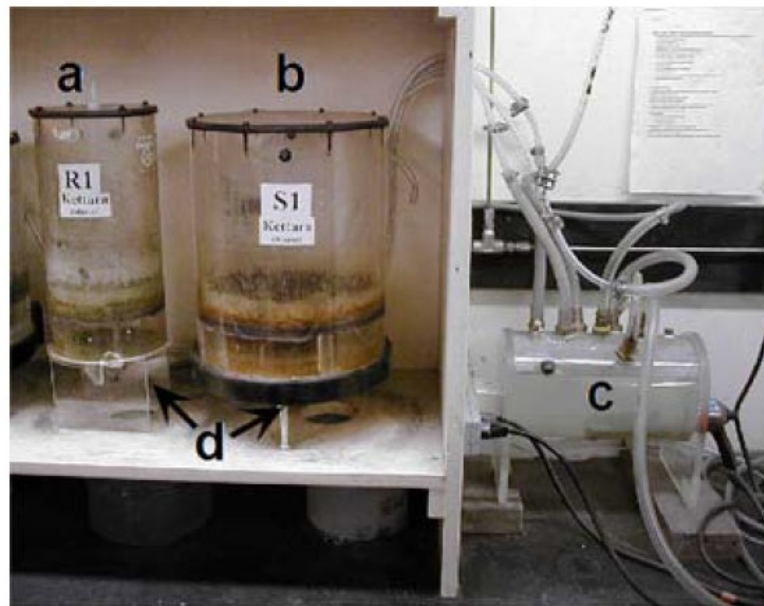


**Figure 2.9** Humidity cell set up example: a) small cell, b) large cell, and c) humidifier (Hakkou, 2008)

### 2.3.2 Physical Properties: Grain Size and Mineralogy

The physical properties of mine waste materials are also essential to understand their characteristics and predicted behavior. Physical properties, such as particle size distribution (PSD), surface area, and mineralogy can be highly supplementary to kinetic tests (USEPA, 1994).

#### 2.3.2.1 Particle size measurements

WRPs consist of waste materials varying in size from meter-scale to micro-scale (e.g., boulders to clay fractions) (Amos, 2014). Particle size analysis can provide important information such as reactivity and the movement of gases and liquids within the waste materials. Particles with high surface area may provide larger influence on mineral-water interaction. The reaction rate of these acid generating and neutralizing minerals increases as surface area increases (Jamieson et al., 2015).

A few approaches are available for measuring PSD, including dry sieving, wet sieving, differential liquid settling procedures, optical scanning, and laser diffraction methods (MEND, 2008). A summary of these approaches is provided by Kroetsch & Wang (2008). Analytical laboratories often apply ASTM C136-06 (Standard Test Method for Sieve Analysis of Fine and Coarse Aggregates) for dry and wet sieving. Dry sieving uses mechanical sieves to measure the sample particle sizes by percentage of weight, separating the sample into gravel (4.75-75 mm), sand (0.075-4.75 mm), as well as silt and clay particles (<0.075 mm). In most cases, wet sieving can help to separate silt and clay particles from sand particles, removing these finer particles so that a more accurate PSD results for the coarse portion of the sample can be obtained, following the procedure from ASTM C117-04 (Standard Test Method for Materials Finer than 75-micron (No.200) Sieve in Mineral Aggregates by Washing) (MEND, 2008).

For materials finer than 75  $\mu\text{m}$ , a differential liquid settling procedure, also known as the hydrometer test, can be used. This method uses visible light or optical density to determine the

particle size distribution and can separate grain particles in silt (2.0-62.5  $\mu\text{m}$ ) and clay ( $<2 \mu\text{m}$ ) (MEND, 2008). For microscopic particles, the automated scanning method can be applied with the electron microscope or laser diffraction method. The procedure for grain size analysis should be chosen according to the particle size range and the use of the data (Price, 2009). It should be noted that any techniques that involve immersing or rinsing sample may result in the loss of Fe sulfate minerals and affect the PSD of the mine waste sample (Jamieson et al., 2015).

#### *2.3.2.2 Mineralogical methods*

It is essential to understand the mineralogy of a mine waste sample to be able to predict what type of drainage will be produced. Waste rock drainage pH and elemental content is heavily dependent on its mineralogical content; therefore, effective prediction methods require the identification and quantification of the reactive minerals residing within the sample. Only two traditional techniques exist that can characterize mine waste mineralogy: optical microscopy, and X-ray diffraction (XRD) (Dold, 2016).

XRD is the most common technique used to determine the mineralogy of finer grained sediments. This method is attractive as it is fast, easy to perform, non-destructive, and only requires small amounts of sample (Poppe et al., 2001). XRD devices are commonly found at universities, government, and commercial laboratories (Jamieson et al., 2015). In XRD, the sample will be bombarded with an incident X-ray that is diffracted at different angles. By matching the diffraction patterns against a database that contains known patterns from thousands of minerals, the mineralogical content of the sample can be identified.

According to Raudsepp & Pani (2003), the relative amounts of crystalline phases present in the mine waste sample can be evaluated with the Rietveld method. This method is often used in mine waste characterization to distinguish between carbonate minerals such as calcite and siderite etc. (Jamieson et al., 2015). It is noted that accurate quantification of reactive minerals in a mine waste sample is very challenging (Dold, 2016). Another challenge with XRD is

successful identification of minerals that make up less than a few percent of the entire sample. Moreover, poorly crystalline, and amorphous materials, typical of many secondary mine waste phases, do not diffract well (Jamieson et al., 2015).

## 2.4 GEOELECTRICAL CHARACTERIZATION OF MINE WASTE

### 2.4.1 Introduction

The main limitations with the various aforementioned tests for mine waste characterization is that they are time-consuming and are based on extracted core samples from WRPs. Mine waste characterization can also be performed at the WRP sites using conventional geoenvironmental site approaches, such as sampling and geochemical analysis from a sparse network of intrusive boreholes; however, these approaches are expensive and provide limited spatial and temporal resolution. This provides the motivation for this work, which aims to answer the following questions: Can geophysical techniques be used to monitor continuously in space and time? Is there a geophysical signature that is best suited to image mine waste? Is there a geophysical signature that will evolve over time as it tracks changes in mine waste at WRPs?

Since sulfide minerals and AMD plumes are typically electrically conductive relative to the surrounding host material and uncontaminated groundwater, geoelectrical methods are an attractive option to provide large-scale continuous mapping of mine waste (Campbell & Fitterman, 2000). Typical geoelectrical methods include direct current (DC) resistivity, induced polarization (IP), electromagnetics (EM), and ground penetrating radar (GPR) (Power et al., 2018).

Among these methods, DC resistivity and IP methods have the most potential due to the electrical conductivity and chargeability associated with AMD-contaminated porewater and sulfide minerals (Joseph, 2016). The other two methods both have limitations: mine waste material with high conductivity can dissipate the radio waves of GPR, while EM is challenging

when the subsurface contains other electrical conductors such as clay lenses (Campbell & Fitterman, 2000; Knodel et al., 2007). For these reasons, only DC resistivity and IP methods will be discussed more in detail.

#### 2.4.2 Direct Current Resistivity

The direct current (DC) resistivity method is one of the most widely used geophysical techniques. This method is well understood as the relationship between resistivity and various hydrological properties has been extensively studied during the past 100 years. DC resistivity method is robust, cost efficient, and is relatively easy to be implemented in the field compared to other geophysical methods (Rubin & Hubbard, 2006).

During DC resistivity field measurements, spatially varied electrical resistivity of the subsurface is recorded using multiple pairs of electrodes that are placed on the ground surface. Figure 2.10 shows the concept of a simple four-electrode array, where the transmitting current is injected into the ground using the current electrodes, and the resulting voltages are measured using the receiver potential electrodes (Knodel et al., 2007). In DC resistivity field surveys, the electrical resistivity of the subsurface can also be measured between boreholes, between a single borehole and ground surface, and underwater by using specially designed cables.

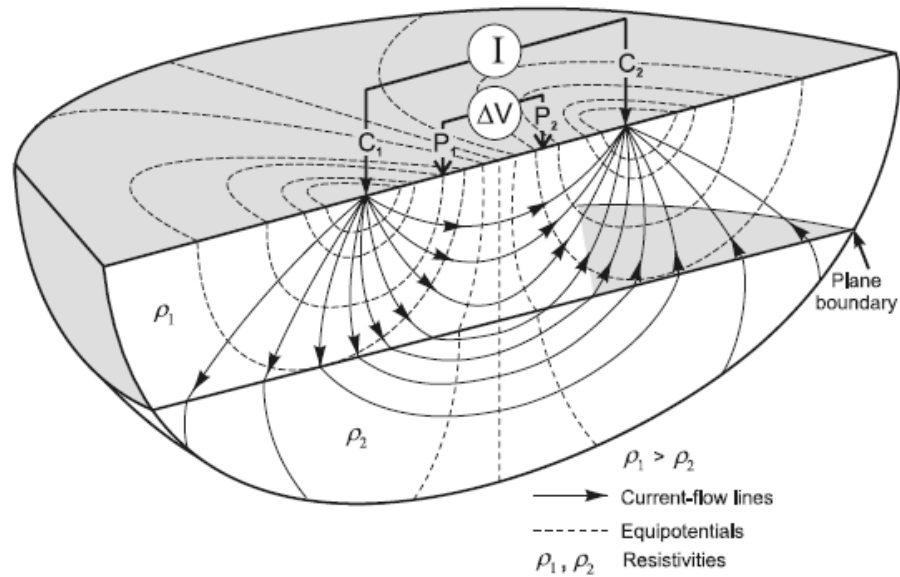


**Figure 2.10** Principle of resistivity measurement with a four-electrodes array (Knodel et al., 2007)

Traditionally, one dimensional (1D) resistivity surveys are carried out either in ‘profiling’ mode, moving electrode array along a line to detect lateral electrical changes, or in ‘sounding’ mode, increasing the electrode separations to detect vertical electrical changes (Rubin & Hubbard, 2006; Dahlin, 2000). When these modes are combined and sufficient measurements are obtained in the field, two- or three-dimensional images of the subsurface condition can be reconstructed via inverse modeling, which can also be known as electrical resistivity tomography (ERT) (Moysey, 2021). If 2D or 3D images of the subsurface are recorded over various timesteps, subsurface processes such as the contaminant transport that are constantly changing can be better delineated. This approach is also known as time-lapse ERT (see Figure 2.11) and is promising to capture subsurface processes at various scales has been highlighted by multiple researchers such as Loke et al. (2013), Binley et al. (2015), and Slater and Binley (2021).

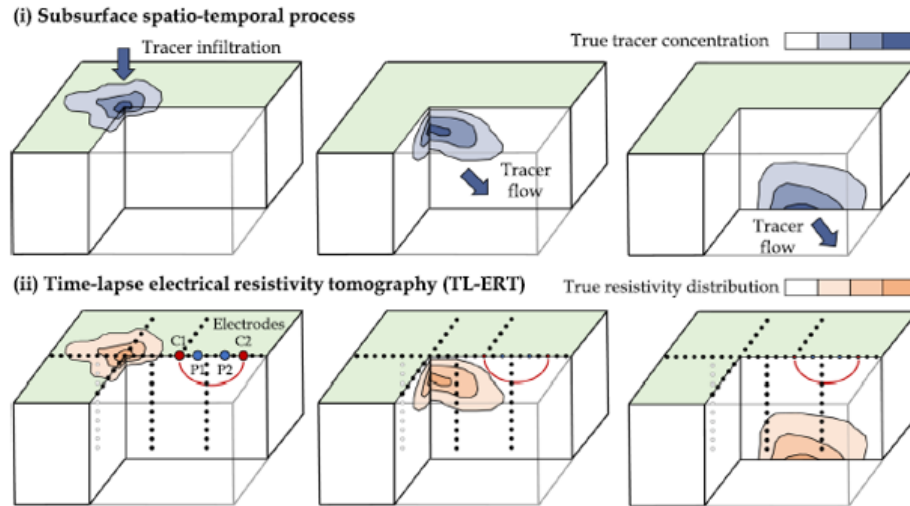


**Figure 2.11** TL-ERT monitoring of a tracer infiltration with surface and borehole electrodes. (i) Top panel shows the true spatial-temporal distribution of tracer concentration, (ii) medium panel presents the distribution of electrical resistivity (Dimech et al., 2022)

DC resistivity is a robust technique in the desalination of subsurface hydrological characteristics as the electrical resistivity values measured by the DC resistivity method are mainly controlled by ionic conduction through the pore fluids. This method is not ideal for geological materials delineation as it is possible that two different geological materials have the same resistivity due to variations in the pore fluid conductivity. The IP method is more suitable for such a task as this method can capture the polarization effects occurring at the fluid-grain interface (Joseph, 2016).

### 2.4.3 Induced Polarization

The IP effect was first discovered by Conard Schlumberger around 100 years ago. During one of Schlumberger's field DC resistivity surveys, it was observed that after shutting off the transmitting current, the voltage measured across the potential electrode did not drop down to zero immediately and showed some decay similar to a charge depleting battery (Martin et al., 2021). Such persistence of the measured voltage after the shutting down of the current source is due to the ability of the ground to polarize, and this phenomenon is called the IP effect (Joseph, 2016).

The IP response is highly complex, but it can be summarized as representing the capability of subsurface to store electrical charge. The polarization phenomenon of the IP effect can occur at both the interface between a pore fluid and metal or non-metal minerals. As an external electrical current is injected into the ground, the ions along these interfaces will be redistributed and polarized as shown in Figure 2.12. Once the external current is switched off, the polarized ions will then gradually relax to their original equilibrium conditions. Such diffusion-controlled relaxation is the source of the subsurface IP response, and the IP method measures the magnitude of this polarization phenomenon (Slater & Lesmes, 2000). In real world IP applications, the polarization effect can be represented as either chargeability ( $M_a$ ), percentage frequency effect (PFE), or phase angle ( $\varphi$ ), and the measurements of the IP method can be made in either time-domain or frequency domain mode (Rubin & Hubbard, 2006; Joseph, 2016).

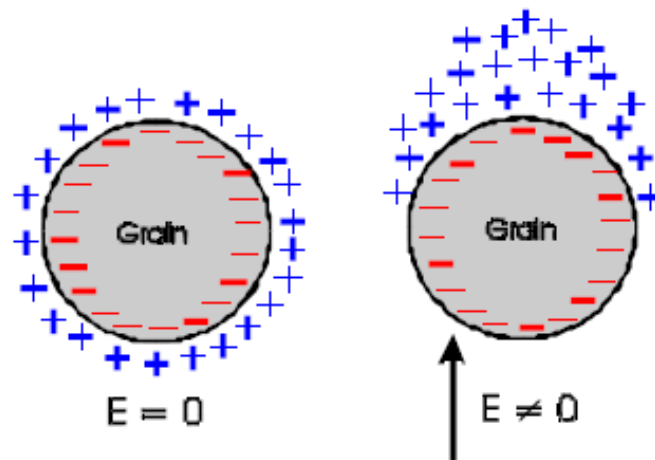


**Figure 2.12** Equilibrium ion distribution (left) and polarization following application of an electric field (right) (Slater & Lesmes, 2000)

Time-domain IP typically injects currents into the ground as a square wave. In this method, the rate of voltage decay upon the termination of the external current source is monitored to represent the polarization characteristics of the subsurface (Moysey, 2021). This is known as the apparent chargeability ( $M_a$ ) (i.e., ratio between secondary voltage ( $V_s$ ) and primary voltage

( $V_p$ ) (see Figure 2.13). In time domain IP measurements, the observed gradual decrease in the measured voltage is a complex function of the electrical charge polarization at the fluid-grain interface, and the conduction within the pore fluid along the grain boundaries (Rubin & Hubbard, 2006).

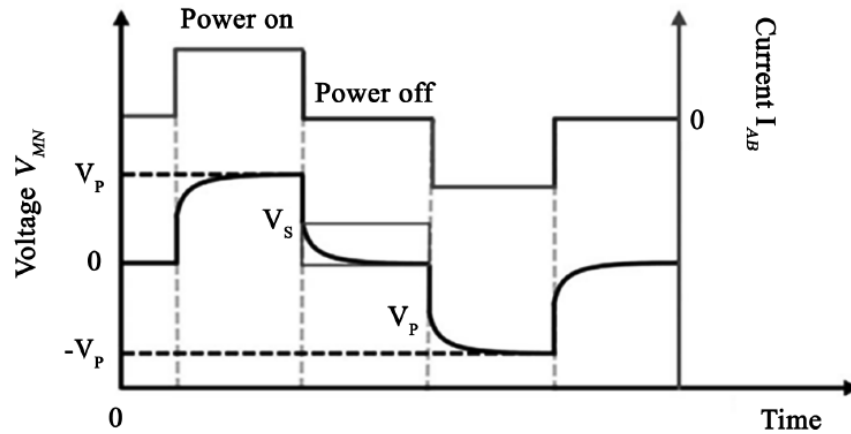


**Figure 2.13** Measurement of time-domain induced polarization (Dusabemariya et al., 2020)

In original frequency-domain IP measurements, subsurface resistivities were measured at two different frequencies. The frequency measured is usually an order of magnitude apart from each other (e.g., 0.05 Hz for low frequency and 10 Hz for high frequency) (Joseph, 2016). Traditionally, the IP effect in frequency domain was represented by the percent frequency effect (PFE), as shown in Equation (2-5), where  $\rho_{a0}$  and  $\rho_{a1}$  are the apparent resistivity values measured at low and higher frequencies, respectively (Zonge et al., 1972).

$$PFE = \frac{\rho_{a0} - \rho_{a1}}{\rho_{a1}} \times 100 \quad (2-5)$$

During the past two decades, an alternative frequency-domain IP method has been ‘re-discovered’ for hydrogeological and environmental investigations (Kemna et al., 2012). This alternative approach measures the complex electrical resistivity (or conductivity) of the subsurface across a range of frequencies (e.g., from 0.001 Hz to 10,000 Hz) to reveal more detailed information about the porous medium. Here, the term ‘complex’ is used to indicate the

measured resistivity (or conductivity) as a complex number that contains both a real component and an imaginary component. This method is known as complex conductivity or spectral IP (SIP) (Joseph, 2016; Rubin & Hubbard, 2006).

#### 2.4.4 Spectral Induced Polarization

SIP measurements inject sinusoidal currents into the ground, as opposed to the square waves used in time-domain IP. The capacitive nature of the subsurface causes a difference in the measured phase angle ( $\phi$ ) between the injected current and the measured voltage waveform as shown in Figure 2.14 (Joseph, 2016).

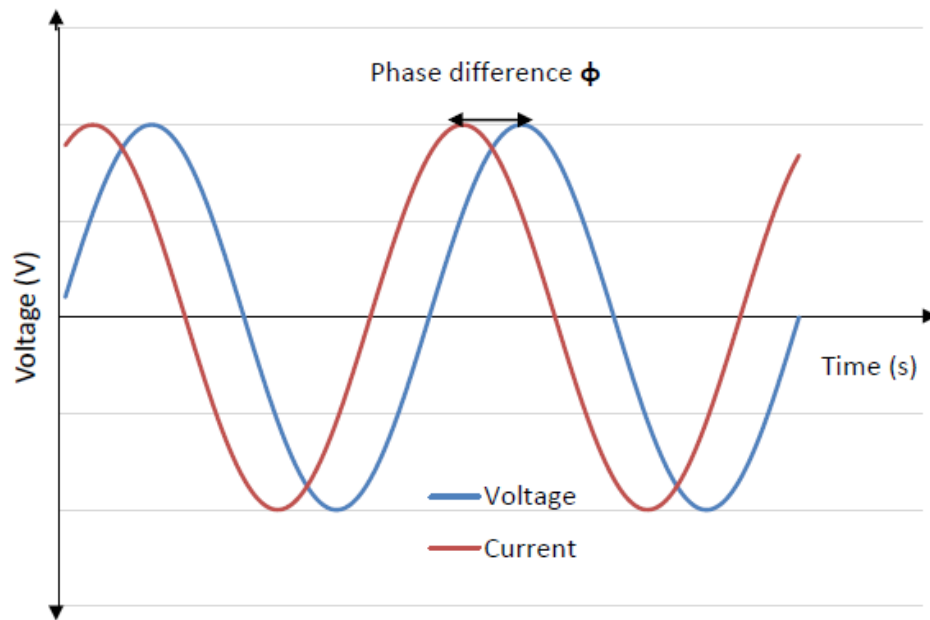


**Figure 2.14** Current and voltage waveforms in SIP measurements showing a phase difference (Joseph, 2016)

The laboratory and field instruments used for SIP measurements store both the injected current and measured voltage waveforms in digital form to then calculate the impedance in terms of its modulus and phase (Joseph, 2016). The real and imaginary parts of the complex conductivity can be expressed in terms of a magnitude and phase angle, or by real and imaginary conductivity components. An extensive overview of SIP theory is provided by

Binley & Slater (2020), with a summary as follows. In polar coordinates, the complex conductivity can be expressed in terms of the real ( $\sigma'$ ) and imaginary ( $\sigma''$ ) components, respectively, as follows:

$$\sigma^* = |\sigma|e^{i\varphi} = \sigma' + i\sigma'' \quad (2-6)$$

where  $|\sigma|$  is the magnitude of the amplitude related to electrical conductivity,  $\varphi$  is the phase angle and  $i = \sqrt{-1}$ . The real component, which is in-phase with the injected current, describes the electrical energy loss due to ohmic conduction currents, and is sensitive to pore water conductivity, moisture content, and porosity. The surface conduction (due to the electrical double layer, EDL) also contributes to the real component. On the other hand, the capacitive properties are represented by the imaginary component, which is out-of-phase with the current waveform. It describes electrical energy storage and is controlled by the physical properties of a porous medium and mediated by various polarization phenomena.

The measured parameters  $|\sigma|$  and  $\varphi$  are functions of both the real and imaginary components of the complex conductivity and are related as follows:

$$\sigma^* = |\sigma|e^{i\varphi} \quad (2-7)$$

Lastly, the phase angle measured in IP defines the ratio of the polarization to the conduction:

$$\varphi = \tan^{-1} \frac{\sigma''}{\sigma'} \quad (2-8)$$

Many fundamental studies have been performed on polarizations occurring in porous media. Three mechanisms have been discovered that can produce polarization effects in porous medium at relevant frequencies: (i) electrochemical polarization, (ii) membrane polarization, and (iii) interfacial polarization. Electrochemical polarization mechanisms arise from the presence of either non-conductive particles (e.g., silicates) or metallic particles in an electrolyte (e.g., pore water), and the formation of the EDL around the particles. These mechanisms are

dependent on the surface electrochemistry of the minerals, as well as the shape and size of the particles (Lesmes and Morgan, 2001). When an electric field is applied to a porous medium, ions in the diffuse layer concentrate in the direction of the electric field, polarizing the particles (Figure 2.15a).

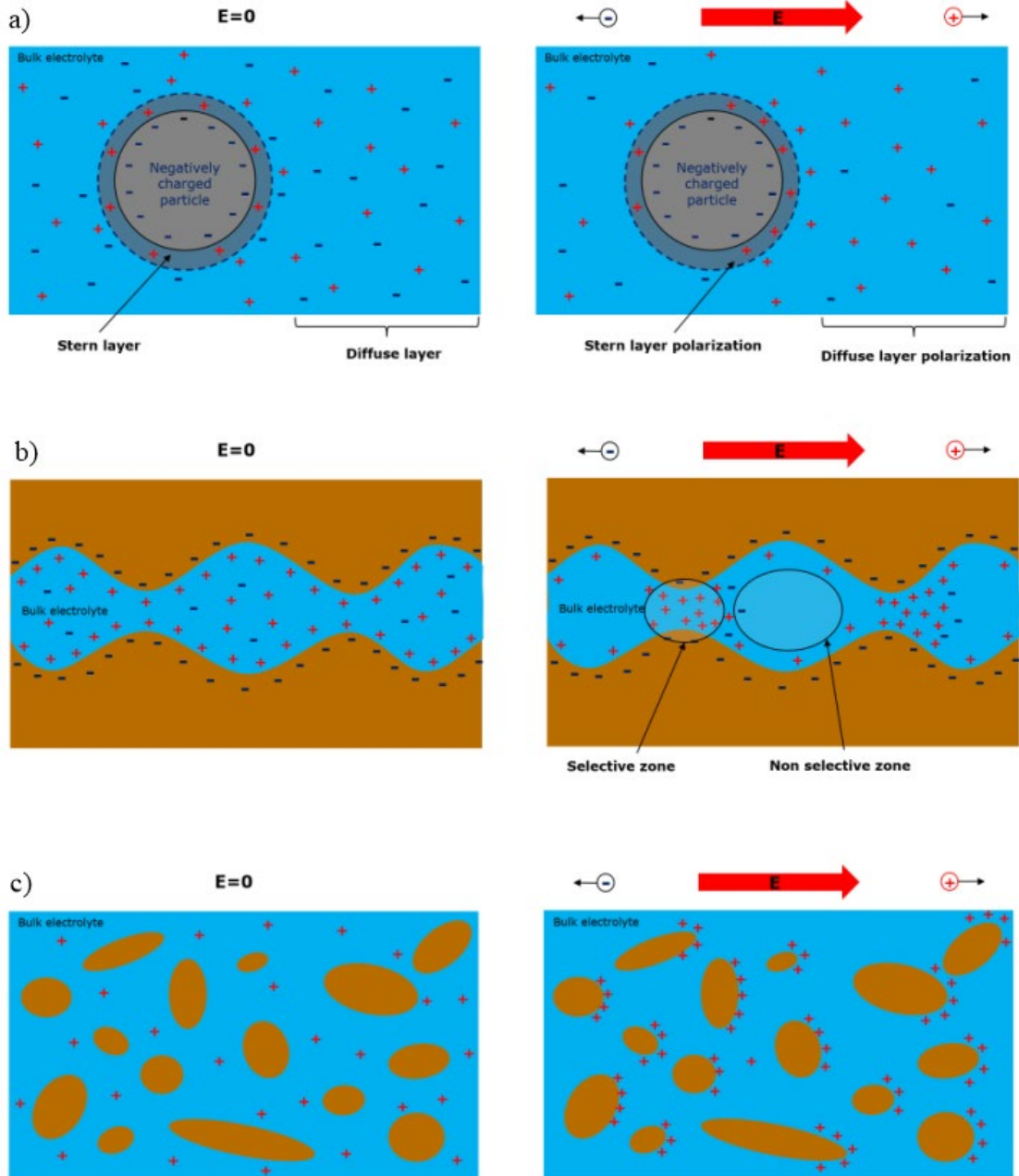


**Figure 2.15** Mechanisms that generate the IP effect in the ground: (a) electrode chemical, (b) membrane and (c) Maxwell-Wagner polarization mechanisms.

The membrane polarization mechanism occurs when non-conductive particles exist and accounts for the so-called background polarization effect (Marshall and Madden, 1959) (see Figure 2.15b). This mechanism results in a series of ion selective and non-selective (with no ion selectivity) zones in the ground. Ion selective zones are passages in the pore system where cations can pass, while anions are blocked, or vice versa, giving rise to polarization effects. The interfacial polarization mechanism, or Maxwell-Wagner mechanism (Figure 2.15 c), also occurs at the interfaces between different materials in a composite material (Johansson, 2016), but only exists at high frequencies ( $>1$  kHz).

#### 2.4.5 The Application of SIP in Mine Waste Characterization and Monitoring

Originally, the application of the SIP method in mine waste characterization was based on the hypothesis that the sulfide minerals residing in the mine waste can give unique phase spectra. This was first demonstrated by the electrochemical model of Wong (1979) on the IP phenomena of disseminated sulfide ores. In this model, the metallic spheres are considered randomly dispersed throughout an electrolytic host medium. As the volume percentage of the conducting mineral increases, the magnitude of the phase response increases. As the grain size of the conducting minerals decreases, the critical frequency of the phase response moves towards higher frequencies. Mahan et al. (1986) provided experimental evidence of Wong's model by testing synthetic samples made from quartz, chalcopyrite, as well as pyrite with known quantity and grain sizes. They concluded that the model fits the data well in frequency range where the phase peak occurs. Between 2013 and 2016, the SIP response of different types of sulfide minerals was further investigated, with results showing the SIP response generally follows the trends presented by Wong's model (e.g., Park et al., 2013; Takakura et al., 2014; Hupfer et al., 2016).

From 1997, a U.S. Geological Survey (USGS) team performed geological, geochemical, hydrogeological, and geophysical studies on eight mine dumps near New Mexico, Silverton Colorado, and Leadville Colorado. All mine waste dumps contained sulfide minerals that give

high IP response (Campbell & Horton, 2001), and the intention was to build a catalog and database of laboratory SIP signatures that could be compared to field SIP signatures. This would allow the mapping of the composition of mine waste dumps, where areas with high sulfide mineral content could be identified as sources of AMD generation (e.g., Campbell et al., 1998; Campbell & Horton, 2000a; Campbell et al., 2000; Anderson et al., 2001; Campbell & Beanland, 2001; Campbell, 2001; Campbell & Horton, 2001, Horton, 2003).

Unfortunately, the USGS team was not able to establish a database due to the lack of agreement between field and laboratory SIP measurements. Some valuable observations were still attained based on the laboratory results. For example, by comparing the sample at different oxidation degrees taken from different sites, observations suggested that as sulfide minerals oxidize, the phase spectra of the sample decreases in magnitude. The USGS experiments also showed that both the resistivity and phase spectra of a mine dump sample can change depending on the water content of the sample; the resistivity and phase spectra of samples change from 'flat shaped' to 'sulfide-looking' as water content increases from 5% to 10% (Campbell & Horton, 2001).

From 2010 to 2015, Placencia-Gomez and co-authors conducted a series of laboratory experiments to investigate the application of SIP for monitoring the generation and release of AMD. Their research objectives include the investigation of the: (i) SIP response during the oxidation of sulfide minerals (pyrite and pyrrhotite) in imitated field samples, (ii) effect of porewater chemistry on the SIP response in the presence of sulfide minerals in imitated field samples, and (iii) SIP response of real mine tailings. The hypothesis of their research assumed that the SIP method has the capability to capture the charge transfer electrochemical reaction at the metal mineral-electrolyte interface that is responsible for the generation of AMD (Placencia-Gomez et al., 2013; Placencia-Gomez et al., 2015; Placencia-Gomez & Slater, 2016).

According to the results of the studies by Placencia-Gomez et al., the phase spectra of the

sulfide minerals (pyrite and pyrrhotite) decreases depending on their degree of oxidation (Placencia-Gomez et al., 2013), which agrees with the work completed by Campbell & Horton (2001). Examples of these responses are shown in Figure 2.16. Such a conclusion was further validated by Wong's 1979 electrochemical model (Placencia-Gomez & Slater, 2014). Furthermore, Placencia-Gomez et al. found that the chemical composition of porewater can have a significant effect on the SIP response of samples containing sulfide minerals (Placencia-Gomez & Slater, 2016). They also demonstrated that the SIP method can provide unique sensitivity to oxidation-based textural features of real mine tailings under saturation conditions. The measurement of polarization can give a distinction between redox-inactive and redox-active ions present in the porewater in scenarios where the sulfide minerals have not been exposed to previous oxidation (Placencia-Gomez et al., 2015). However, their laboratory observations disagree with Campbell & Horton (2001) who had claimed that the phase spectra of the sample are dependent on moisture content (Placencia-Gomez et al., 2015).

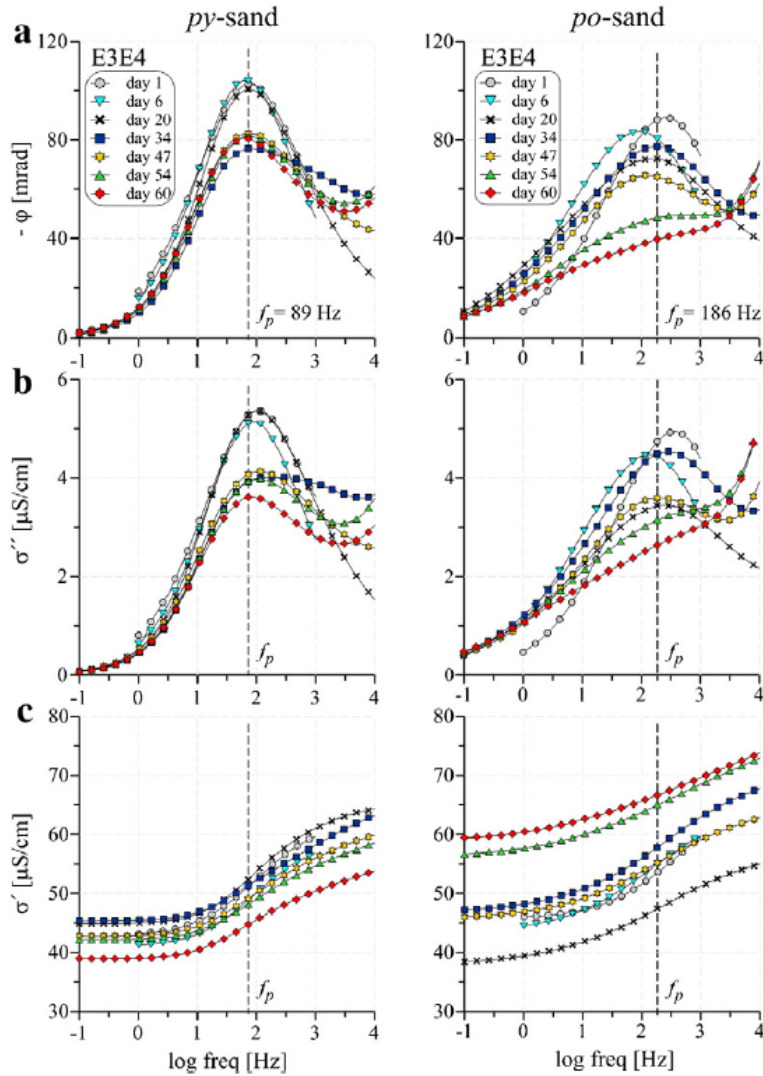


**Figure 2.16** Time-lapse SIP response of pyrite-sand (py-sand) and pyrrhotite-sand (po-sand) mixtures during oxidation: a) phase shift, b) imaginary conductivity and c) real conductivity (Placencia-Gomez et al., 2013)

Other recent SIP-mine waste applications include the use of the SIP method to investigate the residual minerals in abandoned mining waste dumps or slag dumps, which can be treated as a potential resource for mineral reuse. The SIP method can provide valuable information on mineral content, and grain size assuming complementary laboratory measurements are done (e.g., Gunther & Martin, 2016; Martin et al., 2020; Martin et al., 2021).

## 2.5 RESEARCH SUMMARY AND GAPS

This chapter has discussed waste rock production, their storage method, as well as their impacts on the environment. This chapter has also introduced various characterization methods that can be used to track characteristic changes within waste rock. It also highlights the limitation of these conventional approaches and the desire for *in situ* geoelectrical techniques to characterize waste rock due to their capability for continuous and/or large-scale monitoring. The DC and IP techniques were introduced, with emphasis on the SIP method due to its potential for mapping porewater chemistry and mineralogy within mine waste. The chapter finished with a review on previous studies that have assessed the SIP response from imitated samples that added sulfide minerals and/or real mine tailings/waste rock samples.

Following this extensive review of the relevant literature, the following research questions/gaps have been noted:

- Limited information is known on the time lapse SIP response of real waste rock samples. The most robust studies generated imitated waste samples that added known amounts of sulfide minerals.
- Previous studies have only included waste with large amounts of sulfide minerals, so knowledge on the SIP response from real samples with low and weathered sulfide minerals is limited.
- No study has fully characterized real waste rock samples and followed preferred kinetic test methodologies while simultaneously collecting SIP measurements.

## 2.6 REFERENCES

- Acharya, B. S., & Kharel, G. (2020). Acid mine drainage from coal mining in the United States—An overview. *Journal of Hydrology*, 588, 125061.
- Adams, D. J., Ogden, U. T., Pennington, P., Tachie-Menson, S., & Gutierrez, L. A. F. (2005, February). The role of microorganisms in acid rock drainage. In *SME Annual Meeting February*.
- Akcil, A., & Koldas, S. (2006). Acid Mine Drainage (AMD): causes, treatment and case studies. *Journal of cleaner production*, 14(12-13), 1139-1145.
- Amos, R. T., Blowes, D. W., Bailey, B. L., Segó, D. C., Smith, L., & Ritchie, A. I. M. (2015). Waste-rock hydrogeology and geochemistry. *Applied Geochemistry*, 57, 140-156.
- Anderson, A. L., Campbell, D. L., & Beanland, S. (2001). *Laboratory measurements of electrical properties of composite mine dump samples from Colorado and New Mexico*. US Department of the Interior, US Geological Survey.
- Argunhan, Ç. (2014). *Optimum cover design for waste rock storage areas* (Master's thesis, Middle East Technical University).
- ASTM C136–06. (2006). Standard test method for sieve analysis of fine and coarse aggregates. Annual book of ASTM standards. Philadelphia: American Society for Testing and Materials.
- ASTM, N. D5744-96-2001 Standard Test Method for Accelerates Weathering of solid Materials using a Modified Humidity cell. *Book of Standards*, 11(04).
- ASTM. (2013). Standard test method for materials finer than 75- $\mu\text{m}$  (No. 200) sieve in mineral aggregates by washing. *ASTM C117-13*.
- Balaram, V. (2019). Rare earth elements: A review of applications, occurrence, exploration,

- analysis, recycling, and environmental impact. *Geoscience Frontiers*, 10(4), 1285-1303.
- Benzaazoua, M., Bussière, B., & Dagenais, A. M. (2022). Comparison of kinetic tests for sulfide mine tailings. In *Tailings and Mine Waste 2001* (pp. 263-272). CRC Press.
- Benzaazoua, M., Bussière, B., Dagenais, A. M., & Archambault, M. (2004). Kinetic tests comparison and interpretation for prediction of the Joutel tailings acid generation potential. *Environmental geology*, 46, 1086-1101.
- Binley, A., & Slater, L. (2020). *Resistivity and induced polarization: Theory and applications to the near-surface earth*. Cambridge University Press.
- Bradham, W. S., & Caruccio, F. T. (1990). A comparative study of tailings analyses using acid/base accounting, cells, columns and soxhlets. In *Proceedings of the Mining and Reclamation Conference and Exhibition*. (No. 1, pp. 19-25). West Virginia University Publications Service.
- Broda, S., Aubertin, M., Blessent, D., Hirthe, E., & Graf, T. (2014). Improving control of contamination from waste rock piles. *Environmental Geotechnics*, 4(4), 274-283.
- Bussiere B, Guittonny M (2020) Hard rock mine reclamation: from prediction to management of acid mine drainage. CRC Press, USA [https:// doi. org/ 10. 1201/ 97813 15166 698](https://doi.org/10.1201/9781315166698)
- Campbell, D. L., & Beanland, S. (2001). *Spectral Induced Polarization Measurements at the Carlisle Mine Dump, New Mexico*. US Department of the Interior, US Geological Survey.
- Campbell, D. L., & Fitterman, D. V. (2000, May). Geoelectrical methods for investigating mine dumps. In *Proceedings of the 5th International Conference on Acid Rock Drainage (ICARD 2000)*, Denver, Colo (Vol. 2, pp. 1513-1523).
- Campbell, D. L., & Horton, R. J. (2000). *Geoelectrical laboratory and field studies of materials from the Tucson Mine Dump near Leadville, Colorado* (No. 2000-312). US

Department of the Interior, US Geological Survey.

- Campbell, D. L., & Horton, R. J. (2001, March). Spectral induced polarization studies of mine waste piles in Colorado and New Mexico. In *14th EEGS Symposium on the Application of Geophysics to Engineering and Environmental Problems* (pp. cp-192). European Association of Geoscientists & Engineers.
- Campbell, D. L., Fitterman, D. V., Hein, A. S., & Jones, D. P. (1998, March). Spectral induced *Application of Geophysics to Engineering and Environmental Problems* (pp. cp-203). European Association of Geoscientists & Engineers.
- Campbell, D. L., Horton, R. J., & Beanland, S. (2000). *Geoelectrical laboratory measurements of materials from the May Day Mine dump, southwestern Colorado* (No. 2000-382). US Geological Survey,.
- Campbell, D. L., & Horton, R. J. (2001, March). Spectral induced polarization studies of mine waste piles in Colorado and New Mexico. In *14th EEGS Symposium on the Application of Geophysics to Engineering and Environmental Problems* (pp. cp-192). European Association of Geoscientists & Engineers.
- Chen, G., Ye, Y., Yao, N., Hu, N., Zhang, J., & Huang, Y. (2021). A critical review of prevention, treatment, reuse, and resource recovery from acid mine drainage. *Journal of Cleaner Production*, 329, 129666–. <https://doi.org/10.1016/j.jclepro.2021.129666>
- Cohen, M. W., & Coelho, V. N. (2021). Open-pit mining operational planning using multi agent systems. *Procedia Computer Science*, 192, 1677-1686.
- Dahlin, T. (2001). The development of DC resistivity imaging techniques. *Computers & Geosciences*, 27(9), 1019-1029.

- Davey, R. (2022, June 22). *The main types of mining and their differences*. AZoMining.com. Retrieved January 27, 2023, from <https://www.azomining.com/Article.aspx?ArticleID=1690>
- Dimech, A., Cheng, L., Chouteau, M., Chambers, J., Uhlemann, S., Wilkinson, P., ... & Isabelle, A. (2022). A review on applications of time-lapse electrical resistivity tomography over the last 30 years: perspectives for mining waste monitoring. *Surveys in Geophysics*, 43(6), 1699-1759.
- Dold, B. (2017). Acid rock drainage prediction: A critical review. *Journal of Geochemical Exploration*, 172, 120-132.
- Dubuc, J., Pabst, T., & Aubertin, M. (2017, October). An assessment of the hydrogeological response of the flow control layer installed on the experimental waste rock pile at the Lac Tio mine. In *Proceedings of the 70th Canadian Geotechnical Conference, Ottawa, ON, Canada* (pp. 1-4).
- Dusabemariya, C., Qian, W., Bagaragaza, R., Faruwa, A. R., & Ali, M. (2020). Some experiences of resistivity and induced polarization methods on the exploration of sulfide: A review. *Journal of Geoscience and Environment Protection*, 8(11), 68.
- Equeenuddin, S. M., Tripathy, S., Sahoo, P. K., & Panigrahi, M. K. (2010). Hydrogeochemical characteristics of acid mine drainage and water pollution at Makum Coalfield, India. *Journal of Geochemical Exploration*, 105(3), 75-82.
- Gray, N. F. (1997). Environmental impact and remediation of acid mine drainage: a management problem. *Environmental geology*, 30, 62-71.
- Günther, T., & Martin, T. (2016). Spectral two-dimensional inversion of frequency-domain induced polarization data from a mining slag heap. *Journal of Applied Geophysics*, 135, 436-448.

- Hakkou, R., Benzaazoua, M., & Bussiere, B. (2008). Acid mine drainage at the abandoned Kettara mine (Morocco): 2. Mine waste geochemical behavior. *Mine Water and the Environment*, 27, 160-170.
- Horton, R. J. (2003). *Electrical property measurements of mine waste from the Sunday# 2 and Venir mines, Leadville, Colorado*. US Department of the Interior, US Geological Survey.
- Hudson-Edwards, K. A., Jamieson, H. E., & Lottermoser, B. G. (2011). Mine wastes: past, present, future. *Elements*, 7(6), 375-380.
- Hupfer, S., Martin, T., Weller, A., Günther, T., Kuhn, K., Ngninjio, V. D. N., & Noell, U. (2016). Polarization effects of unconsolidated sulphide-sand-mixtures. *Journal of Applied Geophysics*, 135, 456-465.
- Jacobs, J. A., Lehr, J. H., & Testa, S. M. (2013). *Acid mine drainage, rock drainage, and acid sulfate soils : causes, assessment, prediction, prevention, and remediation* (J. A. (James A. Jacobs, J. H. Lehr, & S. M. Testa, Eds.). Hoboken, New Jersey: John Wiley & Sons, Inc.
- Jamieson, H. E., Walker, S. R., & Parsons, M. B. (2015). Mineralogical characterization of mine waste. *Applied Geochemistry*, 57, 85-105.
- Jennings, S. R., Blicher, P. S., & Neuman, D. R. (2008). *Acid mine drainage and effects on fish health and ecology: a review*. Reclamation Research Group.
- Johansson, S. (2016). From microstructure to subsurface characterization. Spectral information from field scale time domain induced polarization. Lunds Universitet. Teknisk Geologi.
- Joseph, S. (2016). The Application of Spectral Induced Polarization to Determination of Hydraulic Conductivity.
- Kefeni, K. K., Msagati, T. A., & Mamba, B. B. (2017). Acid mine drainage: Prevention, treatment options, and resource recovery: A review. *Journal of Cleaner Production*, 151,

475-493.

Kemna, A., Binley, A., Cassiani, G., Niederleithinger, E., Revil, A., Slater, L., ... & Zimmermann, E. (2012). An overview of the spectral induced polarization method for near-surface applications. *Near Surface Geophysics*, *10*(6), 453-468.

Kirby, D. (2014). Effective treatment options for acid mine drainage in the coal region of West Virginia.

Kossoff, D., Hudson-Edwards, K. A., Dubbin, W. E., & Alfredsson, M. A. (2011). Incongruent weathering of Cd and Zn from mine tailings: A column leaching study. *Chemical Geology*, *281*(1-2), 52–71. <https://doi.org/10.1016/j.chemgeo.2010.11.028>

Knödel, K., Lange, G., & Voigt, H. J. (2007). *Environmental geology: handbook of field methods and case studies*. Springer Science & Business Media.

Kossoff, D., Hudson-Edwards, K. A., Dubbin, W. E., & Alfredsson, M. A. (2011). Incongruent weathering of Cd and Zn from mine tailings: a column leaching study. *Chemical Geology*, *281*(1-2), 52-71.

Langmuir, D. (1997). Aqueous environmental geochemistry. Pearson Education, Upper Saddle River, NJ. *Aqueous environmental geochemistry. Pearson Education, Upper Saddle River, NJ.*

Mahan, M. K., Redman, J. D., & Strangway, D. W. (1986). Complex resistivity of synthetic sulphide bearing rocks. *Geophysical Prospecting*, *34*(5), 743-768.

Martin, T., Titov, K., Tarasov, A., & Weller, A. (2021). Spectral induced polarization: frequency domain versus time domain laboratory data. *Geophysical Journal International*, *225*(3), 1982-2000.

Marshall, D. J., & Madden, T. R. (1959). Induced polarization, a study of its causes.

- Geophysics, 24(4), 790-816.
- MEND (Mine Environment Neutral Drainage). (2004). Design, construction and performance monitoring of cover systems for waste rock and tailings: volume 1 – summary, Canadian Mine Environment Neutral Drainage Program, Project 2.21.4a, July 2004. [http://mend-nedem.org/wpcontent/uploads/2.21.4a-Cover-Design Manual.pdf](http://mend-nedem.org/wpcontent/uploads/2.21.4a-Cover-Design%20Manual.pdf). Accessed 10 December 2022.
- MEND (Mine Environment Neutral Drainage). (2008). Acid Rock Drainage Prediction Manual. *Canadian Mine Environment Neutral Drainage Program*, Project 1.61.1b, June 2008
- MEND (Mine Environment Neutral Drainage). (2012). Cold regions cover system design technical guidance document. *Canadian Mine Environment Neutral Drainage Program*, Project 1.61.5c, March 2012.
- Mining Watch Canada. (2020). Mine Waste in Canada: A Growing Liability. Accessed 4 April 2022. Retrieved from <https://miningwatch.ca/blog/2020/10/5/mine-waste-canada-growing-liability>
- Miranda, J. P. (2007). *Handbook of operations research in natural resources* (Vol. 99). Springer Science & Business Media.
- Mudd, G. M. (2001). Critical review of acid in situ leach uranium mining: 1. USA and Australia. *Environmental Geology*, 41, 390-403.
- Parbhakar-Fox, A., & Lottermoser, B. G. (2015). A critical review of acid rock drainage prediction methods and practices. *Minerals Engineering*, 82, 107-124.
- Park, M. K., Park, S., Yi, M. J., Kim, J. H., & Takakura, S. (2013, November). SIP response of sulfide minerals in artificial specimen. In *Proceedings of the 11th SEGJ International*

- Symposium, Yokohama, Japan, 18-21 November 2013* (pp. 407-410). Society of Exploration Geophysicists of Japan.
- Pearce, J., Weber, P., Pearce, S., & Scott, P. (2016, March). Acid and metalliferous drainage contaminant load prediction for operational or legacy mines at closure. In *Mine Closure 2016: Proceedings of the 11th International Conference on Mine Closure* (pp. 663-676). Australian Centre for Geomechanics.
- Plante, B., Benzaazoua, M., & Bussière, B. (2011). Kinetic testing and sorption studies by modified weathering cells to characterize the potential to generate contaminated neutral drainage. *Mine water and the environment*, 30, 22-37.
- Placencia-Gómez, E., & Slater, L. D. (2014). Electrochemical spectral induced polarization modeling of artificial sulfide-sand mixtures. *Geophysics*, 79(6), EN91-EN106.
- Placencia-Gómez, E., & Slater, L. D. (2016). On the pore water chemistry effect on spectral induced polarization measurements in the presence of pyrite. *Journal of Applied Geophysics*, 135, 474-485.
- Placencia-Gómez, E., Slater, L., Ntarlagiannis, D., & Binley, A. (2013). Laboratory SIP signatures associated with oxidation of disseminated metal sulfides. *Journal of Contaminant Hydrology*, 148, 25-38.
- Placencia-Gómez, E., Parviainen, A., Slater, L., & Leveinen, J. (2015). Spectral induced polarization (SIP) response of mine tailings. *Journal of Contaminant Hydrology*, 173, 8-24.
- Poaty, B., Plante, B., Bussière, B., Benzaazoua, M., Pabst, T., Aubertin, M., ... & Nadeau, P. (2018, September). Geochemical behavior of different waste rock configurations from the Lac Tio mine: Comparison between column tests and experimental waste rock pile results. In *Proceedings of Tailings and Mine Waste Conference, Keystone, CO* (Vol. 30, pp. 811-

- 821). Keystone: Tailings and Mine Waste Conference.
- Poppe, L. J., Paskevich, V. F., Hathaway, J. C., & Blackwood, D. S. (2001). A laboratory manual for X-ray powder diffraction. *US Geological Survey open-file report, 1(041)*, 1-88.
- Power, C., Ramasamy, M., MacAskill, D., Shea, J., MacPhee, J., Mayich, D., ... & Mkandawire, M. (2017). Five-year performance monitoring of a high-density polyethylene (HDPE) cover system at a reclaimed mine waste rock pile in the Sydney Coalfield (Nova Scotia, Canada). *Environmental Science and Pollution Research, 24*, 26744-26762.
- Power, C., Tsourlos, P., Ramasamy, M., Nivorlis, A., & Mkandawire, M. (2018). Combined DC resistivity and induced polarization (DC-IP) for mapping the internal composition of a mine waste rock pile in Nova Scotia, Canada. *Journal of Applied Geophysics, 150*, 40-51.
- Rubin, Hubbard, S. S., & Hubbard, S. S. (Susan S. (2005). *Hydrogeophysics*.
- Takakura, S., Sasaki, Y., Takahashi, T., & Matsukuma, Y. (2014). Complex resistivity measurements of artificial samples containing pyrite and magnetite particles. *Butsuri-Tansa, 67(4)*, 267-275.
- United States Environmental Protection Agency (US EPA), 1994. Acid Mine Drainage Prediction. Technical Documents EPA530-R-94-036. US EPA, Washington, DC, USA. 1-52.
- Vriens, B., Plante, B., Seigneur, N., & Jamieson, H. (2020). Mine waste rock: Insights for sustainable hydrogeochemical management. *Minerals, 10(9)*, 728.
- Wong, J. (1979). An electrochemical model of the induced-polarization phenomenon in disseminated sulfide ores. *Geophysics, 44(7)*, 1245-1265.
- Zonge, K. L., Sauck, W. A., & Sumner, J. S. (1972). Comparison of time, frequency, and phase measurements in induced polarization. *Geophysical Prospecting, 20(3)*, 626-648.

## CHAPTER 3 - GEOELECTRICAL SIGNATURES OF ACID-GENERATING MINE WASTE ROCK

### 3.1 INTRODUCTION

Mining activities produce significant amounts of waste rock that are stockpiled on the ground surface and known as waste rock piles (WRPs). Sulfidic minerals such as pyrite and pyrrhotite can reside within the WRP and interact with meteoric water and atmospheric oxygen to produce a highly toxic acidic leachate. This leachate, known as acid mine drainage (AMD), is characterized by low pH, and elevated concentrations of sulfate and dissolved metals (Amos et al., 2014). AMD can then enter the surrounding environment through water runoff over the exposed waste rock surface and/or seepage from the base or toe of the WRP. This can then adversely impact groundwater and surface water quality, vegetation, aquatic species, and ecological stability (Gray, 1996).

To mitigate the negative environmental impacts of AMD, it is important to conduct site-specific characterization, implement strategies to rehabilitate the area, and to carry out long-term monitoring of the WRP (Bao et al., 2022). Several remedial strategies have been deployed to prevent and/or control the generation and release of AMD at WRPs, including the implementation of engineered cover systems to isolate the waste material (e.g., Hersey & Power 2023; Ramasamy & Power, 2019; Power et al., 2017; O’Kane et al., 1998), and constructed wetlands for the passive treatment of discharged AMD (e.g., Pat-Espadas et al., 2018; Howard et al., 1989). Knowledge on the geochemical characteristics and behavior within the waste rock is highly desirable to design and/or implement these remediation programs at WRP sites (MEND, 2004; MEND, 2012; Gusek & Wildeman, 1997; USEPA, 1983). In addition, WRP geochemistry is also critical for the development of solute transport models (e.g., Ramasamy & Power, 2019), and the estimation of the life span of the contamination of the WRP (e.g., Power et al., 2017).

Traditional approaches to assess the geochemical behavior of waste rock within WRPs include the geochemical sampling/analysis of waste rock from coring (e.g., Bao et al., 2020; Skierszkan et al., 2016; Hendry et al., 2015) and porewater from monitoring wells (e.g., Ramasamy & Power 2019; Power et al., 2017; Srasek et al., 2004). The characteristics from extracted waste rock samples can be determined via a range of static and kinetic laboratory tests, including particle size analysis (e.g., Marousek et al., 2023; Shahhosselnl et al., 2020; Azam et al., 2009), x-ray diffraction (XRD) (e.g., Guseva et al., 2021; Hakkou et al., 2009; Frostad et al., 2002), acid base accounting (ABA) (e.g., Shahhosselnl et al., 2020; Kampouroglou et al., 2019; Namaghi & Li et al., 2016), column leaching (e.g., Abreu et al., 2014; Kossoff et al., 2011; Benzaazoua et al., 2004), and humidity cell tests (e.g., Davis et al., 2019; Abreu et al., 2014; Hakkou et al., 2008). Similarly, collected porewater can be analyzed for key AMD indicator parameters, including pH, electrical conductivity (EC), acidity, alkalinity, sulfate, and dissolved concentrations of heavy metals such as iron, manganese, and aluminum (e.g., Power et al., 2017; 2018).

Despite their widespread use, these traditional approaches can be costly and time-consuming to collect and then analyze the waste rock and/or porewater samples. Furthermore, these approaches provide only sparsely distributed point information across the enormous volumes of waste rock at typical WRPs, leading to very low spatial and temporal resolution (Dimech et al., 2022). Geophysical techniques provide an attractive alternative as they are non-invasive and can provide *in situ* characterization of waste rock, while also being more cost-effective and providing rapid, continuous spatial and temporal information (Dimech et al., 2022). Direct current (DC) resistivity and induced polarization (IP) are now the most widely used geophysical techniques (Binley et al., 2015). DC measures the distribution of electrical resistivity within the subsurface, while IP can help to measure the charge storage properties of subsurface materials and give a better indication of mineralogy. DC and IP are being increasingly used for a range of geoenvironmental investigations, such as groundwater-surface water interactions (e.g., Robinson et al., 2022), saline intrusion (e.g., Aladejana et al., 2020;

Sutter & Ingham, 2016), contaminant migration and remediation (e.g., Almpanis et al., 2021), and permafrost monitoring (e.g., Tavakoli et al., 2021; Doetsch et al., 2015).

DC and IP have potential to characterize AMD leachate, which has high electrical conductivity, and mine waste rock, which typically comprises reactive mineralogy (Campbell & Fitterman, 2000). So far at field sites, the DC technique have been used to characterize the internal structure of WRPs (e.g., Fala et al., 2005), map shallow moisture distributions (e.g., Poisson et al., 2009), and monitor water infiltration in an experimental WRP (e.g., Dimech et al., 2019). IP in the time-domain (TDIP) has been used to a much lesser extent for mapping waste rock, being used in combination with DC to characterize the composition of WRPs (e.g., Power et al., 2018b; Power & Almpanis, 2022).

Studies on the temporal DC and IP responses on the generation and release of AMD within evolving waste rock are limited (e.g., no time-lapse monitoring of waste rock). The application of standalone DC to identify sulfide mineral oxidation zones that generate AMD in mine waste rock is challenging. IP can provide enhanced mapping due to its capability to also capture the intrinsic polarization property of the sulfide minerals (Placencia-Gomez et al., 2015). Spectral IP (SIP), which is employed in the frequency-domain, measures real conductivity and imaginary conductivity to map pore fluid conductivity and capacitive properties in a porous medium, respectively. As a result, SIP method has the potential to monitor both geochemical and mineralogical changes occurring during AMD release and generation (Commer et al, 2001). Sulfide minerals residing within the waste rock can give unique phase spectra (Wong, 1979; Mahan et al., 1986). A handful of studies have investigated SIP detection of sulfide minerals in waste rock (Campbell & Horton, 2001); Placencia-Gomez et al. (2013) assessed the SIP response of oxidizing imitated sulfide-containing samples. They have discovered the phase spectra of the sulfide minerals decrease depending on their degree of oxidation and this conclusion was further validated by the modified Wong's 1979 electrochemical model (Placencia-Gomez & Slater, 2014). However, the sample they have used is imitated with

known/large concentrations of sulfides (e.g., 8% wt). Later in the years, Placencia-Gomez et al, (2015) further discovered that the SIP method could be used to detect oxidation-related textural properties of actual mine tailings under saturation conditions, and the chemical composition of pore water can have significant impact on the SIP response samples containing sulfide minerals (Placencia-Gomez & Slater, 2016).

There is currently no study that tracks the SIP response of waste rock samples as they undergo standardized kinetic test procedures, including the generation of AMD leachate and the oxidation of sulfide minerals. Additionally, no studies have compared the time-lapsed SIP response of real site samples with different sulfide concentrations. While previous studies have demonstrated the capability of the SIP method to be used as a tool for detecting sulfide minerals and sulfide mineral oxidation, it is unclear whether if this method is suitable for the tracking the time-lapse characteristic change of actual mine waste rock samples. These gaps are significant for the purpose of comparing data in future studies. Standard methods for AMD generation should be followed, and the SIP method of testing waste rocks should be applied to real site samples.

The objective of this study is to assess the potential of SIP to track the changes associated with acidity generation and release over time in mine waste rock. To fulfill this objective, comprehensive experiments were performed on real waste rock samples extracted from three mine waste rock piles in the Sydney coal field in Nova Scotia, Canada. These samples were first characterized by the x-ray diffraction test method (mineralogy), as well as the modified ABA test method (acid generation characteristics). The AMD experiments were then completed following standardized tests, with both leaching columns and humidity cells, with simultaneous measurements of geochemistry and SIP during these experiments. The measured SIP responses of the waste rock samples were examined to demonstrate its capability in observing the waste rock characteristics change undergoing water influx as well as minor and intense oxidation.

## 3.2 MATERIALS AND METHODS

### 3.2.1 Waste Rock Samples

The mine waste rock samples examined in this study were extracted from mine WRP sites located within the Sydney Coalfield in Nova Scotia, Canada. The coalfield is the oldest in North America, with underground mining occurring from the early 1700s to the early 2000s (Merritt & Power, 2022). In addition to producing ~500 million tonnes of coal, mining activities left behind enormous volumes of coal mine waste, including large WRPs at the former mining sites at Lingan, Summit, and Victoria Junction (see Figure 3.1). The Lingan WRP contains 380,000 m<sup>3</sup> of waste rock from the adjacent Lingan and Phalen collieries stockpiled to a height of ~15 m and a footprint of 82,000 m<sup>2</sup>. The Summit WRP received 1.5 million m<sup>3</sup> of waste rock from nearby collieries between 1911 and 1973 which was spread over 370,000 m<sup>2</sup>. The Victoria Junction WRP is located at the site of a closed coal preparation plant that produced metallurgical and thermal grade coal, with the WRP containing 5.9 million m<sup>3</sup> stretching over 280,000 m<sup>2</sup>.

The mine site closure and reclamation program at each site involved the placement of engineered cover systems over each WRP (e.g., Ramasamy et al., 2018; Hersey & Power, 2023). To allow geochemical sampling for post-reclamation performance monitoring, four monitoring wells were installed at each WRP. During borehole drilling for the wells at Lingan (February 8-13, 2011), Summit (February 16-22, 2011), and Victoria Junction (February 24-March 7, 2011), waste rock and soil samples were collected at 0.5 m depth intervals from auger flight and split spoon samplers. The drilling depths at the Lingan, Summit, and Victoria Junction ranged from 13.7-19.7 m, 10.5-19.8 m, and 21.5-36.4 m. All collected samples were interpreted for material type and measured for paste pH and electrical conductivity (EC). Two waste rock samples from each borehole were analyzed for acid base accounting (ABA) to assess their acid-generating potential (e.g., Power et al., 2017; 2018). The samples were then

sealed and stored in 5-gallon pails.

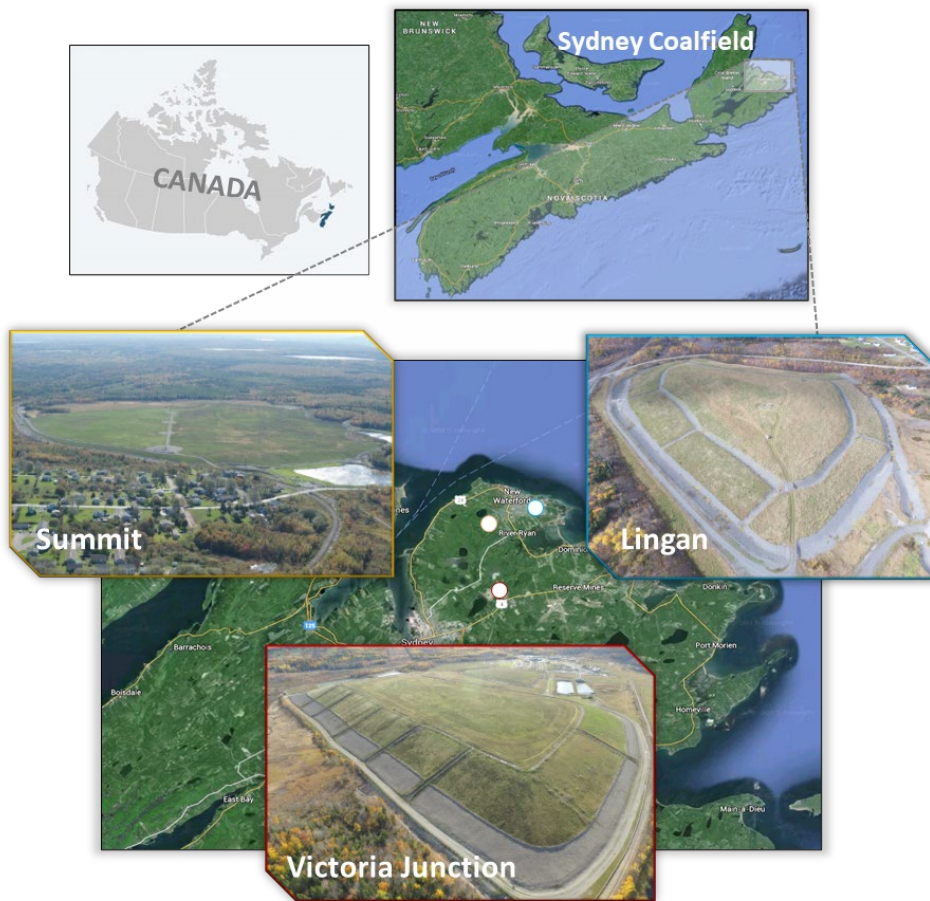


**Figure 3.** Site map of the Sydney Coalfield and the location of Lingan, Summit, and Victoria Junction

### 3.2.2 Waste Rock Characterization

#### 3.2.2.1 *Sample preparation*

The characteristics of the waste rock measured from the 2011 drillings and ABA tests were used to select the most representative samples for this study. The samples with the highest EC and/or acid-generation potential were expected to provide optimal initial conditions for the proposed column leaching and kinetic experiments, i.e., higher acidity provides longer acidity depletion times. Two bulk samples with similar characteristics were selected from each of the four boreholes at the Lingan, Summit, and Victoria Junction WRPs. The samples were taken

from the pails, spread out on aluminum trays and weighed. The samples were then oven-dried under 40°C to prevent any physical and/or chemical changes in their mineral species (ASTM D5744-96). The samples were measured daily throughout the drying process until constant weight was reached, indicating that all sample moisture had evaporated. Details on the various samples and weights measured during drying are provided in Appendix D.

Any cohesive chunks of waste rock within the oven-dried samples were first broken up and reduced to the appropriate size for testing, following the procedure of AASHTO (2014). The selected samples from each WRP were then well-mixed and quartered into different fractions to produce a composite sample to represent each site (AASHTO, 2014). To satisfy the requirements of the columns and humidity cells that will be used in this study, all particles within each composite sample should pass the 6.3 mm screen (ASTM D5744-96). This also ensures that at least six particles can be placed side-by-side across the proposed internal diameter of the columns/cells to ensure sufficient pore structures (MEND, 2008). In any case, the largest aggregates within the waste rock samples were manually crushed down to <4.75 mm diameter (ASTM, 1996). At the opposite end of the size range, sample particles <0.075 mm (i.e., passing No. 200 sieve) were discarded to ensure sufficient permeability for water flow through the columns and humidity cells. A summary of all characterization tests performed on the waste rock samples is shown in Table 3.1.

**Table 3.1** Summary of all characterization tests performed on the waste rock samples

Site	Sample	Tests
Lingan	Initial	PSD, Modified ABA, Mineralogy
	Post-column	Modified ABA
	Post-cell	Modified ABA
Summit	Initial	PSD, Modified ABA, Mineralogy
	Post-column	Modified ABA
	Post-cell	Modified ABA
Victoria Junction	Initial	PSD, Modified ABA, Mineralogy
	Post-column	Modified ABA

### *3.2.2.2 Particle size distribution*

A dry sieve analysis was performed on each composite sample to determine the particle size distribution (PSD) (ASTM C136-06). Wet sieving was not considered to prevent any premature acid leaching and dissolution of sulfide minerals. Sieve No. 4, 8, 10, 20, 40, 80, 100, 140, and 200 were used to provide a range in particle sizes between 0.075 mm to 4.75 mm. Each sample was put into the top of the stacked sieves and then placed in a motorized sieve shaker for 50 minutes to ensure sufficient shaking for representative PSD curves and limit the number of fine particles (<0.075 mm) retained in the sample.

### *3.2.2.2 Mineralogy*

The mineralogy within each of the three composite site samples was determined by X-ray diffraction (XRD) using the Rigaku SmartLab X-ray diffractometer at Surface Science Western. Samples (100 g) were selected to represent the mineralogical composition at each WRP. The elemental composition of the samples (e.g., carbon, sodium, magnesium, iron) was also measured using scanning electron microscopy with energy X-ray spectroscopy (SEM/EDX) using the Hitachi SU8230 Regulus Ultra High-Resolution Field Emission SEM and Bruker X-Flash FQ5060 Annular Quad EDX detector. The SEM/EDX data was used to assist the interpretation of the XRD results.

### *3.2.2.3 Acid base accounting*

ABA was performed using the Modified Sobek method (MEND, 2008) to determine a range of parameters such as total sulfur, sulfide-sulfur, sulfate-sulfur, paste pH, fizz rating, acid generation potential (AGP), acid neutralization potential (ANP), net neutralization potential (NNP), and neutralization potential ratio (NPR). This method determines the sulfide sulfur and sulfate sulfur content by measuring the amount of nitric acid-extractable sulfur and the amount of hot water-extractable and hydrochloric acid-extractable sulfur. ABA was performed on initial samples to estimate the ‘starting’ acidity in the waste rock, and then on the post-column

and post-humidity cell samples to estimate the amount of acidity ‘flushed’ out.

A number of approaches have been used to interpret ABA results to determine whether a sample is acid or non-acid generating (MEND, 2008), including the use of a single ABA parameter (e.g., NNP by Lapakko, 1993) or two or more ABA parameters (e.g., paste pH and NNP by Namaghi & Li, 2016). In this study, the samples were characterized via paste pH and NNP to categorize the waste rock as: (1) potentially acid generating, (2) non-acid generating, and (3) uncertain (e.g., USEPA, 1994; Usher et al., 2003; Foli et al., 2011). If the waste rock is categorized as uncertain, it can be either acidic or non-acidic, with uncertainties existing since static ABA tests do not consider the effect of pyrite oxidation, carbonate material dissolution, and their relative reaction rate of occurrence on the quality of the discharged drainage (Bradham & Caruccio, 1997).

### 3.2.3 SIP monitoring of waste rock kinetics

Two different kinetic experiments were performed on the waste rock samples to comprehensively test the evolving SIP response of mine waste rock: (i) column leaching tests, (ii) humidity cell tests.

#### 3.2.3.1 *Column leaching test*

##### 1) Column preparation

Column leaching tests were conducted with water circulated through 1D columns with simultaneous tracking by SIP. As only water was ever introduced into the column, only minor oxidation of any sulfidic minerals in the samples was expected via the dissolved oxygen content in water. The columns were designed to correctly fuse together column leaching with SIP measurements, with an illustration of the column tests shown in Figure 3.2. The columns were constructed from transparent polyvinyl chloride (PVC) pipe with an internal diameter of 4.08 cm and length of 24 cm, which is similar in size to columns used in previous leaching

(e.g., Al-Abed et al., 2008; Erguler & Erguler, 2015) and SIP (e.g., Placencia-Gomez et al., 2013; Ntarlagiannis et al., 2005) experiments. The end caps were made from PVC flanges that fitted over the ends of the column and sealed to PVC solid caps with a rubber gasket and stainless-steel bolts. The circular rubber gasket was hollow at its center, which provided a small chamber for inflow/outflow reservoirs. A 1/16" diameter soft plastic tubing was screwed into threaded holes at the center of each end cap to provide inflow/outflow ports for the column.

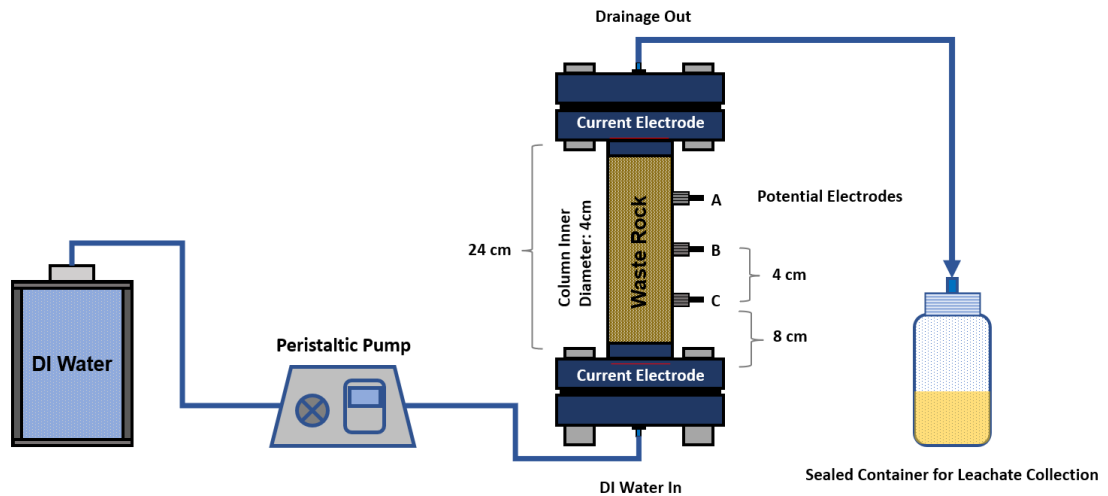


**Figure 3.1** Schematic of the apparatus for the column leaching experiment

A current electrode was added within the reservoir of each end cap of the column. It consisted of stainless-steel wire that was manipulated into a spiral shape to maximize the amount of contact area between the electrode and sample material. The potential electrodes were constructed from silver-silver chloride (Ag-AgCl) wire, which was pure silver wire coated with a thin layer of silver chloride, attached to 1/8" diameter Idex® flangeless standard knurl male nuts. Three potential electrodes were inserted into the sidewall of the column with a spacing of 4 cm, which provided two potential pairs for two sets of SIP measurements (i.e., A-B, B-C) that would provide confidence on the uniformity and repeatability within the sample. The top and bottom potential electrodes (i.e., A and C) were 8 cm from the respective current electrodes at the end caps (see Figure 3.2).

The columns were first packed with the sample material from each respective WRP. Dry packing was performed in 2 cm lifts, with frequent vibrating of the column to ensure maximum compaction of the grain particles. A screen made of 20-micron nylon filter mesh glued to a perforated high-density polyethylene (HDPE) disk was attached to both ends of each column to retain all particles. After packing was completed, the porosity of the Lingan, Summit, and Victoria Junction samples was measured to be 0.32, 0.29, and 0.35, respectively, with corresponding sample pore volumes (PVs) of 100.6 mL, 90.5 mL, and 110.2 mL.

## 2) Spectral induced polarization

The Portable SIP (PSIP) system (Ontash & Ermac, USA) was used in this study to measure the complex conductivity  $\sigma^*$  in terms of magnitude  $|\sigma|$  and phase shift  $\varphi$  at a frequency range from 0.1 Hz to 1,000 Hz, with 31 data points (i.e., timesteps). The system was provided with specific instructions regarding the frequency range and the number of datapoints to be plotted. The specific frequency range selected was intended to capture the response of the sulfide minerals, as observed in previous studies (Placencia-Gomez et al., 2013; Parker et al., 2013). The complex conductivity measurements can also be expressed in terms of real ( $\sigma'$ ) and imaginary ( $\sigma''$ ) conductivity ( $\sigma^* = |\sigma|e^{i\varphi} = \sigma' + i\sigma''$ ), where the real conductivity describes the electrical energy loss due to ohmic conduction current (electrolytic and surface conduction) and the imaginary component describes electrical energy storage controlled by the physical properties of the porous medium (polarization) (Binley & Slater, 2020). The phase shift defines the ratio of the polarization of the conduction ( $\varphi = \tan^{-1} \sigma''/\sigma'$ ).

The PSIP measurements ports were connected to all respective current and potential electrodes via cables and crocodile clips. Frequencies greater than 1,000 Hz were not measured as high errors can exist in four-electrode laboratory SIP measurements that are affected by additional polarization mechanisms at high frequencies, and intensive data correction approaches are required (Lesmes, 1993). Furthermore,  $<0.1$  Hz frequencies were not recorded due to their long measurement times. Using the selected frequency range (0.1-1000 Hz), the SIP measurement

time was approximately three hours.

### 3) Measurement sequence

The inflow port at the bottom end cap was connected to a Masterflex® L/S® high-pressure peristaltic pump (Cole-Parmer, Canada) via PTFE tubing (2.06 mm inner diameter). After preliminary testing, the flow rate was set at 1 PV/day, which corresponds to 0.07 mL/min, 0.06 mL/min, and 0.08 mL/min for the Lingan, Summit, and Victoria Junction samples, respectively. Deionized (DI) water, with a dissolved oxygen (DO) content of 8 mg/L and EC of 5  $\mu$ S/cm, was pumped through the bottom of each column until the inflow rate was equal to the outflow rate, thus indicating full water saturation of the sample.

With the pump switched off, the first set of SIP measurements were recorded. The pump was then restarted to inject the second PV of influent water (PV-2<sub>inf</sub>) into the column over one day, slowly displacing PV-1<sub>inf</sub>, which was pushed out through the outflow port at the top of the column and into a sealed glass beaker via the PTFE tubing (see Figure 3.2). This effluent leachate (i.e., PV-1<sub>eff</sub>) was then collected and filtered with a 0.45  $\mu$ m filter for subsequent geochemical analysis. It should be noted that this PV-1<sub>eff</sub> corresponds to the first set of SIP measurements. This cyclic process was repeated until the geochemical characteristics of the effluent stopped changing, indicating that all available acidity was flushed from the sample material in each column.

The effluent PVs in each beaker throughout the experiment were measured for EC and pH using the Hach HQ Series portable meter (Hach, Canada) which was calibrated daily prior to each measurement. The modified acidity, which is commonly used to represent AMD leachate (e.g., Power et al., 2017; Merritt & Power, 2022), was measured using the hot plate peroxide method (Miner, 2006), while dissolved sulfate concentrations were measured using a high-performance liquid chromatography (HPLC) system with a Waters 717plus Autosampler. An inductively coupled plasma mass spectrometry (ICP-MS) system at Surface Science Western

was used to measure the dissolved concentrations of six metals: iron (Fe), manganese (Mn), aluminum (Al), zinc (Zn), calcium (Ca), and magnesium (Mg). These metals are commonly selected to assess AMD leachate (e.g., Power et al., 2017; 2018). A summary of the geochemical analysis performed on effluent leachate throughout the column experiments is shown in Table 3.2.

### 3.2.3.2 Humidity cell test

#### 1) Column preparation

Humidity cell tests were conducted to assess the SIP signature as the same waste rock undergoes oxidation via the cyclic injection of dry air, humid air, and water. The humidity cell test is the most widely used testing procedure, and modern laboratories have adopted the ASTM D5744-96 method as a standardized measure. Depending on the amount of reactive sulfidic minerals in the waste material, the oxidation process should result in acidity generation, and convert any potential acidity into stored acidity, which is then flushed out by water flow. The Lingan and Summit waste samples were used in these experiments, as an insufficient volume of Victoria Junction material was available.

**Table 3.2** Summary of kinetic tests performed on waste rock samples

Site	Test	Duration (days)	PVs	Geochemical Parameters
Lingan	Column leaching	86	86	EC, pH, sulfate, acidity, metals <sup>1</sup>
	Humidity cell	84	12	EC, pH, sulfate, metals
Summit	Column leaching	86	86	EC, pH, sulfate, metals
	Humidity cell	84	12	EC, pH, sulfate, metals
Victoria Junction	Column leaching	86	86	EC, pH, sulfate, acidity, metals

<sup>1</sup>Dissolved concentrations of iron, manganese, aluminum, zinc, calcium, magnesium

The columns were designed and constructed in the same way as those for the column leaching experiments; however, these columns had a larger inner diameter (4.9 cm) and a shorter length (20 cm) to permit the easier flow of dry air and humid air through the waste material (Hakkou et al., 2008). It should be noted that due to SIP constraints (i.e., typical SIP cell diameters are <5 cm), the humidity cell diameter in this study was smaller compared to the suggested 10 cm diameter cells for coarse materials (ASTM D5744-96). For these cells, only two potential electrodes were placed along the sidewall of the column to allow a single set of SIP measurements within the column. A potential electrode spacing of 4 cm was again used, with 8 cm distance to the current electrodes. The end caps were also constructed the same, but with a larger diameter. Figure 3.3 illustrates the columns used in the humidity cell experiments.

The sample columns were again dry packed with the waste material in 2 cm lifts, with 20-micron filter mesh screens at each end cap to ensure all particles remained in the columns. The Lingan and Summit columns were packed with 486.6 g and 517.6 g of waste material, respectively. The porosity of the Lingan and Summit samples was 0.32 and 0.29, respectively, with corresponding sample PVs of 120.7 mL and 94.3 mL.

## 2) Measurement sequence

The humidity cell experiments followed the following seven-day injection cycle: (1) three days of dry water, (2) three days of humid air, and (3) one day of water, which was then repeated over 12 weeks. Prior to the start of this cycle, the dry-packed samples were saturated with DI water being injected through the bottom of the columns with an approximate flow rate of 0.3 mL/min until full saturation. The saturated columns are then left to stabilize with SIP measurements collected one day later. Following this initial saturation, SIP measurements were recorded across the 0.1 Hz to 1,000 Hz frequency range (Figure 3.3a).

The water inflow tube at the bottom of each column was disconnected and replaced with tubing connected to an air chamber for dry air injection. This dry air slowly pushed porewater out of

the column and into a sealed graduated cylinder, as illustrated in Figure 3.3b. The optimal air flow was tested to maximize the volume of porewater displaced, while also preventing excessive pressures within the column that could cause cracking in the sample material and/or push off the end caps. The dry air injection was continuous for three days and the total volume of displaced porewater (i.e., effluent leachate) was measured (i.e.,  $PV-1_{\text{eff}}$ ). It should be noted that the effluent volume was much less than the sample PV, with the injected air unable to displace most of the porewater. The average effluent volume for Lingan and Summit was 40.1 mL and 38.6 mL, respectively, meaning the average water saturation remaining in the Lingan and Summit column was 67% (80.6/120.7 mL) and 59% (55.7/94.3 mL). The effluent leachate was then analyzed for EC, pH, dissolved sulfate, and dissolved metals. The modified acidity was not measured due to the insufficient volume of effluent during each cycle.

After three days of dry air (Figure 3.3c), the columns were then connected to a humidifier for the injection of humid air over three days, as shown in Figure 3.3d. The humidifier was designed and constructed following procedures outlined in ASTM D5744-96, with more details provided in Appendix A. The humid air introduces both oxygen and moisture into the samples to encourage the oxidation of any reactive minerals. After three days of humid air injection, the columns were reconnected to the water inflow tubing to re-saturate the sample with DI water (see Figure 3.3a), before the next of SIP measurements were recorded. This seven-day cycle was repeated for 12 PVs of water, with a total experimental duration of 12 weeks.

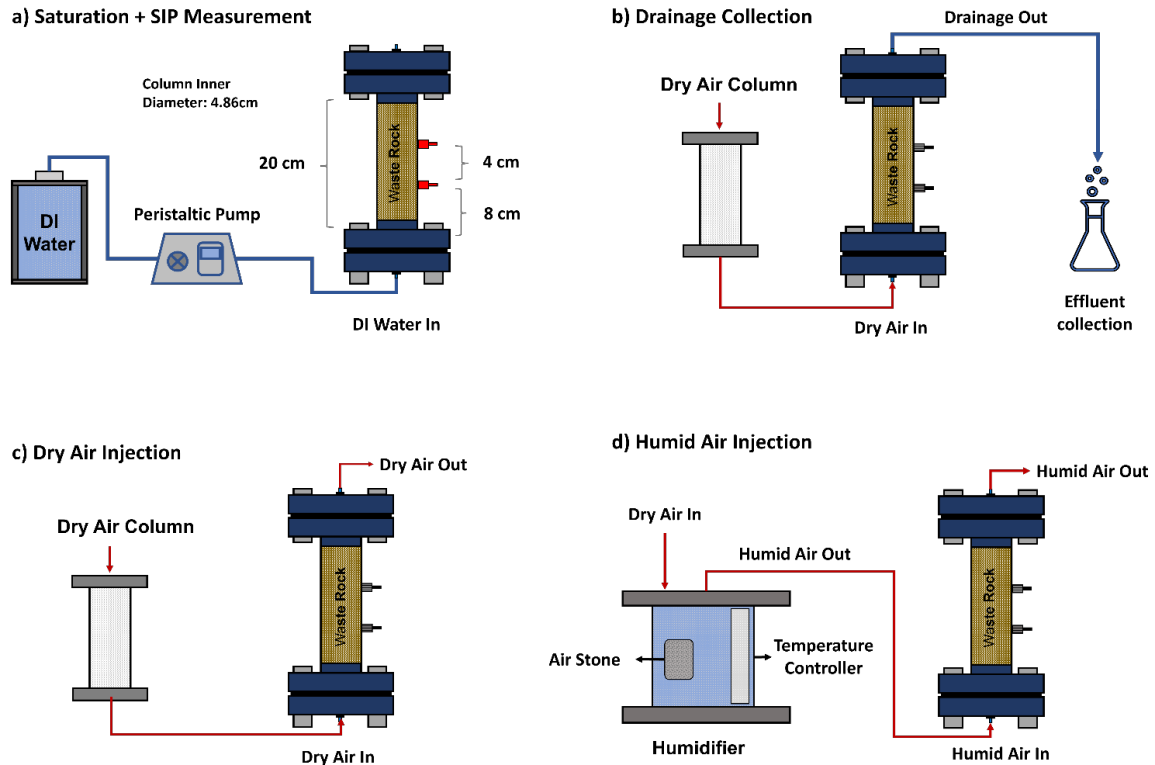


**Figure 3.2** Illustration of the apparatus for the humidity cell during each stage of the experiment: (a) saturation and SIP measurement, (b) air displacement of porewater and effluent collection, (c) three days of dry air, and (d) three days of humid air.

### 3.3 RESULTS AND DISCUSSIONS

#### 3.3.1 Mine Waste Characterization

##### 3.3.1.1 Particle size distribution

The PSD curves for the prepared Lingan, Summit, and Victoria Junction waste rock samples are shown in Figure 3.4. Due to the lower and upper limits of the sieve sizes that were intentionally used (0.075-4.75 mm), all particle sizes within each sample resembled sand sizes. The mean grain size (i.e.,  $d_{50}$ ) of the Lingan and Summit samples is 0.58 mm and 0.71 mm, respectively, matching medium sand, while the mean grain size of Victoria Junction is 0.33 mm and matches fine sand.

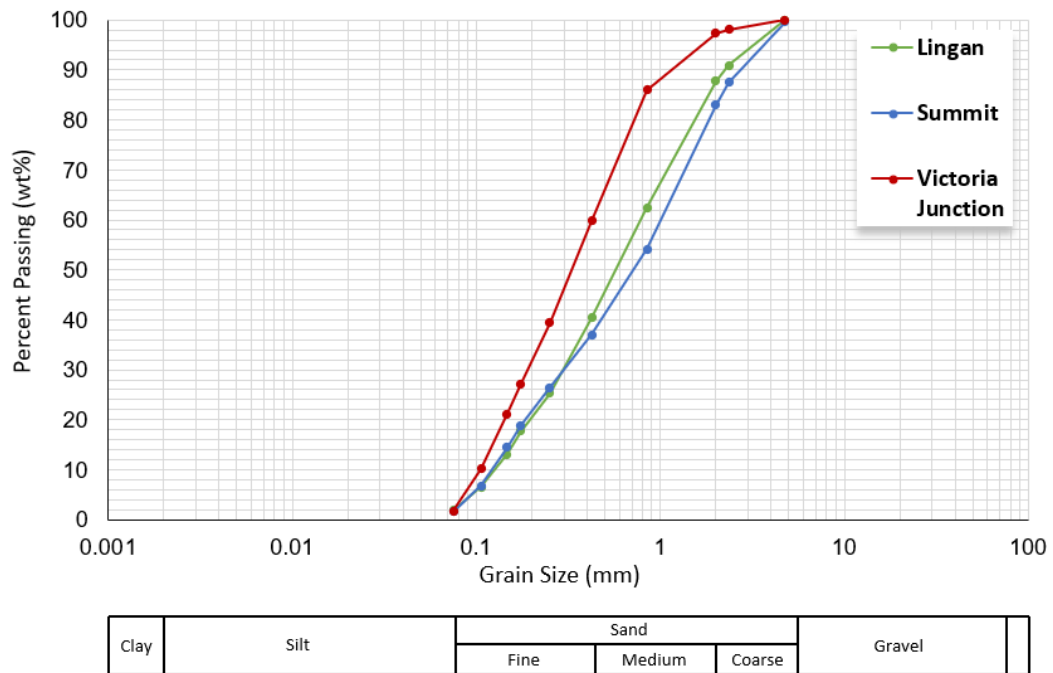


**Figure 3.3** Particle size distribution curve for each of the prepared waste rock samples.

The uniformity coefficient ( $C_u$ ) of the Ligan, Summit, and Victoria Junction samples were 6.3, 8.3, 4.0, respectively, with respective curvature coefficients ( $C_c$ ) of 0.9, 0.7, 0.8. A sample is considered uniform if its  $C_u$  value is less than 4 and poorly graded if its  $C_c$  value lies outside the 1 and 4 range (Shahhosselnl et al., 2020). The Ligan and Summit samples were considered nonuniform but poorly graded, while the Victoria Junction sample was uniform and poorly graded. Therefore, these samples were feasible for the column and humidity cell experiments since the effluent samples and SIP measurements are being used to represent the entire column/cell. More details on the sample particle sizes are shown in Appendix D.

### 3.3.1.2 Mineralogy

The minerals in the waste material can be divided into the following groups: (i) primary sulfide minerals such as pyrite, and pyrrhotite, (ii) primary non-sulfide minerals (i.e., carbonate minerals) such as calcite and dolomite, (iii) secondary minerals (i.e., sulfide oxidation product) such as jarosite and goethite, and (iv) undesirable gangue minerals such as quartz and

muscovite (e.g., Hudson-Edwards et al., 2011; Shahhosseini et al., 2020). Table 3.3 presents the identifiable mineral composition of the Lingan, Summit and Victoria Junction samples following interpretation of the XRD results. The Victoria Junction sample contains the secondary mineral jarosite, indicating the potential occurrence of sulfide oxidation before the onset of the kinetic experiments. In contrast, the Lingan sample contains carbonate mineral calcite, which is an AMD neutralizing agent. Quartz, muscovite, kaolinite, and clinocllore were the identifiable silicate gangues associated with the waste rock samples.

**Table 3.3** Mineralogy of the Lingan, Summit and Victoria Junction samples based on XRD results

<b>Mineral</b>	<b>Lingan</b>	<b>Summit</b>	<b>Victoria Junction</b>
Primary mineral	-	-	-
Secondary mineral	-	-	Jarosite
Carbonate mineral	Calcite	-	-
Gangue mineral	Quartz, Muscovite, Kaolinite	Quartz, Muscovite	Quartz, Clinocllore
Amorphous	No	Yes	Yes
Unknown phases	Yes	Yes	Yes

Amorphous phases were found in the Summit and Victoria Junction samples; these phases represent the materials that contain no crystalline diffraction peaks. Amorphous materials are commonly found in coal, glasses, polymers, as well as alloys (e.g., Ward & French, 2005; Zubrik et al., 2010). The XRD results also indicated that each sample contained unidentified phases that make up less than a few percent of the samples; these phases could represent the missing phases of sulfide minerals, such as pyrite and pyrrhotite, and other secondary minerals such as goethite, gibbsite, and gypsum. Detailed XRD analysis reports are attached to Appendix E.

### 3.3.1.3 Acid base accounting

The modified ABA results are shown in Table 3.4. The total sulfur content in each sample refers to their stored and potential acidities, which are important in determining the overall level of acidity of the samples. Sulfur in mine waste comes in two forms: (1) sulfide-sulfur (potential acidity), which is associated with sulfide minerals that correspond to a sample's AGP, and (2) sulfate-sulfur (stored acidity), which is the result of weathering and oxidation of the sulfide-sulfur (Jacob et al., 2013). The sulfide-sulfur content for the Lingan, Summit, and Victoria Junction samples were 0.59 wt%, 0.39 wt%, and 1.03 wt%, respectively, indicating that each sample contains some level of oxidizable sulfide minerals. However, it should be noted that these levels are relatively low compared to waste rock in other studies (e.g., 2.41 to 3.91 wt% of sulfide-sulfur in Hakkou et al., 2008). The sulfate-sulfur content was 0.40 wt%, 0.43 wt%, and 0.97 wt% for Lingan, Summit, and Victoria Junction, respectively, with the Victoria Junction sample containing the largest amount of releasable stored acidity. It should be noted that the measured sulfate-sulfur is assumed to be non acid-generating in modified ABA tests; therefore, the value of AGP of the samples can be underestimated if the sample did in fact contain acid-generating sulfate minerals (USEPA, 1994).

The positive ANP value of the Lingan sample (15.4 kg CaCO<sub>3</sub>/tonne) confirmed its capability to neutralize acidity, with the XRD results indicating this neutralization potential was mainly the result of carbonate minerals such as calcite (Table 3.3). In contrast, the Summit and Victoria Junction samples exhibit negative ANP values, with -5.5 kg CaCO<sub>3</sub>/tonne and -11.1 kg CaCO<sub>3</sub>/tonne, respectively. All samples contained positive AGP, and all NNP values were negative.

**Table 3.4** Summary of acid base accounting test results for each pre- and post-experiment waste rock sample

	Lingan			Summit			Victoria Junction	
	Initial	Final Col	Final HC	Initial	Final Col	Final HC	Initial	Final Col
Paste pH	6.64	7.64	7.40	3.95	4.70	4.40	3.72	4.45
Total S	0.99	0.53	0.88	0.82	0.49	0.59	2.00	1.28
Sulfate S	0.40	0.02	0.34	0.43	0.07	0.20	0.97	0.29
Sulfide S	0.59	0.51	0.54	0.39	0.42	0.39	1.03	0.99
AGP	18.4	15.9	16.9	12.2	13.1	12.2	32.2	30.9
ANP	15.4	13.9	15.3	-5.50	-2.50	-1.20	-11.1	-3.00
NNP	-3.00	-2.00	-1.60	-17.7	-15.6	-13.4	-43.3	-33.9

Figure 3.5 plots paste pH versus NNP for each sample, with Summit and Victoria Junction classified as ‘potentially acid-generating’, and Lingan classified as ‘uncertain’ and can be either acidic or neutral (Namaghi & Li, 2016). The kinetic test results will enhance the interpretation of the acid generation characteristics of Lingan, Summit, and Victoria Junction.

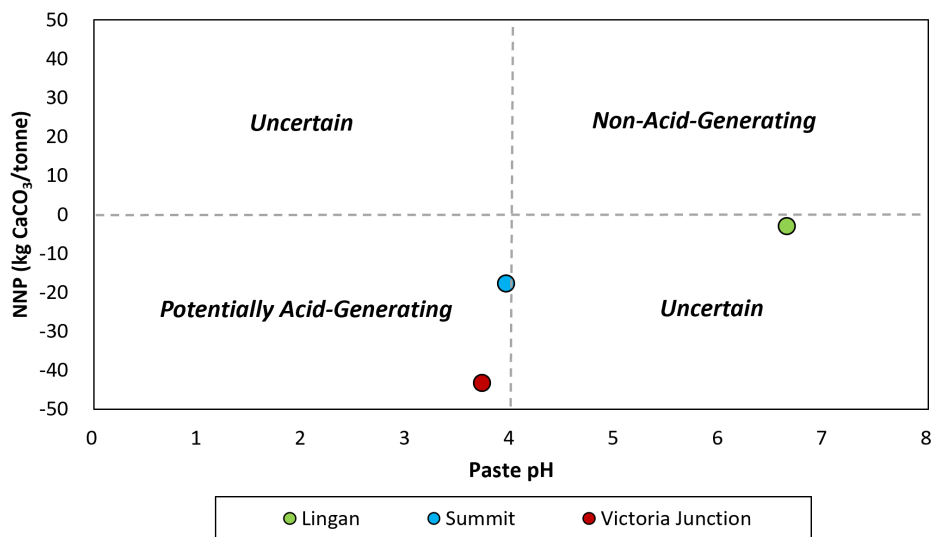


**Figure 3.4** Classification of waste rock samples in terms of NNP and paste pH

### 3.3.2 Kinetic Tests

#### 3.3.2.1 Column leaching test

The column leaching tests were conducted to observe the changes in waste rock and drainage characteristics over time during water flushing and minor oxidation. Figure 3.6 plots the modified acidity, sulfate, pH, and EC in the effluent leachate over the 86 days of the experiment (1 PV/day) for Lingan (green), Summit (blue), and Victoria Junction (red), while Figure 3.7 plots the dissolved concentrations of selected metals.

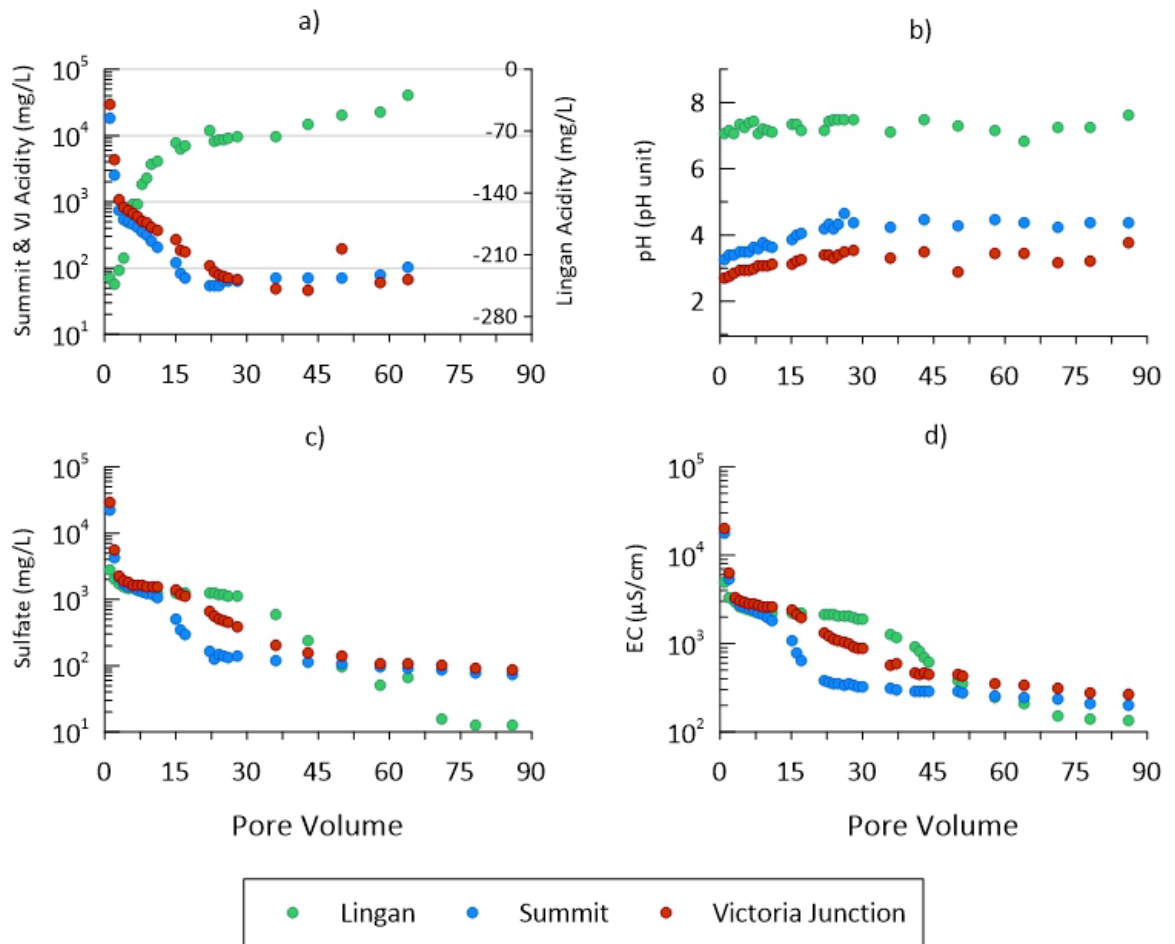


**Figure 3.5** Temporal evolution of (a) modified acidity, (b) pH, (c) sulfate, and (d) EC of effluent leachate during the duration of the column leaching experiments.

The modified acidity and pH of the first effluent leachate in the Lingan sample (PV-1) was -

236 mg/L and 7.08, respectively. The neutral pH and negative acidity (i.e., net alkaline) was likely due to the buffering effect of the carbonate minerals (calcite) that was previously identified by XRD analysis (Table 3.3). The carbonate minerals will consume acids to maintain pH at a neutral level. As the column is continuously flushed, the modified acidity rapidly increases to -84 mg/L at PV-15, followed by a slower but steady increase to -30 mg/L at PV-64 (note that it was not possible to measure acidity after PV-64). The pH also increases over time, to a final pH of 7.62 at PV-86. As more drainage is produced over time, the carbonate minerals are flushed from the column and the acidity increases.

The initial effluent leachate from the Summit and Victoria Junction samples were significantly higher in modified acidity (17,800 mg/L and 28,800 mg/L, respectively) and lower in pH (3.27 and 2.71, respectively). This is likely due to the dissolution of soluble weathering products produced by the oxidation of sulfide minerals prior to the experiments (i.e., within the WRP and during drilling/storage/preparation). Over time, the acidity greatly changes in Summit and Victoria Junction, with three different rates observed: (i) rapid initial decrease to 756 mg/L and 1,080 mg/L at PV-3, (ii) steady decrease to 55 mg/L and 80 mg/L at PV-24, and (iii) slight increase to 103 mg/L and 68 mg/L at PV-64. Similarly, pH increases steadily to 4.20 and 3.29 at PV-24 in Summit and Victoria Junction, respectively, with slight increases until a final pH of 4.36 and 3.78 at PV-86. The slight increases in acidity, and decreases in pH, at later times suggest the occurrence of minor sulfide oxidation and the generation of additional acidity, with similar behavior observed in other column leaching studies (Abreu et al., 2014; Hakkou et al., 2009).

As shown in Figures 3.6c, the evolution of sulfate was similar for all samples. The sulfate for the PV-1 effluent at Lingan was 2,778 mg/L, which is a lot more comparable to Summit (22,883 mg/L) and Victoria Junction (29,895 mg/L). At PV-3, the sulfate at Summit and Victoria Junction has rapidly decreased to 2,133 mg/L and 2,254 mg/L, respectively, and now relatively similar to the corresponding sulfate at Lingan (1,726 mg/L). The sulfate is relatively similar in

each sample, with only a slight decrease until PV-8, before each sample exhibited significantly different behavior and values before converging again at PV-50. While Victoria Junction steadily decreased until PV-50, Summit rapidly decreased after PV-8 before slowing at PV-20 and only slightly decreasing until PV-50. In contrast, Lingan only slightly decreased after PV-8 until PV-30, with a more delayed, rapid decrease then occurring until PV-50. This behavioral difference is likely due to differences in the mineralogy, elemental composition, and unique flow patterns within each sample. After PV-50, Lingan continued its steady decrease with a final sulfate value of 13 mg/L at PV-86, whereas Summit and Victoria Junction only slightly decreased until PV-86, with respective sulfate values of 73 mg/L and 86 mg/L.

Figure 3.6d indicates that EC followed the same trend as sulfate over time, with respective EC values for Lingan, Summit and Victoria Junction equal to 4,860  $\mu\text{S/cm}$ , 17,570  $\mu\text{S/cm}$ , and 19,830  $\mu\text{S/cm}$  at PV-1, 2,290  $\mu\text{S/cm}$ , 2,260  $\mu\text{S/cm}$ , and 2,690  $\mu\text{S/cm}$  at PV-8, and 133  $\mu\text{S/cm}$ , 202  $\mu\text{S/cm}$ , and 266  $\mu\text{S/cm}$  at PV-86. The similarity in sulfate and EC is further demonstrated in Appendix X where a relatively linear relationship occurs below 5,000  $\mu\text{S/cm}$ .

EC measurements can be used to represent the behavior of major elements (Abreu et al., 2014; Hakkou et al., 2009; Benzaazoua et al., 2004). Figure 3.7 shows the evolution of Fe, Mn, Al, Mg, Ca, and Zn concentrations at PVs of most interest, namely PV-1, PV-8, PV-24, PV-50, and PV-86. The concentration of these selected elements decreased to nearly 0 mg/L on day 50. The effluent from Lingan was high in Mg, and Ca. Summit drainage was high in Mg, Al, and Mn. The Victoria Junction effluent was high in Mg, Al, Ca, Mn, and Fe. Dissolution is likely to occur for all elements. This may involve the dissolution of ultrafine particles (Furrer & Stumm, 1986) and/or dissolution at high reactive surface sites on the mineral surface (Wehrli, 1989).

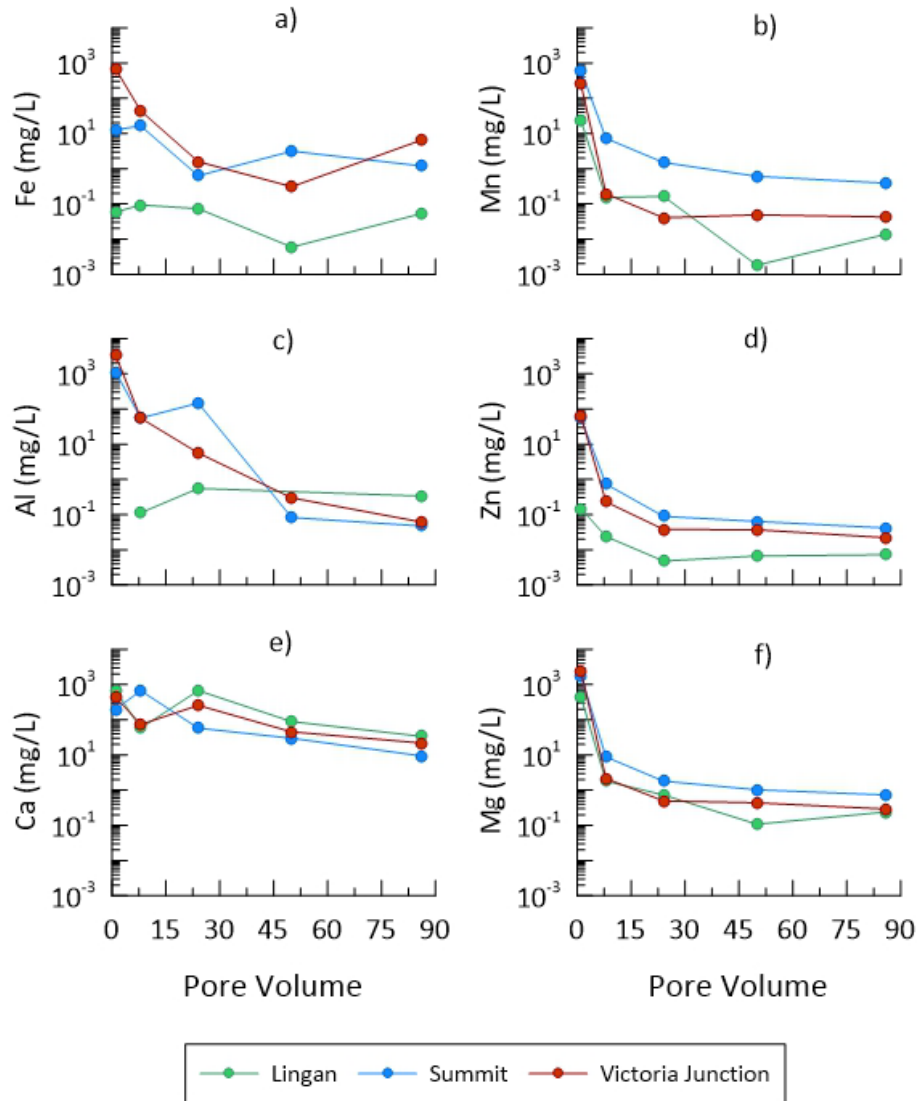


**Figure 3.6** Column leaching test selected dissolved metal evolution of a) Fe, b) Mn, c) Al, d) Zn, e) Ca, and f) Mg

### 3.3.2.2 Humidity cell test

In the humidity cell experiment, the waste rock samples were subject to higher oxidation. While this experiment had the same 86-day time duration as the column leaching experiment, PVs of effluent leachate were only collected at the end of each 7-day cycle for a total of 12 PVs. Therefore, while the leaching columns had one day of water flushing through fully saturated waste between each PV, the humidity cells had six days of air flow through partially saturated waste, and one day of water flushing through fully saturated waste between each PV.

Figure 3.8 plots the evolution of pH, sulfate, and EC measured in the effluent leachate collected over the 12 PVs. Note that the values were not normalized by either drainage volume or the weight of the materials. Figure 3.8a indicates that the initial pH in Lingan and Summit was 7.09 and 3.22, respectively, again indicating their respective neutrality and acidity. The pH in both samples then fluctuates with small increases and decreases over time. In Figure 3.8b, the sulfate of the PV-1 effluent is 2,683 mg/L and 36,323 mg/L at Lingan and Summit, respectively, before decreasing to 1,832 mg/L and 2,517 mg/L at PV-3, and then fluctuating with increases and decreases until PV-12. The EC of the effluents in Lingan and Summit follow the same trend as sulfate, as shown in Figure 3.8c, starting at 5,340  $\mu\text{S}/\text{cm}$  and 23,000  $\mu\text{S}/\text{cm}$ , respectively, and decreasing to 3,250  $\mu\text{S}/\text{cm}$  and 3,470  $\mu\text{S}/\text{cm}$  by PV-3.

Figure 3.8 also shows the corresponding evolution of pH, sulfate, and EC over the first 12 PVs in the column leaching experiment. As shown, the values for each parameter in Lingan were similar between the leaching columns and humidity cells; for example, the pH remained neutral throughout both experiments. In contrast, the acidic Summit showed some differences between the leaching columns and humidity cells. The pH did increase a little in the leaching columns between PV-1 and PV-11 (3.27 to 3.61) but remained relatively steady with only small fluctuations in the humidity cells (3.22 to 3.27). Similarly, sulfate was larger at every PV in the humidity cell than the leaching columns; for example, sulfate increased between PV-3 and PV-5 (2,517 mg/L to 2,751 mg/L) in the humidity cell but decreased from 2,133 mg/L to 1,547 mg/L in the leaching column.

While they are small, these differences possibly indicate the occurrence of more sulfide oxidation in the humidity cells for the Summit sample. The Lingan sample was neutral from the beginning so was not affected by any increases in oxidation between the columns and cells.

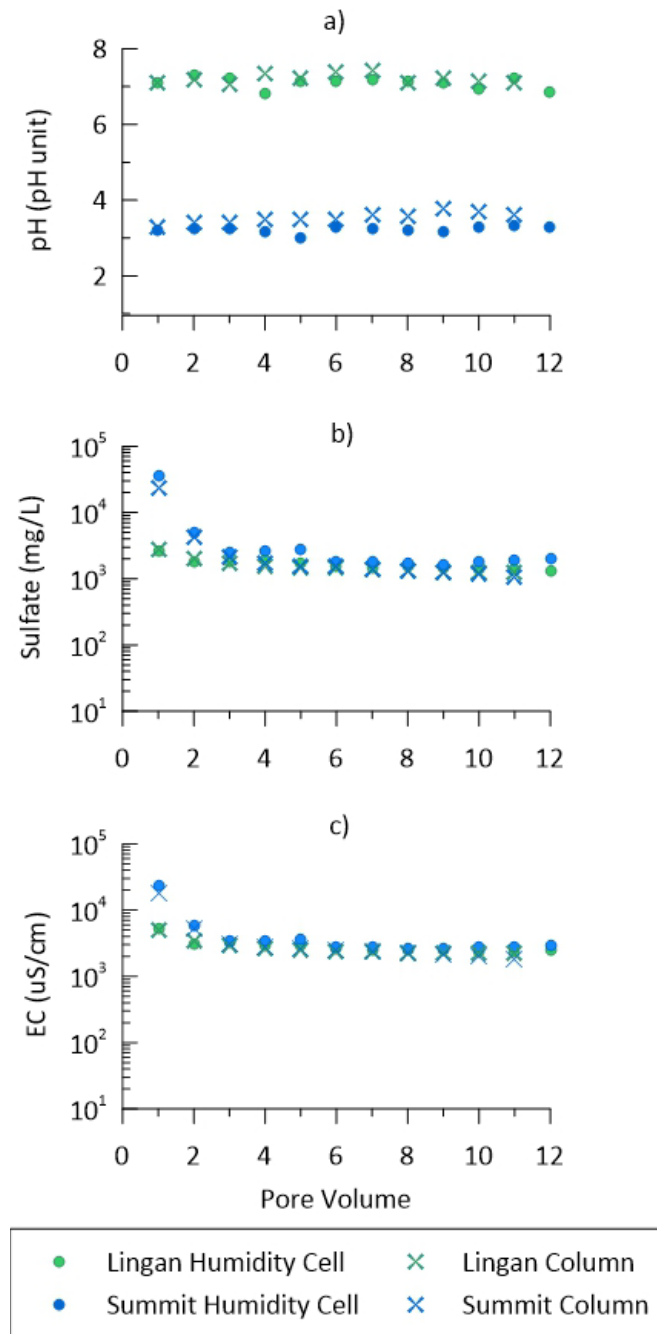


**Figure 3.7** Humidity cell test, temporal evolution of (a) pH, (b) sulfate, and (c) EC in the effluent

Figure 3.9 presents the evolution of dissolved concentrations of Fe, Mn, Al, Zn, Ca, and Mg at PV-1, PV-6, and PV-12. Lingan drainage was high in Ca and Mg, whereas the Summit drainage was high in Mn, Al, and Mg. Elements (except Ca) with high initial concentrations were depleted within the first six weeks of the experiment for both samples.

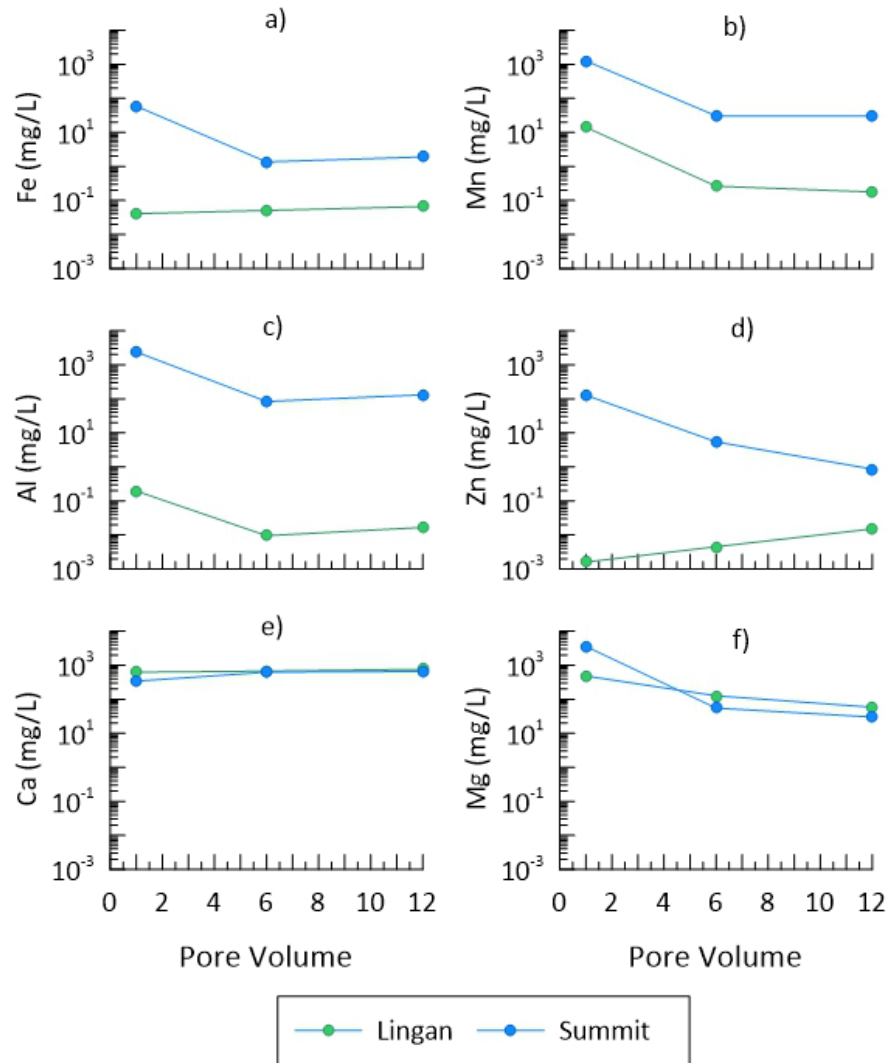


**Figure 3.8** Humidity cell test selected dissolved metal evolution of a) Fe, b) Mn, c) Al, d) Zn, e) Ca, and f) Mg

### 3.3.2.3 Acid generation characteristics of the waste rock samples

The characteristics related to the acid generation of the waste rock samples are summarized in Table 3.5, using the ABA results of the pre- and post-experiment samples (Table 3.4). The pre-experiment samples were classified based on their NNP and paste pH (Figure 3.5), while the post-experiment samples were based on their end pH (Prestia et al., 2015).

The initial Lingan sample had ‘uncertain’ acid generating potential and did not generate acid in both column leaching and humidity cell experiments (i.e., end pH > 5), suggesting the

sample was non-acidic (neutralized by carbonate minerals). However, since the Lingan effluent collected during both the leaching columns and humidity cells did contain elevated concentrations of sulfate, Mn, Al, and Mg (see Figure 3.7 and Figure 3.9), the Lingan sample generated neutral drainage (metal leaching) that can also be a potential threat to the environment (Plante et al., 2011).

In contrast, the Summit and Victoria Junction samples did generate acid in the leaching column and humidity cell experiments (note that only column leaching experiment was performed for Victoria Junction), which agrees with the ABA results prediction. As a result, the samples can be considered acid generating and the leachates collected from these samples can be treated as AMD with elevated acidity, sulfate, and dissolved metals (Figure 3.7 and Figure 3.9).

**Table 3.5** Waste rock acid generation characteristics classification

Site	ABA		Column Test		Humidity Cell Test	
	NNP	AP Defined	End pH	AP Defined	End pH	AP Defined
Lingan	-3.0	Uncertain	7.62	Non-Acid	6.86	Non-Acid
Summit	-17.7	Potentially Acid Gen	4.36	Acid	3.37	Acid
Victoria Junction	-43.3	Potentially Acid Gen	3.78	Acid	-	-

### 3.3.3 SIP Response of the Acid Generating Waste Rocks

#### 3.3.3.1 Real conductivity

Figure 3.10 presents the real conductivity of the SIP response from the (a) Lingan, (b) Summit, and (c) Victoria Junction waste rock samples during the column leaching experiment. The response from both potential pairs A-B (diamonds) and B-C (crosses) are shown for each sample, demonstrating relatively high repeatability of SIP measurements and sample

uniformity. A slight delay is observed in the conductivity decrease in each sample, particularly Lingan. Each potential pair measures the response within their own sensitivity area with B-C below A-B and closer to the water injection at the bottom of the column (see Figure 3.2). The measurements at B-C capture the conductivity decrease before A-B, suggesting that the water quality through the depth of the column was not completely uniform, which is a common assumption in 1D flow columns. The EC of the porewater is lowest at the bottom of the column where the fresh water initially entered the sample. As this water is continuously pushed through the pore spaces, its quality decreases (e.g., more metals are leached into the water with longer travel distance, which agrees with the metal leaching experiments by Liu et al. (2019), which corresponds to increasing EC with vertical distance through the column.

Looking at the real conductivity at A-B (diamonds) in Figure 3.10, the first PV was somewhat similar for Lingan (646  $\mu\text{S}/\text{cm}$ ) and Summit (973  $\mu\text{S}/\text{cm}$ ), but much higher for Victoria Junction (1569  $\mu\text{S}/\text{cm}$ ). This was the first interaction of the initially dry sample with injected water, with high dissolution of available minerals occurring. Each sample exhibits large decreases in real conductivity before PV-30, albeit at different rates and PVs. Summit has an early steep decline from 388  $\mu\text{S}/\text{cm}$  at PV-4 to 113  $\mu\text{S}/\text{cm}$  at PV-15, while Lingan has a late steep decline from 458  $\mu\text{S}/\text{cm}$  at PV-17 to 115  $\mu\text{S}/\text{cm}$  at PV-30. In contrast, Victoria Junction has a gradual uniform decline from 572  $\mu\text{S}/\text{cm}$  at PV-4 to 188  $\mu\text{S}/\text{cm}$  at PV-30. After PV-30, the real conductivity starts to plateau with small increases and decreases until the end of the experiments.

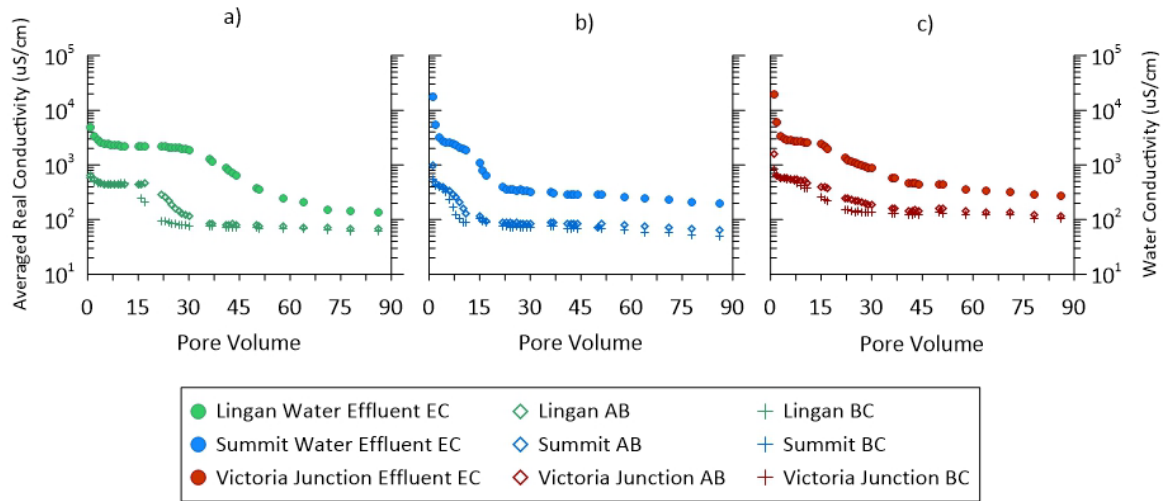


**Figure 3.9** Real conductivity for (a) Lingan, (b) Summit, and (c) Victoria Junction leaching columns. The EC of corresponding effluent (solid circles) is included on the secondary axes. Note that the real conductivity is shown from the A-B (diamonds) and B-C (plus sign) potential pairs.

The evolution of effluent water EC has also been added to Figure 3.10 for direct comparison with the SIP real conductivity. In terms of the evolving pattern during the experiment, a strong correlation is evident between the real conductivity and water EC. The difference in magnitude is based on comparing a fluid EC with a bulk material EC. The ‘water EC’ is based fully on the fluid (electrolytic conduction), whereas the real conductivity represents a ‘bulk EC’ based on the fluid and solid (electrolytic and surface conduction). As electrolytic conduction is typically the most dominant contribution, water EC (water content = 100%) will be significantly larger than bulk EC (water content  $\leq$  porosity) (Archie, 1942). Using Archie’s law (i.e., bulk EC = porosity x water EC) and their respective porosities, the real conductivity measured at Lingan, Summit, and Victoria Junction will be approximately 32%, 29%, and 35% of their corresponding effluent EC values. It should be noted that this assumes that surface conduction has negligible contribution to the real conductivity measurement, which may not always be the case for typical mine waste minerals.

Similar to the measurement differences at potential pairs A-B and B-C, any time (i.e., PV) lag between real conductivity and effluent EC may be associated with the non-uniformity in water

quality. Lingan and to a lesser degree, Summit, show some lag between the large changes in real conductivity and effluent EC, whereas Victoria Junction does not show any lag. Therefore, even though the experimental samples are relatively uniform and small in scale, measurements of effluent quality may be insufficient to understand the behavior of the waste material that is generating and releasing that effluent.

Figure 3.11 presents the evolving real conductivity of the Lingan and Summit samples that had more potential for oxidation in the humidity cells, though air saturations of only 33% and 41% were attained during the air injection cycles. The measured real conductivity decreases as the experiments proceed, similar to the drainage EC measured in Figure 3.8c, which is likely due to the depletion of measured sulfate and the dissolution of major elements. This again shows the potential of the real conductivity measured with the SIP method to monitor the water quality change within the pore spaces of the waste rock samples. The real conductivity in the humidity cells show changes similar to the leaching columns, which corresponds to the similarity between the geochemical characteristics of the porewater in the columns and cells (see Figure 3.8).

It is evident from the evolution of all samples in both the leaching columns and humidity cells that the real conductivity was highly effective in tracking the evolution of porewater quality within the waste material. The decrease in real conductivity is associated with the depletion of the sulfate and metals within the porewater, as shown in Figures 3.6 and 3.7.

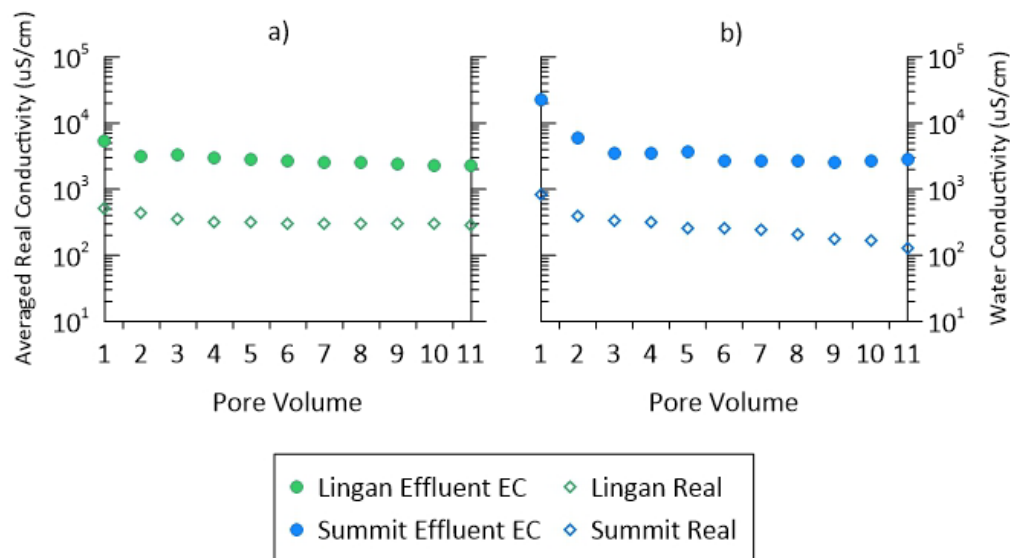


**Figure 3.10** Real conductivity (diamonds) for (a) Lingan, and (b) Summit humidity cells. The EC of corresponding effluent (circles) is included on the secondary axes.

### 3.3.3.2 Imaginary conductivity

While SIP responses were collected for all 86 PVs in the column leaching experiments, only a subset of PVs is presented. Figure 3.12 plots the imaginary conductivity and phase shift for PV-1, PV-8, PV-24, PV-44, and PV-86, which were selected as they showed the largest differences in the EC of the effluent leachate.

At each site, the imaginary conductivity generally displayed similar spectra which decreased with increasing PVs during the experiment, with values highest at Victoria Junction and lowest at Lingan. The imaginary conductivity increased with increasing frequency at PV-1 (red) of each site. Victoria Junction had higher imaginary conductivity, ranging from 0.0002  $\mu\text{S}/\text{cm}$  at 0.1 Hz to 0.001  $\mu\text{S}/\text{cm}$  at 1000 Hz, compared to Summit (0.0001  $\mu\text{S}/\text{cm}$  to 0.0005  $\mu\text{S}/\text{cm}$ ) and Lingan (0.00001  $\mu\text{S}/\text{cm}$  to 0.0005  $\mu\text{S}/\text{cm}$ ). The imaginary conductivity changed very little at PV-8 (orange), except for increases at frequencies <10 Hz at Lingan and Summit. At PV-17 (yellow), the imaginary conductivity at Victoria Junction and Summit decreased at the same rate across all frequencies, with Lingan continuing to increase in imaginary conductivity at frequencies <10 Hz. Each site now displays similar patterns, with no changes below 10 Hz and

increasing imaginary conductivity with increasing frequency above 10 Hz. From PV-24 to PV-86, all sites show gradually decreasing imaginary conductivity. The phase shift for PV-1 was similar at Lingan, Summit, and Victoria Junction, with very small values across all frequencies (<5 mrad). The phase shift then increased steadily with increasing PVs, with Victoria Junction having the highest phase and Lingan having the lowest.

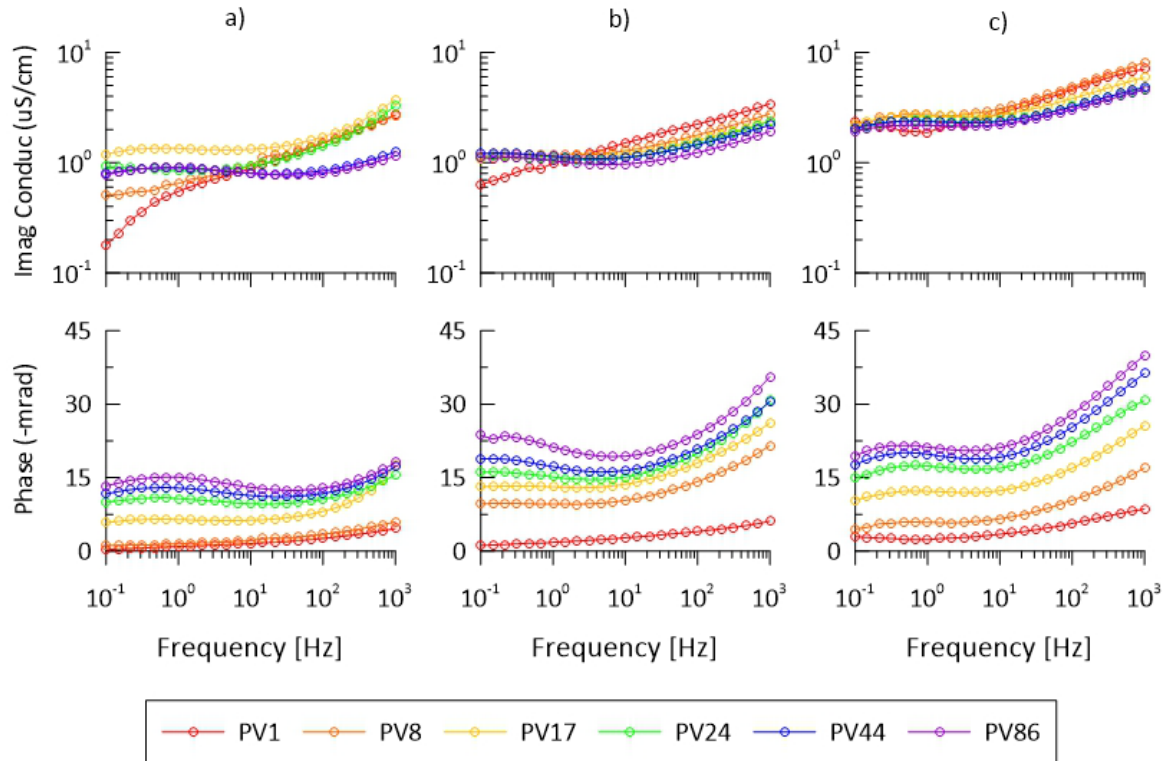


**Figure 3.11** Imaginary conductivity and phase shift for (a) Lingan, (b) Summit, and (c) Victoria Junction humidity cells at selected PVs

The responses in Figure 3.12 did not have the same strong signatures as observed in other studies of SIP on sulfidic minerals, where the magnitude of the signal is based on the concentration and degree of oxidation, while its location along the frequency range is based on the particle sizes within the waste rock (e.g., Wong, 1979; Campbell et al., 1998; Park et al., 2013). It was suspected that the waste material was coated with oxidized minerals (such as jarosite) that would inhibit the surface electrochemical reactions (i.e., coating prevents SIP detecting the actual sulfides) that give rise to strong SIP signatures, similar to the observations

by Campbell et al. (1998). A total of 86 PVs of water were flushed through the samples and clearly leached metals/minerals into the effluent water over time; however, the signature of the sulfide minerals was not obvious. It is suspected that the weight percentages of sulfides in the waste material were too low, with <1 wt% sulfide in this study (Table 3.4) compared to >8 wt% in other studies (e.g., Placencia-Gomez et al., 2014).

The imaginary conductivities of the Summit and Victoria Junction samples fluctuated within ranges and were relatively stable compared to the Lingan measurements. Even though the spectrum of the samples did not distinctly show the presence of oxidizable sulfides, it was evident that Victoria Junction had a higher storage capability of charge compared to Lingan and Summit.

Figure 3.13 plots the imaginary conductivity and phase shift for every second PV in the humidity cell experiments, namely PV-1, PV-3, PV-5, PV-7, PV-9, and PV-11. The spectra of the imaginary conductivity and phase shift in the humidity cells were close to the leaching columns, also indicating that the extra oxidation did not greatly change the mineralogical changes and/or existence of sulfide minerals.

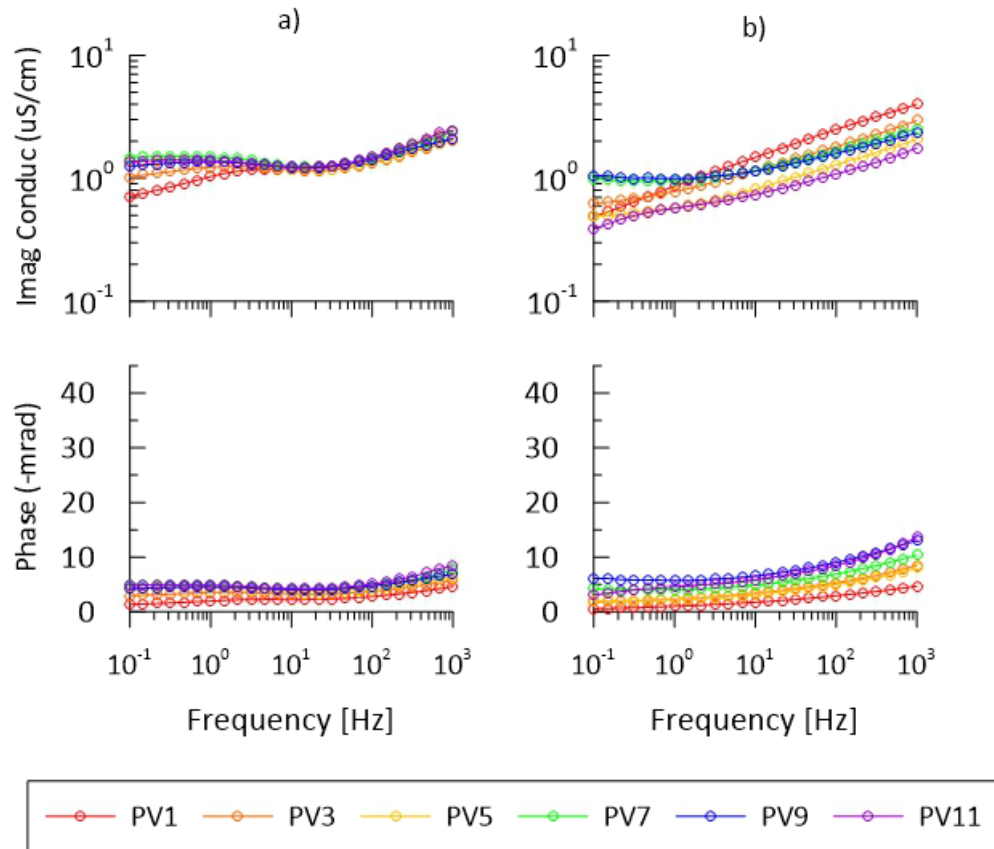


**Figure 3.12** Imaginary conductivity and phase shift for (a) Lingan, and (b) Summit humidity cells at selected PVs

It should be noticed that both column leaching and humidity cell tests ceased on Day 86 (Week 12) as all measured geochemical parameters plateaued off. If the experiment had continued, it would be expected that the measured acidity, sulfate, and EC would continue to decrease, while pH of the discharged drainage would continue to increase. In terms of SIP measurements, the measured real would decrease to capture with the depletion in drainage EC, whereas the imaginary conductivity would remain unchanged. The phase shift, which is typically defined as the ratio between the imaginary and real conductivities, would also increase until the pore water EC was completely depleted.

### 3.3 CONCLUSIONS

In this study, the potential of the SIP to be used as a mine waste rock monitoring tool for the generation and release of AMD was evaluated. Previous studies demonstrated the potential of SIP for detecting sulfide minerals, leading to investigations on its potential to detect mine waste rock. The SIP method could be used as an attractive alternative to overcome limitations posed by the traditional WRP monitoring techniques such as well monitoring and core sampling.

For the purpose of data diversity, real waste rock samples were extracted from the Lingan, Summit, and Victoria Junction WRPs in the Sydney Coalfield in Nova Scotia, Canada. Samples were reconstructed to the size suitable for leaching experiments and then characterized using a series of traditional mine waste characterization methods. Modified ABA test result shows sulfide sulfur content of all samples accounted for nearly 50% of their total sulfur content. This is an indication of the existence of oxidizable sulfide minerals. Unfortunately, the X-ray diffraction test was not able to identify the exact composition of these sulfide minerals and their relative weight percentage. According to the Modified ABA test, both Summit and Victoria Junction were classified as potentially acid generating, whereas the Lingan sample was classified into the uncertain category.

Kinetic column and humidity cell tests were then carried out to determine the exact acid generation characteristics of the waste rock samples. Minor oxidation was introduced to the sample in the column leaching experiment by injecting circulated oxygenated DI water. The humidity cell test experiment was used to simulate intense accelerate oxidation with periodic wetting and drying period. According to the kinetic test experiments, both the Summit and Victoria Junction samples generated acid in the kinetic test experiments. These samples can be classified as acid generating which agrees with the classification made by the ABA analysis. On the other hand, the uncertain Lingan sample did not produce acid during the kinetic experiments, though its drainage did contain elevated dissolved metals (metal leaching) and

can be characterized as neutral drainage.

During the kinetic test experiment, the SIP response of the waste rock samples was simultaneously measured. Phase and imaginary conductivity measured with the SIP instrumentation did not show the existence of sulfide minerals. In general, this study suggests that the SIP method is not suitable for monitoring acid generating waste rock with low oxidizable sulfide. However, the real component showed great capability to monitor the EC evolution within the WRP. This can be used to reflect sulfate, and the level of dissolved metal concentration. It should be noticed that the real component measured with the SIP method cannot be used to indicate the level of acidity of the generated drainage.

### 3.3 REFERENCES

- AASHTO. (2014). *Reducing Sample of Aggregate to Testing Size (T-248)*. Washington, D.C., USA: American Association of State Highway and Transportation.
- Abreu, A. T. D., Faria, E. M. D., Chaves, C. T. F., Leite, A. D. L., & Lena, J. C. D. (2014). Assessment of two kinetic tests to predict the acid mine drainage in waste rock samples of a uranium mine. *Rem: Revista Escola de Minas*, 67, 107-113.
- Aladejana, J. A., Kalin, R. M., Sentenac, P., & Hassan, I. (2020). Hydrostratigraphic characterisation of shallow coastal aquifers of Eastern Dahomey Basin, S/W Nigeria, using integrated hydrogeophysical approach; implication for saltwater intrusion. *Geosciences*, 10(2), 65.
- Al-Abed, S. R., Jegadeesan, G., Purandare, J., & Allen, D. (2008). Leaching behavior of mineral processing waste: comparison of batch and column investigations. *Journal of hazardous materials*, 153(3), 1088-1092.
- Almpanis, A., Gerhard, J., & Power, C. (2021). Mapping and monitoring of DNAPL source zones with combined direct current resistivity and induced polarization: a field-scale numerical investigation. *Water Resources Research*, 57(11), e2021WR031366.
- Amos, R. T., Blowes, D. W., Bailey, B. L., Segó, D. C., Smith, L., & Ritchie, A. I. M. (2015). Waste-rock hydrogeology and geochemistry. *Applied Geochemistry*, 57, 140-156.
- Archie, G.E. (1942) The Electrical Resistivity Log as an Aid in Determining Some Reservoir Characteristics. *Transactions of the AIME*, 146, 54-62.
- ASTM C136–06. (2006). Standard test method for sieve analysis of fine and coarse aggregates. Annual book of ASTM standards. Philadelphia: American Society for Testing and Materials.

- ASTM, N. D5744-96-2001 Standard Test Method for Accelerates Weathering of solid Materials using a Modified Humidity cell. *Book of Standards, 11(04)*.
- ASTM. (2013). Standard test method for materials finer than 75- $\mu\text{m}$  (No. 200) sieve in mineral aggregates by washing. *ASTM C117-13*.
- Azam, S., Wilson, G. W., Fredlund, D. G., & Van Zyl, D. (2011). Geotechnical characterization of mine waste rock. In *Proceedings of the 17th International Conference on Soil Mechanics and Geotechnical Engineering: 5-9 October 2009, Alexandria, Egypt (volume 5)* (pp. 3421-3425). IOS Press.
- Bao, Z., Bain, J., Holland, S. P., Wilson, D., MacKenzie, P., Ptacek, C. J., & Blowes, D. W. (2020). Faro Waste Rock Project: Characterizing geochemical heterogeneity in sulfide-and carbonate-rich waste rock. *Applied Geochemistry, 121*, 104691.
- Bao, Z., Bain, J., Holland, S. P., Wilson, D., Ptacek, C. J., & Blowes, D. W. (2022). Hydrogeochemical Response of a Variably Saturated Sulfide-Bearing Mine Waste-Rock Pile to Precipitation: A Field-Scale Study in the Discontinuous Permafrost Region of Northern Canada. *Water Resources Research, 58*(1), e2021WR031082.
- Benzaazoua, M., Bussière, B., Dagenais, A. M., & Archambault, M. (2004). Kinetic tests comparison and interpretation for prediction of the Joutel tailings acid generation potential. *Environmental geology, 46*, 1086-1101.
- Binley, A., Hubbard, S. S., Huisman, J. A., Revil, A., Robinson, D. A., Singha, K., & Slater, L. D. (2015). The emergence of hydrogeophysics for improved understanding of subsurface processes over multiple scales. *Water resources research, 51*(6), 3837-3866.
- Binley, A., & Slater, L. (2020). *Resistivity and induced polarization: Theory and applications to the near-surface earth*. Cambridge University Press.

- Bradham, W. S., & Caruccio, F. T. (1997). *Acid base accounting success rates in acid mine drainage laboratory predictive tests* (No. CONF-9705128-). American Society for Surface Mining and Reclamation, Princeton, WV (United States).
- Campbell, D. L., Fitterman, D. V., Hein, A. S., & Jones, D. P. (1998, March). Spectral induced polarization studies of mine dumps near Silverton, Colorado. In *11th EEGS Symposium on the Application of Geophysics to Engineering and Environmental Problems* (pp. cp-203). European Association of Geoscientists & Engineers.
- Campbell, D. L., & Fitterman, D. V. (2000, May). Geoelectrical methods for investigating mine dumps. In *Proceedings of the 5th International Conference on Acid Rock Drainage (ICARD 2000), Denver, Colo* (Vol. 2, pp. 1513-1523).
- Campbell, D. L., & Horton, R. J. (2001, March). Spectral induced polarization studies of mine waste piles in Colorado and New Mexico. In *14th EEGS Symposium on the Application of Geophysics to Engineering and Environmental Problems* (pp. cp-192). European Association of Geoscientists & Engineers.
- Commer, M., Newman, G. A., Williams, K. H., & Hubbard, S. S. (2011). 3D induced-polarization data inversion for complex resistivity. *Geophysics*, 76(3), F157-F171.
- Davis, A., Whitehead, C., Lengke, M., & Collord, J. (2019). Acid–base accounting tests in combination with humidity cells help to predict waste rock behavior. *Mine Water and the Environment*, 38, 467-487.
- Dimech, A., Chouteau, M., Aubertin, M., Bussière, B., Martin, V., & Plante, B. (2019). Three-dimensional time-lapse geoelectrical monitoring of water infiltration in an experimental mine waste rock pile. *Vadose Zone Journal*, 18(1), 1-19.
- Dimech, A., Cheng, L., Chouteau, M., Chambers, J., Uhlemann, S., Wilkinson, P., ... & Isabelle, A. (2022). A review on applications of time-lapse electrical resistivity tomography over the

- last 30 years: perspectives for mining waste monitoring. *Surveys in Geophysics*, 43(6), 1699-1759.
- Doetsch, J., Ingeman-Nielsen, T., Christiansen, A. V., Fiandaca, G., Auken, E., & Elberling, B. (2015). Direct current (DC) resistivity and induced polarization (IP) monitoring of active layer dynamics at high temporal resolution. *Cold Regions Science and Technology*, 119, 16-28.
- Erguler, Z. A., & Erguler, G. K. (2015). The effect of particle size on acid mine drainage generation: Kinetic column tests. *Minerals engineering*, 76, 154-167.
- Fala, O., Molson, J., Aubertin, M., & Bussière, B. (2005). Numerical modelling of flow and capillary barrier effects in unsaturated waste rock piles. *Mine water and the environment*, 24(4), 172.
- Foli, G., Apeah, O. B., & Amedjoe, C. G. (2011). Pre-mining water quality prediction from non-weathered sulphide ores along the Ashanti metallogenic belt in Ghana using Acid-Base accounting procedure. *American journal of scientific and industrial research*, 2(5), 827-833.
- Frostad, S., Klein, B., & Lawrence, R. W. (2002). Evaluation of laboratory kinetic test methods for measuring rates of weathering. *Mine Water and the Environment*, 21, 183-192.
- Furrer, G., & Stumm, W. (1986). The coordination chemistry of weathering: I. Dissolution kinetics of  $\delta$ -Al<sub>2</sub>O<sub>3</sub> and BeO. *Geochimica et Cosmochimica Acta*, 50(9), 1847-1860.
- Gray, N. F. (1997). Environmental impact and remediation of acid mine drainage: a management problem. *Environmental geology*, 30, 62-71.
- Gusek, J., & Wildeman, T. (1997). Treatment of Acid Mine Drainage Part I [short course]. *4th International Conference on Acid Rock Drainage*. Vancouver, BC, Canada.
- Guseva, O., Opitz, A. K., Broadhurst, J. L., Harrison, S. T., & Becker, M. (2021).

- Characterisation and prediction of acid rock drainage potential in waste rock: Value of integrating quantitative mineralogical and textural measurements. *Minerals Engineering*, 163, 106750.
- Hakkou, R., Benzaazoua, M., & Bussiere, B. (2008). Acid mine drainage at the abandoned Kettara mine (Morocco): 2. Mine waste geochemical behavior. *Mine Water and the Environment*, 27, 160-170.
- Hakkou, R., Benzaazoua, M., & Bussiere, B. (2009). Laboratory evaluation of the use of alkaline phosphate wastes for the control of acidic mine drainage. *Mine Water and the Environment*, 28, 206-218.
- Hendry, M. J., Biswas, A., Essilfie-Dughan, J., Chen, N., Day, S. J., & Barbour, S. L. (2015). Reservoirs of selenium in coal waste rock: Elk Valley, British Columbia, Canada. *Environmental science & technology*, 49(13), 8228-8236.
- Hersey, D., & Power, C. (2023). Assessing the importance of drainage layers over geomembrane liners within engineered cover systems: Seven years of field monitoring at three mine waste rock piles. *Geotextiles and Geomembranes*, 51(3), 381-389.
- Howard, E. A., Wildeman, T. R., Laudon, L. S., & Machemer, S. D. (1989). Design considerations for the passive treatment of acid mine drainage. In *In Proceedings of the Conference "Reclamation, A Global Perspective". Alberta Land Conservation and Reclamation Council Report# RRTAC* (pp. 89-2).
- Jacobs, J. A., Lehr, J. H., & Testa, S. M. (2013). *Acid mine drainage, rock drainage, and acid sulfate soils : causes, assessment, prediction, prevention, and remediation* (J. A. (James A. Jacobs, J. H. Lehr, & S. M. Testa, Eds.). Hoboken, New Jersey: John Wiley & Sons, Inc.
- Hudson-Edwards, K. A., Jamieson, H. E., & Lottermoser, B. G. (2011). Mine wastes: past, present, future. *Elements*, 7(6), 375-380.

- Kampouroglou, E., Kollias, K., Arvaniti, L., Stouraiti, C., & Papassiopi, N. Acid generation and heavy metal leachability from waste lignite disposal sites, Oropos basin, North Attica. An assessment on preliminary data.
- Kossoff, D., Hudson-Edwards, K. A., Dubbin, W. E., & Alfredsson, M. A. (2011). Incongruent weathering of Cd and Zn from mine tailings: a column leaching study. *Chemical Geology*, 281(1-2), 52-71.
- Lapakko, K. 1993b. Mine Waste Drainage Quality Prediction: A Literature Review. Draft Paper. Minnesota Department of Natural Resources, Division of Minerals, St. Paul, MN.
- Lesmes, D. P. (1993). *Electrical-impedance spectroscopy of sedimentary rocks*. Texas A&M University.
- Liu, Z. S., Huang, C., Ma, L., Dy, E., Xie, Z., Tufa, K., ... & Tallon, L. (2019). The characteristic properties of waste rock piles in terms of metal leaching. *Journal of contaminant hydrology*, 226, 103540.
- Mahan, M. K., Redman, J. D., & Strangway, D. W. (1986). Complex resistivity of synthetic sulphide bearing rocks. *Geophysical Prospecting*, 34(5), 743-768.
- Maroušek, L., Dollinger, S., Elmer, S., Öfner, W., Nussbacher, H., Melcher, F., & Flachberger, H. (2023). Re-Mining of Waste Rock Dumps from a Closed Lead–Zinc Mine—Characterisation of the Residuals. *Minerals*, 13(3), 361.
- MEND (Mine Environment Neutral Drainage). (2004). Design, construction and performance monitoring of cover systems for waste rock and tailings: volume 1 – summary, Canadian Mine Environment Neutral Drainage Program, Project 2.21.4a, July 2004. <http://mend-nedem.org/wpcontent/uploads/2.21.4a-Cover-Design Manual.pdf>. Accessed 10 December 2022.

- MEND (Mine Environment Neutral Drainage). (2008). Acid Rock Drainage Prediction Manual. *Canadian Mine Environment Neutral Drainage Program, Project 1.61.1b, June 2008*
- MEND (Mine Environment Neutral Drainage). (2012). Cold regions cover system design technical guidance document. *Canadian Mine Environment Neutral Drainage Program, Project 1.61.5c, March 2012.*
- Merritt, P., & Power, C. (2022). Assessing the long-term evolution of mine water quality in abandoned underground mine workings using first-flush based models. *Science of The Total Environment, 846*, 157390.
- Miner, G. (2006). Standard methods for the examination of water and wastewater. *American Water Works Association. Journal, 98(1)*, 130
- Namaghi, H. H., & Li, S. (2016). Acid-generating and leaching potential of soils in a Coal Waste Rock Pile in Northeastern China. *Soil and Sediment Contamination: An International Journal, 25(7)*, 776-791.
- Ntarlagiannis, D., Williams, K. H., Slater, L., & Hubbard, S. (2005). Low-frequency electrical response to microbial induced sulfide precipitation. *Journal of Geophysical Research: Biogeosciences, 110(G2)*.
- O'kane, M., Wilson, G. W., & Barbour, S. L. (1998). Instrumentation and monitoring of an engineered soil cover system for mine waste rock. *Canadian Geotechnical Journal, 35(5)*, 828-846.
- Park, M. K., Park, S., Yi, M. J., Kim, J. H., & Takakura, S. (2013, November). SIP response of sulfide minerals in artificial specimen. In *Proceedings of the 11th SEGJ International Symposium, Yokohama, Japan, 18-21 November 2013* (pp. 407-410). Society of Exploration Geophysicists of Japan.

- Pat-Espadas, A. M., Loredó Portales, R., Amabilis-Sosa, L. E., Gómez, G., & Vidal, G. (2018). Review of constructed wetlands for acid mine drainage treatment. *Water*, *10*(11), 1685.
- Plante, B., Benzaazoua, M., & Bussière, B. (2011). Kinetic testing and sorption studies by modified weathering cells to characterize the potential to generate contaminated neutral drainage. *Mine water and the environment*, *30*, 22-37.
- Placencia-Gómez, E., Slater, L., Ntarlagiannis, D., & Binley, A. (2013). Laboratory SIP signatures associated with oxidation of disseminated metal sulfides. *Journal of Contaminant Hydrology*, *148*, 25-38.
- Placencia-Gómez, E., & Slater, L. D. (2014). Electrochemical spectral induced polarization modeling of artificial sulfide-sand mixtures. *Geophysics*, *79*(6), EN91-EN106.
- Placencia-Gómez, E., Parviainen, A., Slater, L., & Leveinen, J. (2015). Spectral induced polarization (SIP) response of mine tailings. *Journal of Contaminant Hydrology*, *173*, 8-24.
- Placencia-Gómez, E., & Slater, L. D. (2016). On the pore water chemistry effect on spectral induced polarization measurements in the presence of pyrite. *Journal of Applied Geophysics*, *135*, 474-485.
- Poisson, J., Chouteau, M., Aubertin, M., & Campos, D. (2009). Geophysical experiments to image the shallow internal structure and the moisture distribution of a mine waste rock pile. *Journal of Applied Geophysics*, *67*(2), 179-192.
- Power, C., & Almpanis, A. (2022). Improved imaging efficiency of large mine waste rock piles with integrated electrical and electromagnetic geophysical techniques. *Journal of Applied Geophysics*, *206*, 104824.
- Power, C., Ramasamy, M., MacAskill, D., Shea, J., MacPhee, J., Mayich, D., ... & Mkandawire,

- M. (2017). Five-year performance monitoring of a high-density polyethylene (HDPE) cover system at a reclaimed mine waste rock pile in the Sydney Coalfield (Nova Scotia, Canada). *Environmental Science and Pollution Research*, 24, 26744-26762.
- Power, C., Ramasamy, M., & Mkandawire, M. (2018). Performance assessment of a single-layer moisture store-and-release cover system at a mine waste rock pile in a seasonally humid region (Nova Scotia, Canada). *Environmental monitoring and assessment*, 190, 1-20.
- Power, C., Tsourlos, P., Ramasamy, M., Nivorlis, A., & Mkandawire, M. (2018). Combined DC resistivity and induced polarization (DC-IP) for mapping the internal composition of a mine waste rock pile in Nova Scotia, Canada. *Journal of Applied Geophysics*, 150, 40-51.
- Prestia, A., Bowell, R., Warrender, R., Brough, C., & Fallowfield, K. (2015). Application of Acid Base Accounting Methods to Barite Projects in Nevada. In *Proceedings of 27 th International Applied Geochemistry Symposium at Tucson* (pp. 1-6).
- Ramasamy, M., & Power, C. (2019). Evolution of acid mine drainage from a coal waste rock pile reclaimed with a simple soil cover. *Hydrology*, 6(4), 83.
- Ramasamy, M., Power, C., & Mkandawire, M. (2018). Numerical prediction of the long-term evolution of acid mine drainage at a waste rock pile site remediated with an HDPE-lined cover system. *Journal of contaminant hydrology*, 216, 10-26.
- Robinson, K., Robinson, C. E., Roy, J. W., Vissers, M., Almpanis, A., Schneidewind, U., & Power, C. (2022). Improved interpretation of groundwater-surface water interactions along a stream reach using 3D high-resolution combined DC resistivity and induced polarization (DC-IP) geoelectrical imaging. *Journal of Hydrology*, 613, 128468.
- Shahhosseini, M., Doulati Ardejani, F., Amini, M., & Ebrahimi, L. (2020). The spatial assessment of acid mine drainage potential within a low-grade ore dump: the role of preferential flow paths. *Environmental earth sciences*, 79(1), 28.

- Skierszkan, E. K., Mayer, K. U., Weis, D., & Beckie, R. D. (2016). Molybdenum and zinc stable isotope variation in mining waste rock drainage and waste rock at the Antamina mine, Peru. *Science of the Total Environment*, 550, 103-113.
- Sracek, O., Choquette, M., G elinas, P., Lefebvre, R., & Nicholson, R. V. (2004). Geochemical characterization of acid mine drainage from a waste rock pile, Mine Doyon, Quebec, Canada. *Journal of contaminant hydrology*, 69(1-2), 45-71.
- Sutter, E., & Ingham, M. (2017). Seasonal saline intrusion monitoring of a shallow coastal aquifer using time-lapse DC resistivity traversing. *Near Surface Geophysics*, 15(1), 59-73.
- Tavakoli, S., Gilbert, G., Lysdahl, A. O. K., Frauenfelder, R., & Forsberg, C. S. (2021). Geoelectrical properties of saline permafrost soil in the Adventdalen valley of Svalbard (Norway), constrained with in-situ well data. *Journal of Applied Geophysics*, 195, 104497.
- United States Environmental Protection Agency (US EPA), 1983. Neutralization of Acid Mine Drainage. Design Manual EPA-600/2-83-001. US EPA, Chicago, Illinois, USA.
- United States Environmental Protection Agency (US EPA), 1994. Acid Mine Drainage Prediction. Technical Documents EPA530-R-94-036. US EPA, Washington, DC, USA. 1-52.
- Usher, B. H., Cruywagen, L. M., De Necker, E., & Hodgson, F. D. I. (2003). On-site and laboratory investigations of spoil in opencast collieries and the development of acid-base accounting procedures. *Water Research Commission Report*, 1055(1), 03.
- Ward, C. R., & French, D. (2005). Relation between coal and fly ash mineralogy, based on quantitative X-ray diffraction methods. *World Coal Ash (WOCA)*, April, 11, 15.
- Wehrli, B. (1989). Monte Carlo simulations of surface morphologies during mineral dissolution. *Journal of Colloid and Interface Science*, 132(1), 230-242.
- Wong, J. (1979). An electrochemical model of the induced-polarization phenomenon in

disseminated sulfide ores. *Geophysics*, 44(7), 1245-1265.

Zubrik, A., Hredzák, S., Turčániová, E., Lovás, M., Bergmann, I., Becker, K. D., & Šepelák, V. (2010). Distribution of inorganic and organic substances in the hydrocyclone separated Slovak sub-bituminous coal. *Fuel*, 89(8), 2126-2132.

## CHAPTER 4 - CONCLUSION

### 4.1 SUMMARY & CONCLUSIONS

Toxic acid mine drainage (AMD) generated from waste rock piles (WRPs) can pose significant threats to the environment (Chen et al., 2021; Bao et al., 2022). Impacts of AMD can be minimized by several approaches, which include the prevention of AMD formation, control of AMD migration, and/or the treatment of AMD effluent (Power et al., 2017). Understanding the changes in the physical and geochemical characteristics within the WRPs is highly desirable for the successful design and implementation of these remediation strategies (MEND, 2004; MEND, 2012; Gusek & Wildeman, 1997; USEPA, 1983). Traditional WRP monitoring methods include monitoring wells and core sampling (e.g., Bao et al., 2020; Ramasamy & Power, 2019); however, these approaches are invasive, expensive, laborious, and can only provide data with limited spatial and temporal resolution. Since both AMD and mine waste materials are electrically conductive, geoelectrical methods, particularly spectral induced polarization (SIP), can be used to provide large-scale monitoring of WRPs.

The ability of the SIP method to carry out this task has been evaluated in previous studies (e.g., Wong, 1979; Mahan et al., 1986; Campbell & Horton, 2001; Placencia-Gomez et al., 2013); however, its performance for monitoring real site samples remains unclear. To the best of the author's knowledge, no studies existed that (i) compared the time-lapse SIP signal change for different waste rock samples taken from different real WRP sites, and (ii) supplemented their SIP responses with detailed mine waste geochemistry.

The objective of this study was to assess the potential of the SIP method to be used as a waste rock monitoring tool. This includes the tracking of the waste rock characteristic change, as well as their generation and release of AMD. To achieve this objective, comprehensive characterization test and laboratory experiments were performed on real site waste rock samples extracted from three WRPs in the Sydney Coalfield in Nova Scotia, Canada. These

tests and experiments included particle size distribution analysis, determination of waste mineralogy and acid generation capacity, and monitoring evolving SIP responses undergoing water influx and/or oxidation.

Based on the mine waste characterization results, all samples tested in this study contained oxidizable sulfides at low weight percentages. Two of the three sites (samples) were acid generating, with the remaining site producing neutral drainage. The measurements of imaginary conductivity and the phase shift indicated that the SIP method was not suitable for monitoring waste rock mineralogy changes with low sulfide concentrations (<1% wt).

Although the SIP method failed to capture the response of sulfide minerals, the real component of the complex conductivity showed great capability in monitoring the changes in porewater chemistry within the waste rock. This information can help to understand the evolution of sulfate and the presence of dissolved metals. The real conductivity measured using the SIP method is equivalent to that measured with the DC resistivity method, which is already a reliable field technique for a range of geoenvironmental applications.

In summary, the experiments conducted in this study contribute to improving the understanding of the SIP method for tracking real mine waste rock and established a robust approach for future laboratory-based time-lapse SIP monitoring. This study also demonstrated the potential of the DC resistivity method to be used as a field monitoring tool at WRP sites.

## 4.2 LIMITATIONS

This is the first study that has combined the SIP method with traditional kinetic test procedures, with some limitations existing, which include:

- The humidity cell apparatus used in this study was not fully optimized. The continuous air injection process caused sample disturbance, potentially leading to compaction, and loss

of fines during the drainage collection process. This could result in changes to the sample porosity as the experiment proceeds.

- The column leaching and humidity cell tests performed in this study were highly accelerated. Furthermore, water flow was from the bottom to top for all kinetic experiments, unlike actual WRP sites where water flowed from top to bottom.
- The samples used in this study were not in their original condition as they were crushed to allow better air flow during the kinetic experiment to prevent clogging issues.
- The effect of temperature, degree of saturation, grain size, and surface texture of the waste rock material (e.g., sphere vs square grain shape) was not considered. These factors could potentially influence the recorded SIP response of the waste rock samples.

It is important to acknowledge these limitations to better understand the scope and applicability of the findings from this study. Further research addressing these limitations would be valuable to enhance the understanding of SIP technique in monitoring the time-lapse change of mine waste rock characteristics.

### 4.3 RECOMMENDATIONS

Considering the limitations mentioned in the previous section, the experiments conducted in this study can only provide preliminary insights into the potential use of the SIP method for monitoring acid generating waste rock with low oxidizable sulfides. Nevertheless, SIP can still be valuable for monitoring the change in the characteristics of high sulfide concentration waste rock. To further advance the application of the SIP method, additional laboratory column experiments are necessary to assess the impact of various factors on the recorded SIP signals before progressing towards field-scale applications. Recommendations for future laboratory SIP experiments include:

- Conduct experiments for waste rock samples with high sulfide concentration and determine the minimum sulfide concentration that can be detected by SIP. The SIP response of waste rocks produced from other mining activities should also be investigated (e.g., gold mine, copper mine, etc.).
- Actual WRPs can be highly complex and heterogeneous. The effect of grain size, surface texture, and degree of saturation on the waste rock SIP response should be extensively studied. The time-lapse SIP response of various mixtures, including clay, silt, sand, and multiple sulfide minerals should also be evaluated.
- Investigate the effect of temperature on the waste rock SIP response as *in situ* waste rock temperature can vary significantly during different seasons. A single suite of experiments at room temperature is insufficient to represent the diverse field conditions.
- In future experiments, consider switching the injected DI water to synthetic rainwater. Bacteria and microbes can also be added to the sample to better simulate natural conditions.

Lastly, this study has demonstrated the potential of the DC resistivity method to capture the changes in pore water characteristics within mine waste rock over time. It is recommended to proceed with experimental tanks and/or field test piles using DC to monitor the generation and release of AMD. This can eventually be transferred to field scale applications to gain insights into the behavior of AMD quality within WRPs.

### 4.3 REFERENCES

- Bao, Z., Bain, J., Holland, S. P., Wilson, D., MacKenzie, P., Ptacek, C. J., & Blowes, D. W. (2020). Faro Waste Rock Project: Characterizing geochemical heterogeneity in sulfide-and carbonate-rich waste rock. *Applied Geochemistry*, *121*, 104691.
- Bao, Z., Bain, J., Holland, S. P., Wilson, D., Ptacek, C. J., & Blowes, D. W. (2022). Hydrogeochemical Response of a Variably Saturated Sulfide-Bearing Mine Waste-Rock Pile to Precipitation: A Field-Scale Study in the Discontinuous Permafrost Region of Northern Canada. *Water Resources Research*, *58*(1), e2021WR031082.
- Campbell, D. L., & Horton, R. J. (2001, March). Spectral induced polarization studies of mine waste piles in Colorado and New Mexico. In *14th EEGS Symposium on the Application of Geophysics to Engineering and Environmental Problems* (pp. cp-192). European Association of Geoscientists & Engineers.
- Chen, G., Ye, Y., Yao, N., Hu, N., Zhang, J., & Huang, Y. (2021). A critical review of prevention, treatment, reuse, and resource recovery from acid mine drainage. *Journal of cleaner production*, *329*, 129666.
- Mahan, M. K., Redman, J. D., & Strangway, D. W. (1986). Complex resistivity of synthetic sulphide bearing rocks. *Geophysical Prospecting*, *34*(5), 743-768.
- MEND (Mine Environment Neutral Drainage). (2004). Design, construction and performance monitoring of cover systems for waste rock and tailings: volume 1 – summary, Canadian Mine Environment Neutral Drainage Program, Project 2.21.4a, July 2004. [http://mend-nedem.org/wpcontent/uploads/2.21.4a-Cover-Design Manual.pdf](http://mend-nedem.org/wpcontent/uploads/2.21.4a-Cover-Design%20Manual.pdf). Accessed 10 December 2022.
- MEND (Mine Environment Neutral Drainage). (2012). Cold regions cover system design

- technical guidance document. *Canadian Mine Environment Neutral Drainage Program*, Project 1.61.5c, March 2012.
- Placencia-Gómez, E., Slater, L., Ntarlagiannis, D., & Binley, A. (2013). Laboratory SIP signatures associated with oxidation of disseminated metal sulfides. *Journal of Contaminant Hydrology*, 148, 25-38.
- Power, C., Ramasamy, M., MacAskill, D., Shea, J., MacPhee, J., Mayich, D., ... & Mkandawire, M. (2017). Five-year performance monitoring of a high-density polyethylene (HDPE) cover system at a reclaimed mine waste rock pile in the Sydney Coalfield (Nova Scotia, Canada). *Environmental Science and Pollution Research*, 24, 26744-26762.
- Ramasamy, M., & Power, C. (2019). Evolution of acid mine drainage from a coal waste rock pile reclaimed with a simple soil cover. *Hydrology*, 6(4), 83.
- Wong, J. (1979). An electrochemical model of the induced-polarization phenomenon in disseminated sulfide ores. *Geophysics*, 44(7), 1245-1265.

# **APPENDICES**

## List of Appendix Tables

<b>Table B. 1</b> Electrode materials comparison.....	114
<b>Table C. 1</b> Summarization of leaching column geometric factors.....	118
<b>Table C. 2</b> Summarization of humidity cell geometric factors.....	118
<b>Table D. 1</b> Results from the field leachate tests on each WRP composite sample .....	129
<b>Table D. 2</b> Detailed sieve analysis results .....	129
<b>Table F. 1</b> Elemental composition of the pretreatment Victoria Junction Sample.....	133
<b>Table F. 2</b> Elemental composition of the pretreatment Lingan Sample .....	134
<b>Table F. 3</b> Elemental composition of the pretreatment Summit Sample.....	135

## List of Appendix Figures

<b>Figure A. 1</b> Leaching columns with practice waste rock samples and sand .....	111
<b>Figure A. 2</b> Leaching columns (right) and humidity cells (left) during SIP measurement .....	111
<b>Figure A. 3</b> Dry air column (left) and humidity cells (right) during dry air injection period .....	112
<b>Figure A. 4</b> Humidifier (left) and humidity cells (right) during humid air injection period .....	112
<b>Figure A. 5</b> Construction of humidifier.....	113
<b>Figure B. 1</b> Electrode materials .....	115
<b>Figure B. 2</b> Electrode materials phase responses (NaCl fluid conductivity: 0.01 S/m). 115	
<b>Figure B. 3</b> Electrode materials phase errors (NaCl fluid conductivity: 0.01 S/m).....	116
<b>Figure C.1</b> Column 1 electrodes phase responses and phase errors (NaCl fluid conductivity: 0.1680 S/m) .....	118
<b>Figure C.2</b> Column 1 electrodes phase responses and phase errors (NaCl fluid conductivity: 0.1012 S/m) .....	119
<b>Figure C.3</b> Column 1 electrodes phase responses and phase errors (NaCl fluid conductivity: 0.0471 S/m) .....	119
<b>Figure C.4</b> Column 1 electrodes phase responses and phase errors (NaCl fluid conductivity: 0.0128 S/m) .....	119
<b>Figure C. 5</b> Column 1: measured impedance vs the reciprocal of fluid conductivity ...	120
<b>Figure C.6</b> Column 2 electrodes phase responses and phase errors (NaCl fluid conductivity: 0.18 S/m).....	120
<b>Figure C.7</b> Column 2 electrodes phase responses and phase errors (NaCl fluid conductivity: 0.12 S/m).....	121
<b>Figure C.8</b> Column 2 electrodes phase responses and phase errors (NaCl fluid conductivity: 0.0548 S/m) .....	121
<b>Figure C.9</b> Column 2 electrodes phase responses and phase errors (NaCl fluid conductivity: 0.0177 S/m) .....	121

<b>Figure C.10</b> Column 2: measured impedance vs the reciprocal of fluid conductivity ..	122
<b>Figure C.11</b> Column 3 electrodes phase responses and phase errors (NaCl fluid conductivity: 0.1556 S/m) .....	122
<b>Figure C.12</b> Column 3 electrodes phase responses and phase errors (NaCl fluid conductivity: 0.1072 S/m) .....	122
<b>Figure C.13</b> Column 3 electrodes phase responses and phase errors (NaCl fluid conductivity: 0.053 S/m) .....	123
<b>Figure C.14</b> Column 3 electrodes phase responses and phase errors (NaCl fluid conductivity: 0.01563 S/m) .....	123
<b>Figure C.15</b> Column 3: measured impedance vs the reciprocal of fluid conductivity ..	124
<b>Figure C.16</b> Humidity cell electrodes phase responses and phase errors (NaCl fluid conductivity: 0.201 S/m) .....	124
<b>Figure C.17</b> Humidity cell electrodes phase responses and phase errors (NaCl fluid conductivity: 0.1289 S/m) .....	124
<b>Figure C.18</b> Humidity cell electrodes phase responses and phase errors (NaCl fluid conductivity: 0.0471 S/m) .....	125
<b>Figure C.19</b> Humidity cell electrodes phase responses and phase errors (NaCl fluid conductivity: 0.0284 S/m) .....	125
<b>Figure C. 20</b> Humidity cells: measured impedance vs the reciprocal of fluid conductivity .....	126
<b>Figure D.1</b> Sample preparation and oven drying summary sheet (all samples are oven dried under 40 degrees Celsius .....	127
<b>Figure D.2</b> Sample preparation – quartering and mixing (1) .....	128
<b>Figure D.3</b> Sample preparation – quartering and mixing (2) .....	128
<b>Figure E. 1</b> Lingan XRD result.....	130
<b>Figure E. 2</b> Summit XRD result .....	131
<b>Figure E. 3</b> Victoria Junction XRD result .....	132
<b>Figure F. 1</b> SEM Scan, spectrum 1 & 2 for the Victoria Junction sample .....	133
<b>Figure F. 2</b> SEM Scan, spectrum 3 for the Victoria Junction sample .....	133

<b>Figure F. 3</b> SEM Scan, spectrum 7&8 for the Lingan sample.....	134
<b>Figure F. 4</b> SEM Scan, spectrum 9 for the Lingan sample .....	134
<b>Figure F. 5</b> SEM Scan, spectrum 13&14 for the Summit sample .....	135
<b>Figure F. 6</b> SEM Scan, spectrum 15 for the Summit sample .....	135
<b>Figure. G.1</b> Column leaching test SIP AB responses for: a) Lingan; b) Summit; c) Victoria Junction .....	136
<b>Figure. G.2</b> Lingan column leaching test potential pair AB PV1 & PV 86 Comparison (0.01 Hz to 1,000 Hz).....	137
<b>Figure. G.3</b> Lingan column leaching test potential pair BC PV1 & PV 86 Comparison (0.01 Hz to 1,000 Hz).....	137
<b>Figure. G.4</b> Summit column leaching test potential pair AB PV1 & PV 86 Comparison (0.01 Hz to 1,000 Hz).....	138
<b>Figure. G.5</b> Summit column leaching test potential pair BC PV1 & PV 86 Comparison (0.01 Hz to 1,000 Hz).....	138
<b>Figure. G.6</b> Victoria Junction column test potential pair AB PV1 & PV 86 Comparison (0.01 Hz to 1,000 Hz).....	139
<b>Figure. G.7</b> Victoria Junction column test potential pair BC PV1 & PV 86 Comparison (0.01 Hz to 1,000 Hz).....	139

## Appendix A: Experiment Apparatus Photos

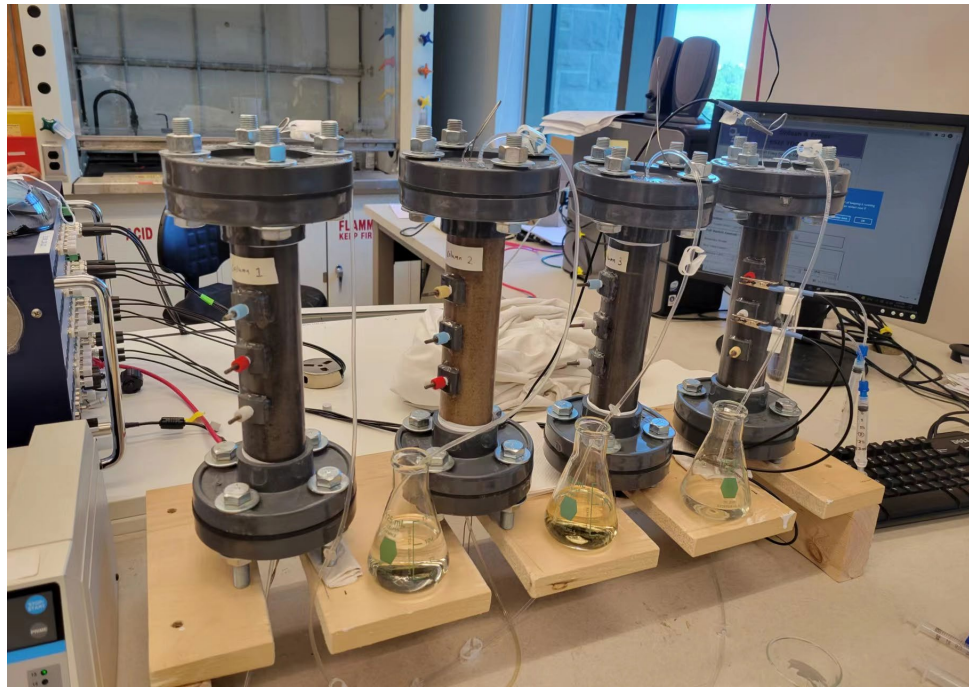


**Figure A. 1** Leaching columns with practice waste rock samples and sand



**Figure A. 2** Leaching columns (right) and humidity cells (left) during SIP measurement



**Figure A. 3** Dry air column (left) and humidity cells (right) during dry air injection period



**Figure A. 4** Humidifier (left) and humidity cells (right) during humid air injection period



**Figure A. 5** Construction of humidifier

## Appendix B: SIP Measurement Electrode Selection

Potential electrodes for SIP measurements can be made from different materials. These materials include graphite, silver disc, and silver rod. Each of these electrodes has its own advantages. Prior to the experiments, these electrodes have been tested for their accuracy and performance to decide which one is the most suitable for column leaching and humidity cell experiments.

According to the test results, the silver disc gives the highest accuracy. However, silver disc electrode is very difficult to handle as the electrode chamber is required to be filled with electrolytes before testing. The selection of electrolytes can be either agar gel or water. Air bubbles might arise in the electrode chamber to reduce the stability of the measurements. In comparison, silver rod and silver disc electrodes do not contain a chamber in their design, the electrodes are designed to be directly in contact with the sample surface. Graphite is less expensive, but it is easy to break and gives relatively high phase error. By soaking the silver rod in bleach, a stable Ag-AgCl electrode can be made to obtain reliable data.

Due to the above considerations, silver rod has been selected as the electrode material for the experiments.

**Table B. 1** Electrode materials comparison

<b>Materials</b>	<b>Advantages</b>	<b>Disadvantages</b>
Graphite	Low cost, easy to handle	Relatively high phase error
Silver Rod	Easy to handle, reliable results, durable	Expensive
Silver Disc	Give perfect results	Expensive, difficult to handle



**Figure B. 1** Electrode materials

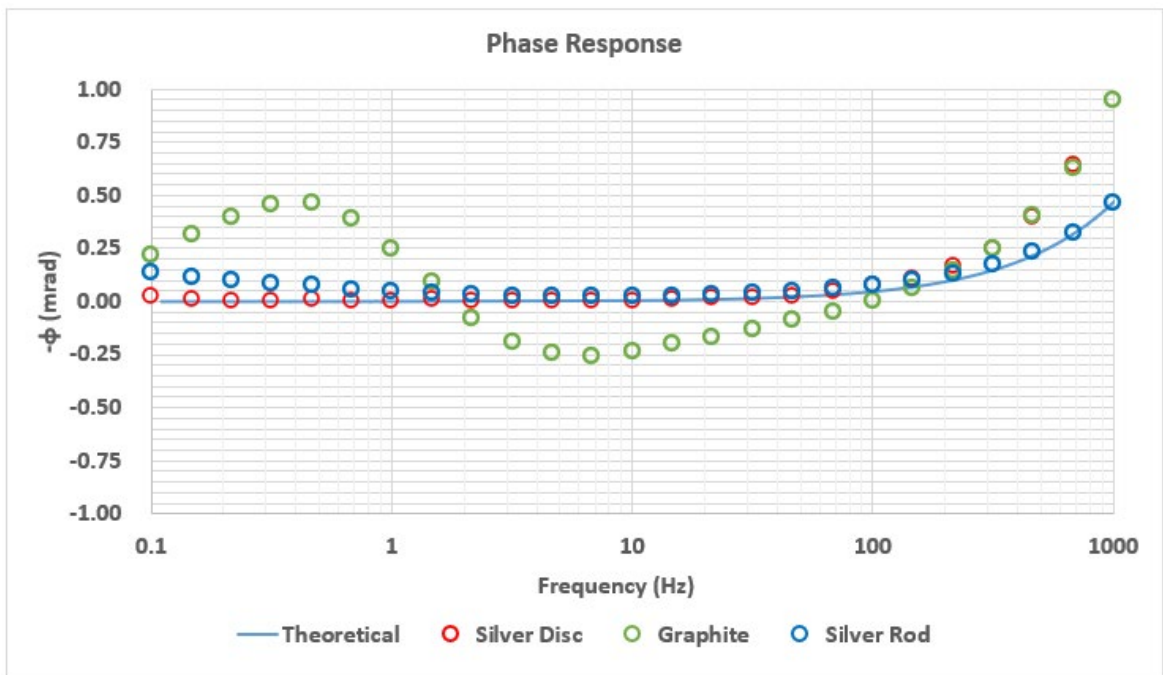


**Figure B. 2** Electrode materials phase responses (NaCl fluid conductivity: 0.01 S/m)

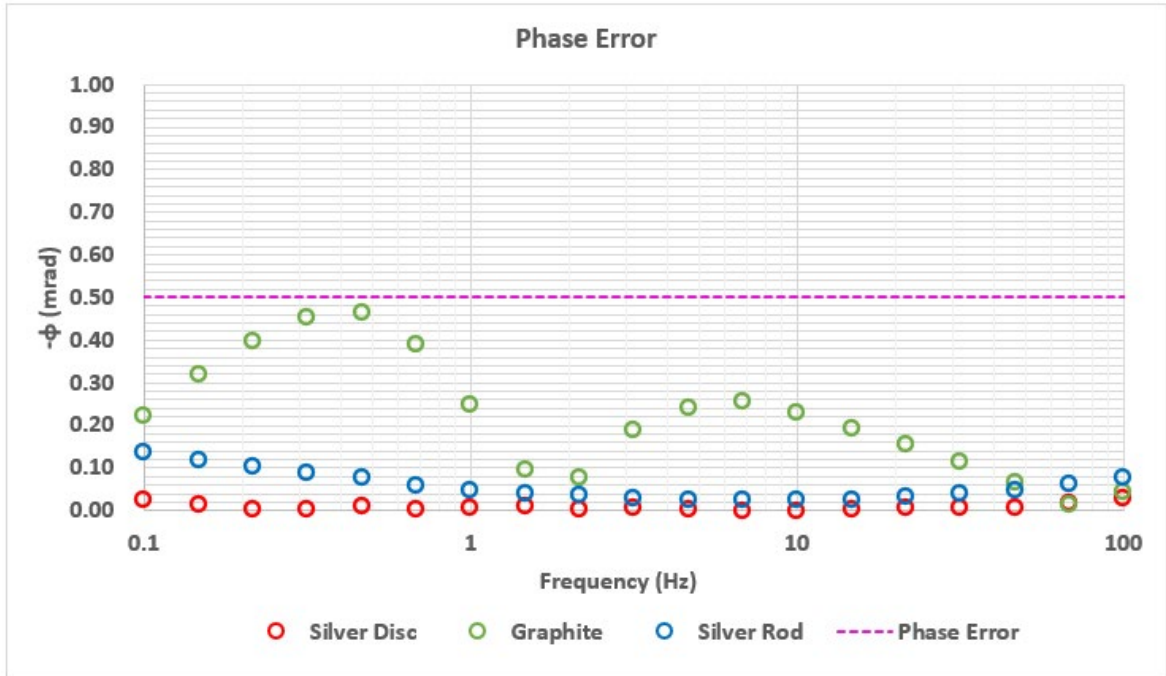


**Figure B. 3** Electrode materials phase errors (NaCl fluid conductivity: 0.01 S/m)

## Appendix C: Geometric Factors

According to Binley & Slater, (2020), the resistivity of a material is a characteristic that explains the resistance it exerts to the conduction of electrical current. This characteristic is determined by measuring the resistance that occurs during the transfer of electrical current, by taking into consideration of a geometric factor (K). In SIP measurements, each sample holder has a unique K that is required for the calculation of real and imaginary components of complex conductivity. There is a simple analytical expression for K,

$$K = \left(\frac{A}{L}\right) \quad (C-1)$$

Where A is the-cross-sectional area of the sample holder and L is the length of between the measuring potential electrodes. However, this analytical expression may not provide an accurate representation of the actual K of the sample holder.

A more reliable and effective method is to determine K experimentally. This can be achieved by filling the sample holder with fluids with different known conductivities. The resistance (impedance) between the potential electrode pair is then recorded. The best estimate of K can be determined once enough measurements are made and is the reciprocal of the slope of the best fitting linear relation between measured impedance and the fluid conductivity,

$$R = \left(\frac{1}{K}\right) \frac{1}{\sigma_w} \quad (C-2)$$

Where R = complex resistance or impedance (ohms),  $\sigma_w$  = water conductivity (S/m), k = geometric factor (configuration specific, m).

In this study, geometric factor K was calculated for all leaching columns. According to the result, the geometric factor K calculated for each column is nearly identical. All humidity cells were assumed to have the same geometric factor K as the cells (identical) and were carefully constructed to follow the proposed design. The sample holders were first filled with NaCl to reach desired conductivities, and the complex conductivity of the solution was measured with Hatch EC probe calibrated daily with certified standards. The impedance of the solution was measured with the PSIP unit. Table C.1 and Table C.2 summarize the detailed geometric factors for each column and cell. Detailed phase response, phase errors, and the relationships between measured impedance and fluid conductivities are summarized in the figures below for each sample holder.

**Table C. 1** Summarization of leaching column geometric factors

Column #	Potential Pair AB	Potential Pair BC	Potential Pair AC
1	0.031137	0.030669	0.015412
2	0.030982	0.030764	0.015286
3	0.031683	0.030682	0.015585

**Table C. 2** Summarization of humidity cell geometric factors

Humidity Cell #	Geometric Factor
1, 2, 3	0.046492

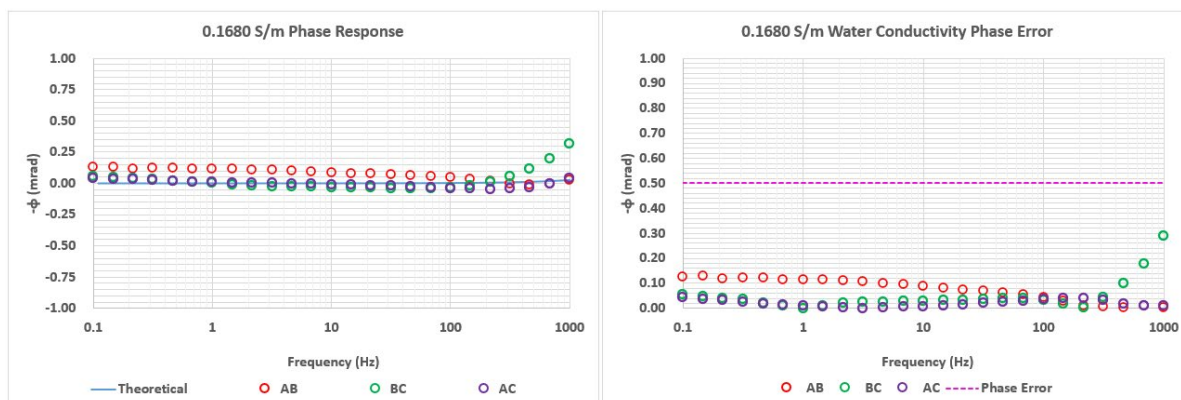


**Figure C. 1** Column 1 electrodes phase responses and phase errors (NaCl fluid conductivity: 0.1680 S/m)

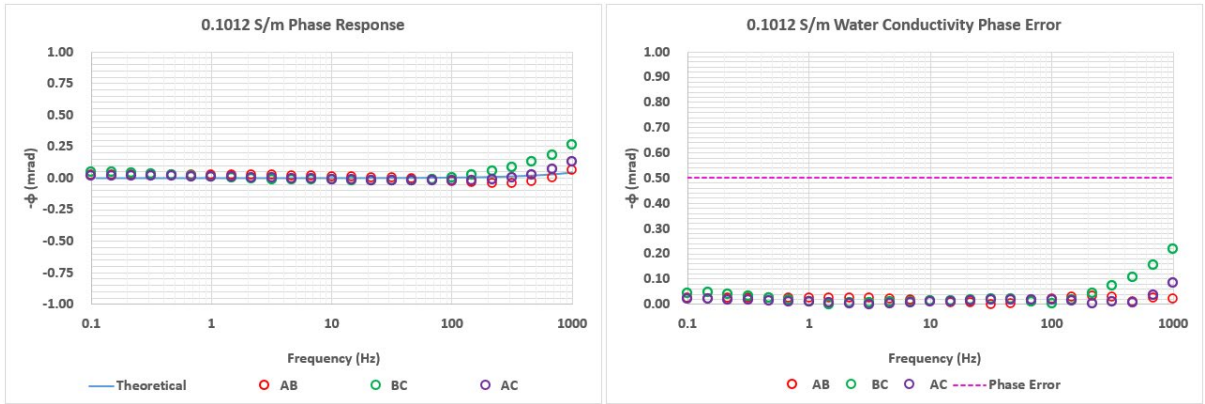


**Figure C. 2** Column 1 electrodes phase responses and phase errors (NaCl fluid conductivity: 0.1012 S/m)

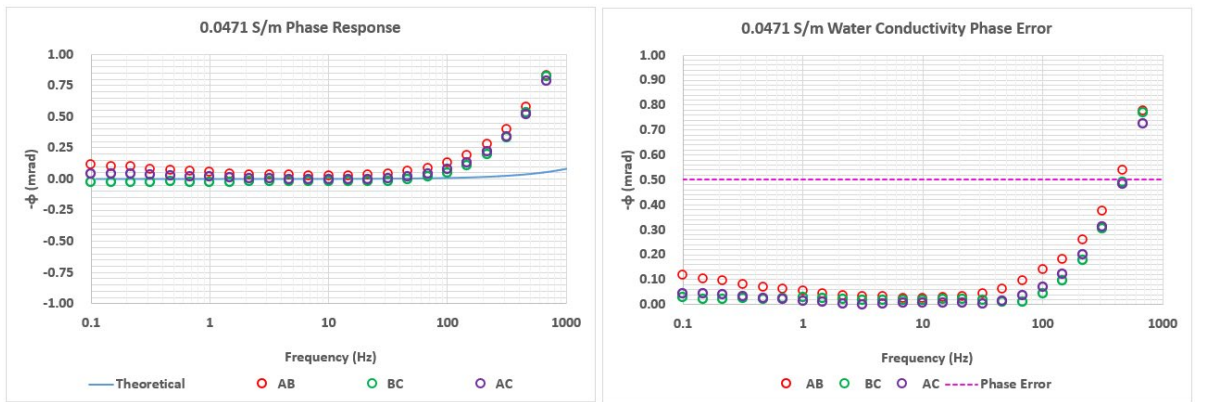


**Figure C. 3** Column 1 electrodes phase responses and phase errors (NaCl fluid conductivity: 0.0471 S/m)

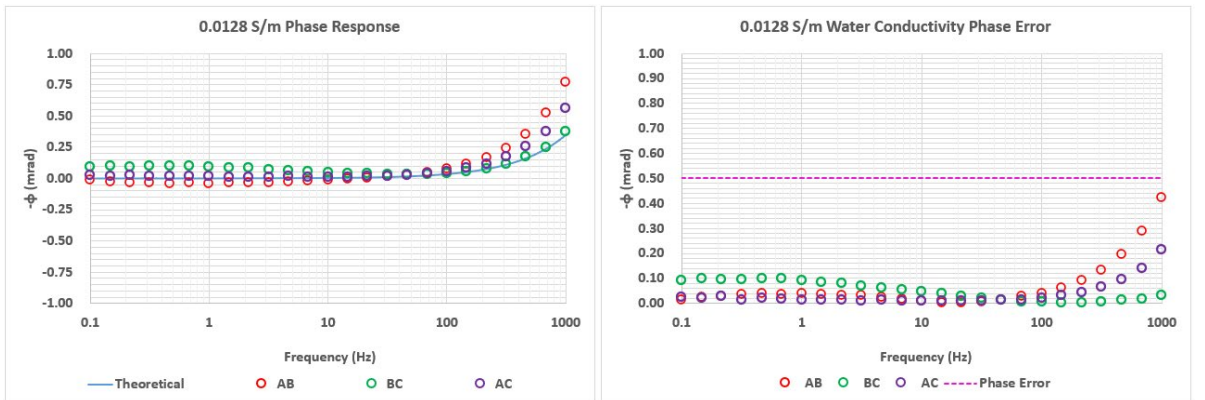


**Figure C. 4** Column 1 electrodes phase responses and phase errors (NaCl fluid conductivity: 0.0128 S/m)

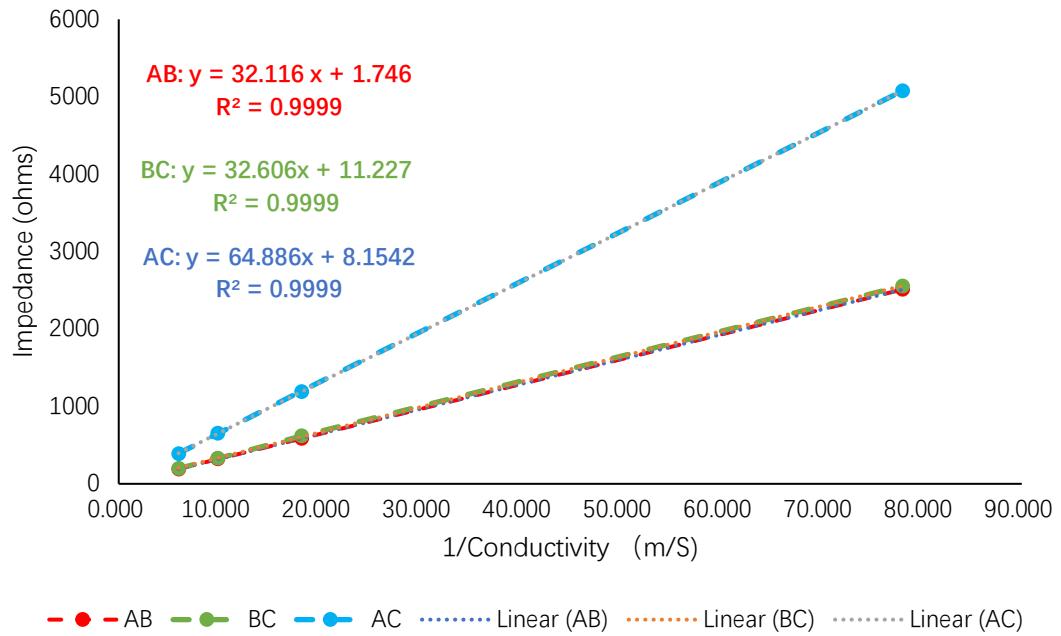


**Figure C. 5** Column 1: measured impedance vs the reciprocal of fluid conductivity

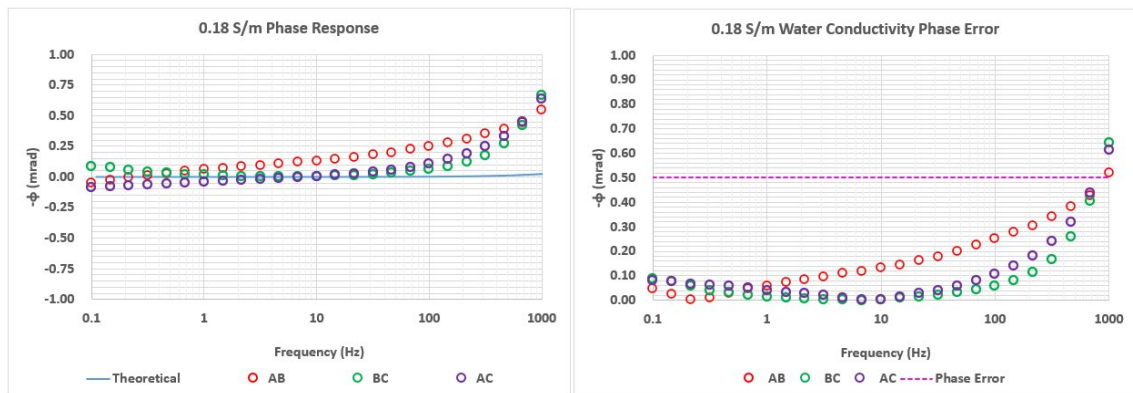


**Figure C. 6** Column 2 electrodes phase responses and phase errors (NaCl fluid conductivity: 0.18 S/m)

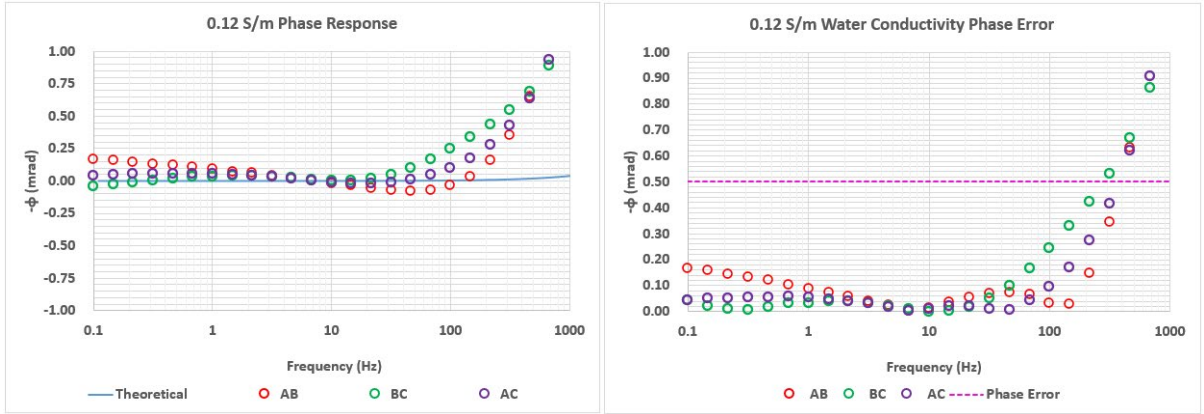


**Figure C. 7** Column 2 electrodes phase responses and phase errors (NaCl fluid conductivity: 0.12 S/m)

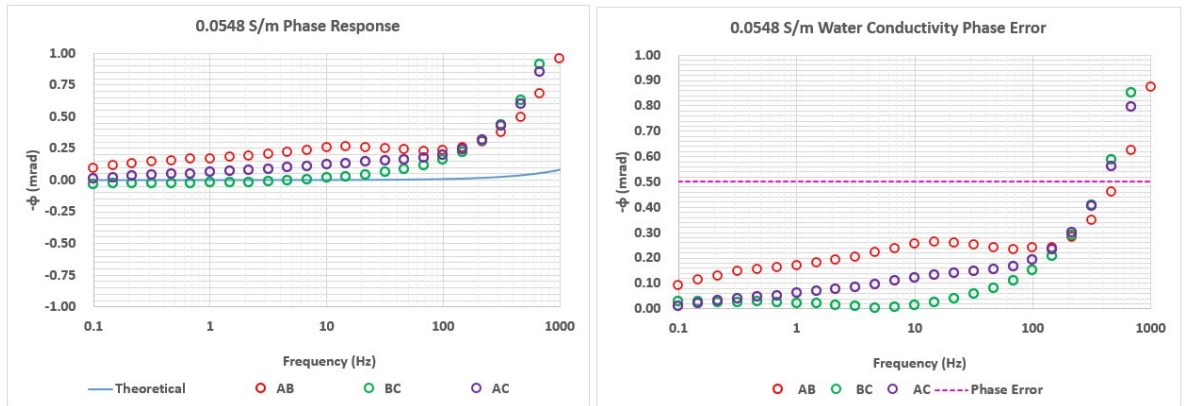


**Figure C. 8** Column 2 electrodes phase responses and phase errors (NaCl fluid conductivity: 0.0548 S/m)

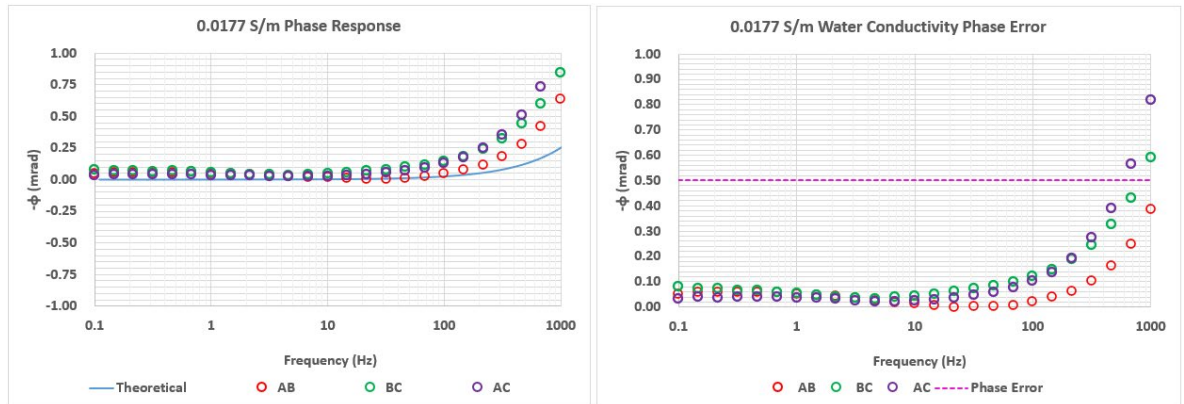


**Figure C. 9** Column 2 electrodes phase responses and phase errors (NaCl fluid conductivity: 0.0177 S/m)

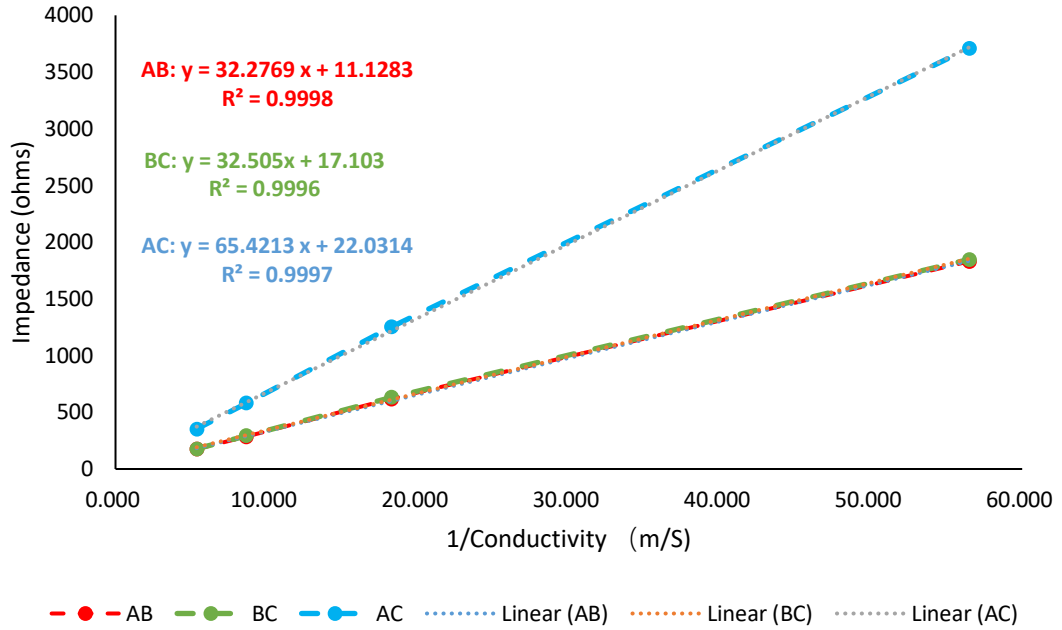


**Figure C. 10** Column 2: measured impedance vs the reciprocal of fluid conductivity

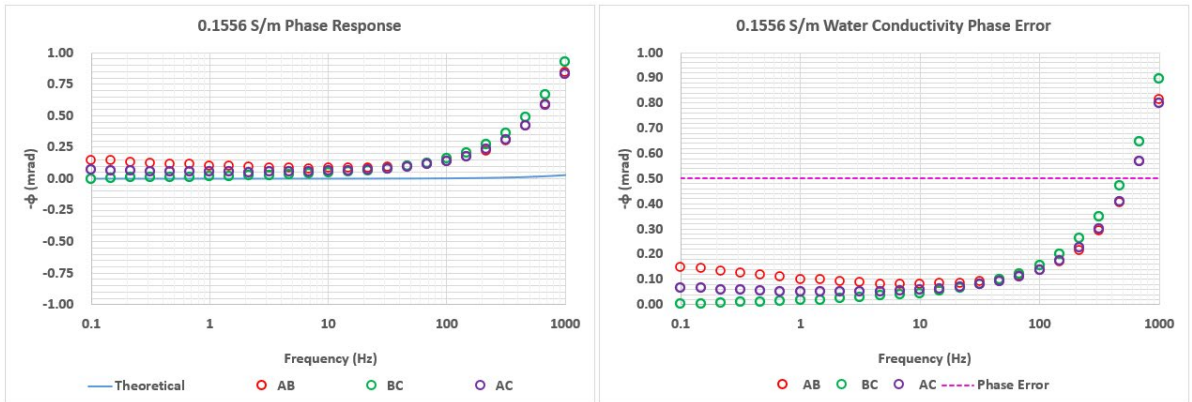


**Figure C. 11** Column 3 electrodes phase responses and phase errors (NaCl fluid conductivity: 0.1556 S/m)

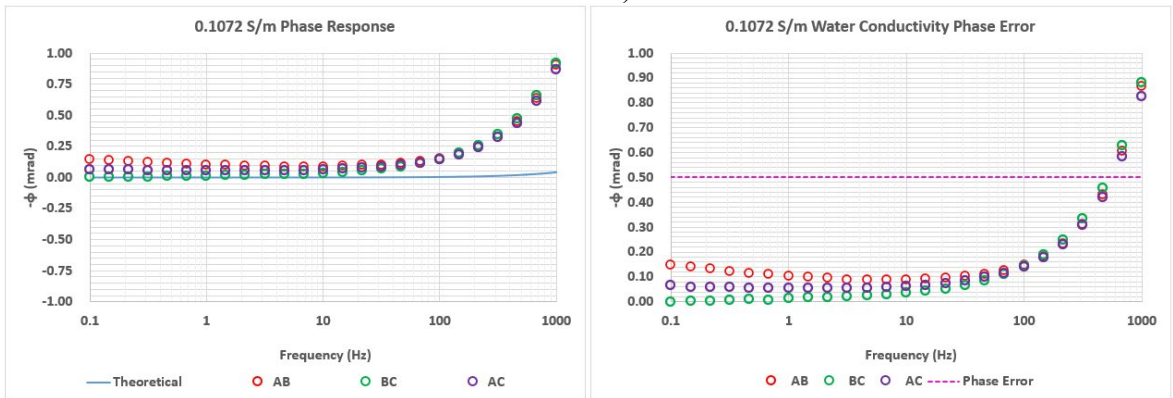


**Figure C. 12** Column 3 electrodes phase responses and phase errors (NaCl fluid conductivity: 0.1072 S/m)

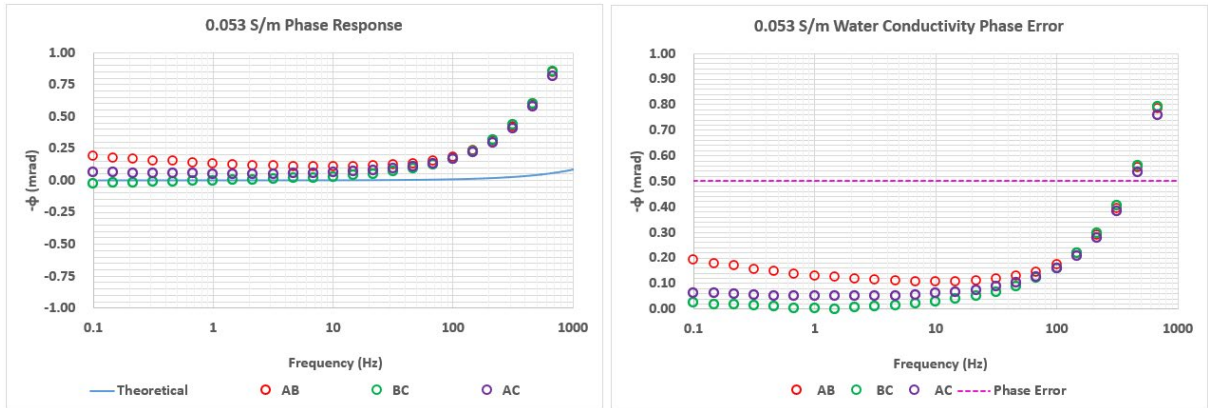


**Figure C. 13** Column 3 electrodes phase responses and phase errors (NaCl fluid conductivity: 0.053 S/m)

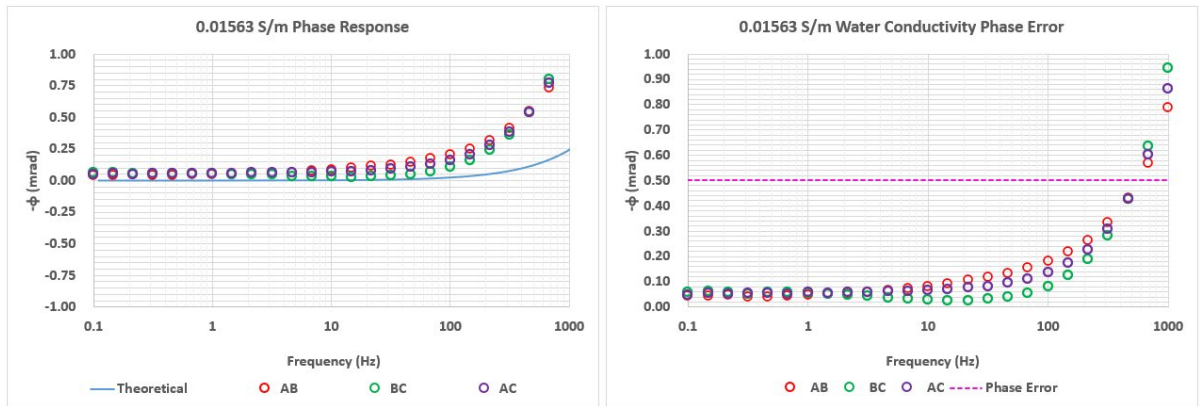


**Figure C. 14** Column 3 electrodes phase responses and phase errors (NaCl fluid conductivity: 0.01563 S/m)

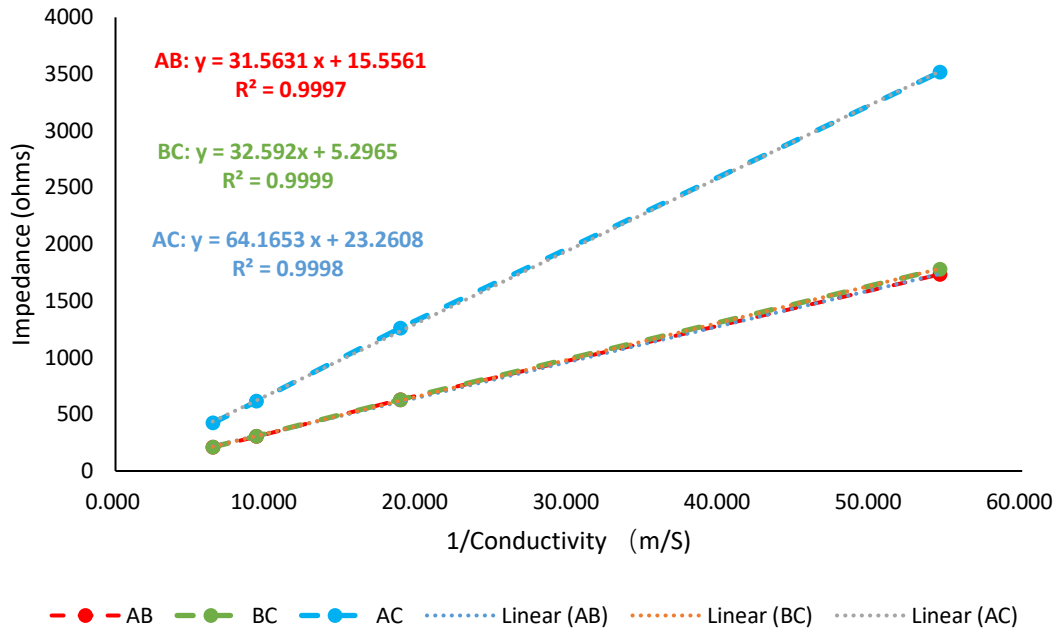


**Figure C. 15** Column 3: measured impedance vs the reciprocal of fluid conductivity

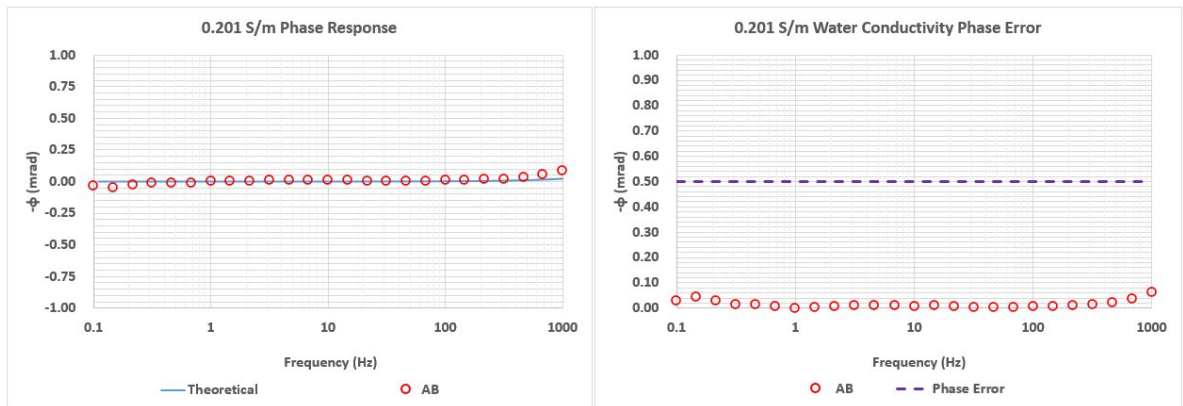


**Figure C. 16** Humidity cell electrodes phase responses and phase errors (NaCl fluid conductivity: 0.201 S/m)

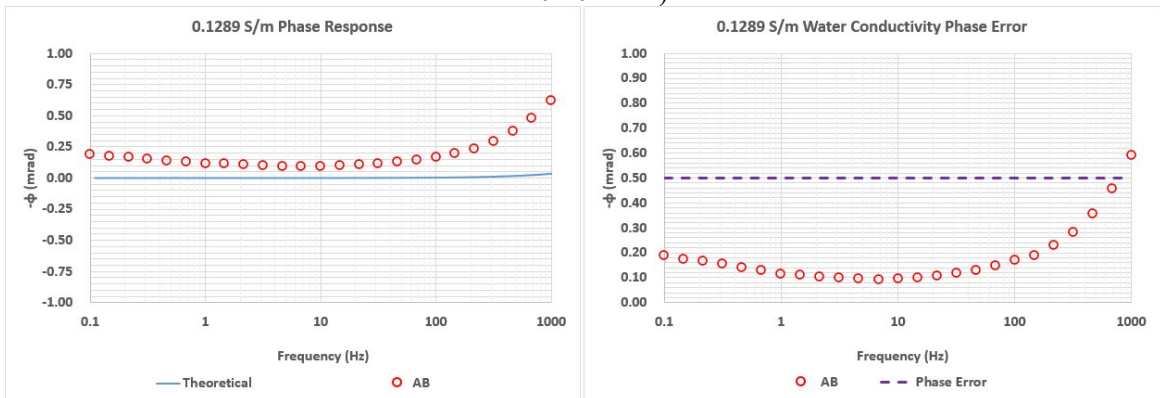


**Figure C. 17** Humidity cell electrodes phase responses and phase errors (NaCl fluid conductivity: 0.1289 S/m)

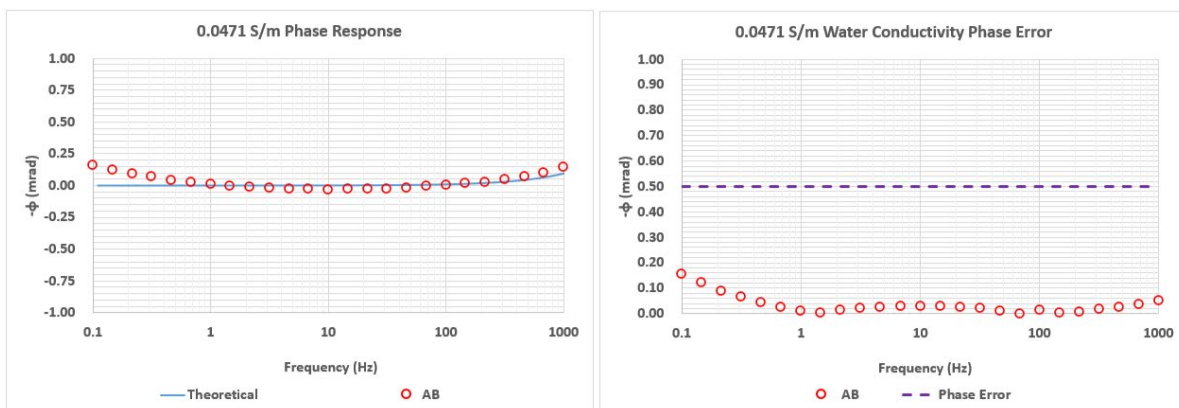


**Figure C. 18** Humidity cell electrodes phase responses and phase errors (NaCl fluid conductivity: 0.0471 S/m)

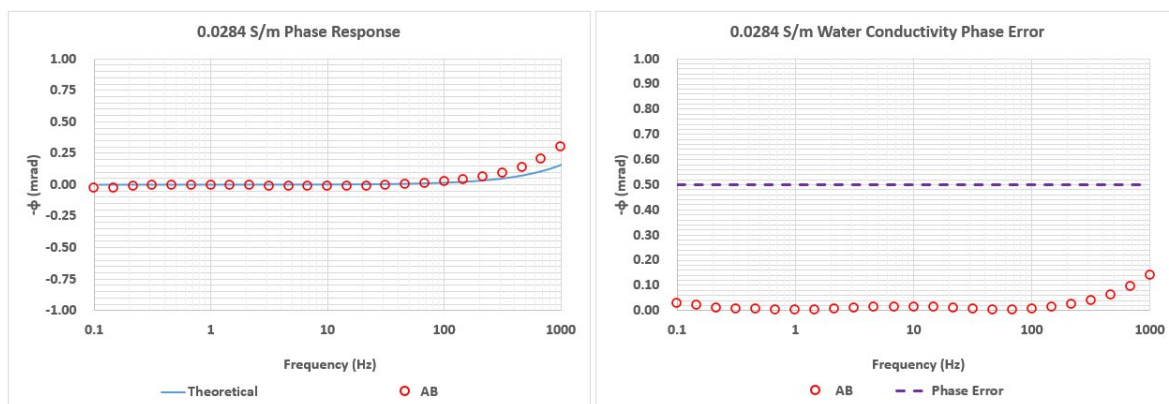


**Figure C. 19** Humidity cell electrodes phase responses and phase errors (NaCl fluid conductivity: 0.0284 S/m)

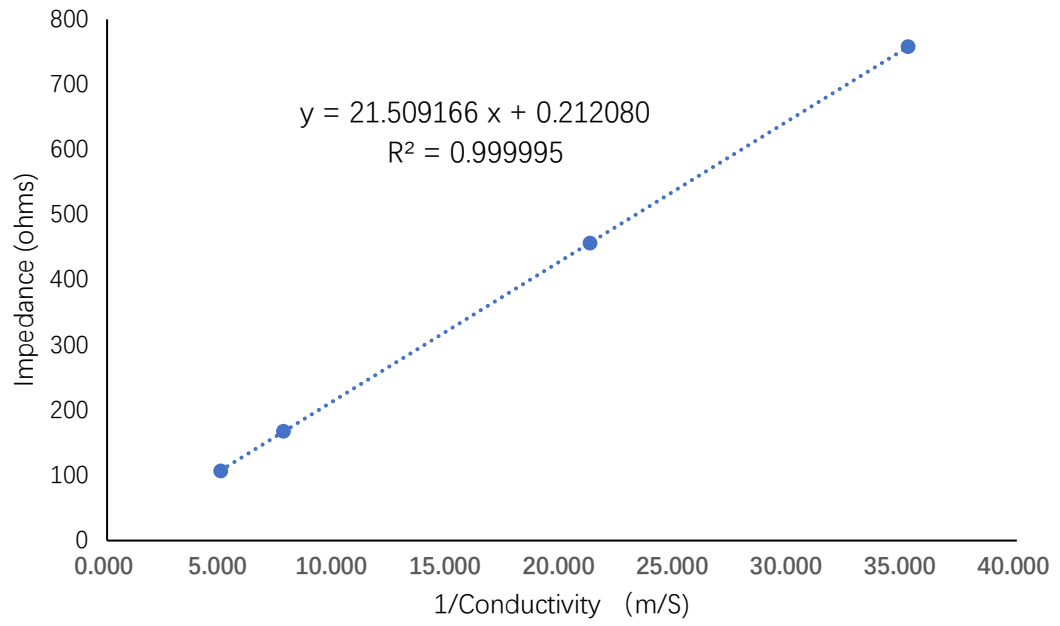


**Figure C. 20** Humidity cells: measured impedance vs the reciprocal of fluid conductivity

## Appendix D: Sample Preparation

### Lingan

Tray #	Tray Weight (g)	Bucket / Bag Sample ID	Moist Sample + Tray Weight (g)	Oven Dry Start Time	1st Check Time	1st Check Weight (g)	2nd Check Time (g)	2nd Check Weight (g)	3rd Check Time	3rd Check Weight (g)
1	59.57	L-W2-01, 10, 11	4182.7	2022/6/25 15:00	2022/6/27 12:03	3561.9	2022/6/28 11:36	3557.4	2022/6/28 13:36	3557.2
2	59.47	L-W2-06, 07, 08	2891.5	2022/6/22 15:16	2022/6/23 15:16	2653.8	2022/6/25 14:55	2625.4	2022/6/27 11:41	2655.1
3	59.5	L-W2-09, 12, 13	4094.3	2022/6/25 15:00	2022/6/27 11:58	3419.2	2022/6/28 11:36	3413.1	2022/6/28 13:36	3413.1
4	59.42	L-W2-14, 15, 16, 17, 18	5361.2	2022/6/22 15:16	2022/6/23 15:16	4989.2	2022/6/25 15:00	4492.6	2022/6/27 11:53	4492.5
5	61.21	L-W4-05, 08	2067.6	2022/6/28 13:40	2022/6/29 13:40	1951.2	2022/6/29 15:40	1942.1	2022/6/29 18:40	1942.1
6	59.9	L-W4-09, 10	2319.1	2022/6/28 13:40	2022/6/29 13:40	2190.1	2022/6/29 15:45	2186.9	2022/6/29 18:38	2186.6

### Summit

Tray #	Tray Weight (g)	Bucket / Bag Sample ID	Moist Sample + Tray Weight (g)	Oven Dry Start Time	1st Check Time	1st Check Weight (g)	2nd Check Time (g)	2nd Check Weight (g)	3rd Check Time	3rd Check Weight (g)
1	59.05	S-W2-14, 17, 18, 19	4520.5	2022/7/1 9:05	2022/7/2 9:05	4315.9	2022/7/2 11:05	4309.7	2022/7/2 13:05	4309.5
2	59.41	S-W4-05, 06, 07, 08, 09, 10	4840.4	2022/7/1 9:05	2022/7/2 9:05	3562.8	2022/7/2 11:05	3560.2	2022/7/2 13:05	3559.8
3	58.58	S-W3-16, 17, 18, 19, 20, 21	4188.6	2022/7/2 13:05	2022/7/3 13:05	3696.7	2022/7/3 14:05	3689.5	2022/7/3 15:05	3688.9

### Victoria Junction

Tray #	Tray Weight (g)	Bucket / Bag Sample ID	Moist Sample + Tray Weight (g)	Oven Dry Start Time	1st Check Time	1st Check Weight (g)	2nd Check Time (g)	2nd Check Weight (g)	3rd Check Time	3rd Check Weight (g)
1	59.5	VJ-W4-003 (14'-20')	3342.9	2022/7/3 15:05	2022/7/4 15:10	2998.1	2022/7/4 19:10	2813.4	2022/7/4 21:10	2813.3
2	59.44	VJ-W4-003 (14'-20')	2851.8	2022/7/3 15:00	2022/7/4 15:00	2302.1	2022/7/4 17:00	2282.2	2022/7/4 19:00	2282.2

Figure D. 1 Sample preparation and oven drying summary sheet (all samples are oven dried under 40 degrees Celsius)



**Figure D. 2** Sample preparation – quartering and mixing (1)



**Figure D. 3** Sample preparation – quartering and mixing (2)

A fast, effective, and simple leach test was performed on a portion of each WRP composite sample for a preliminary assessment of the leachate generated by the waste rock (USGS Techniques and Methods 5-D3). Table D.1 presents the characteristics of this initial leachate of these leach tests, with the most acidic leachate at Victoria Junction, and the least acidic at Lingan, which also corresponds to the range of EC values.

**Table D. 1** Results from the field leachate tests on each WRP composite sample

<b>Sample</b>	<b>pH</b>	<b>Acidity (mg/L as CaCO<sub>3</sub>)</b>	<b>Conductivity (mS/cm)</b>
Lingan	6.82	400	6,100
Summit	2.98	5,200	10,000
Victoria Junction	2.76	12,000	11,860

**Table D. 2** Detailed sieve analysis results

	<b>Lingan</b>	<b>Summit</b>	<b>Victoria Junction</b>
D <sub>10</sub> (mm)	0.1245	0.1218	0.1063
D <sub>30</sub> (mm)	0.3005	0.2970	0.1902
D <sub>50</sub> (mm)	0.5836	0.7073	0.3324
D <sub>60</sub> (mm)	0.7875	1.0114	0.4305
C <sub>u</sub>	6.33	8.30	4.05
C <sub>c</sub>	0.92	0.72	0.79
Coarse Sand (wt%)	17	12	3
Medium Sand (wt%)	46	48	37
Fine Sand (wt%)	35	38	58
Silt and Clay (wt%)	2	2	2
Calculated Porosity	0.33	0.31	0.37
Actual Porosity	0.32	0.29	0.35
Soil Classification	Poorly Graded	Poorly Graded	Poorly Graded

# Appendix E: XRD Test Results

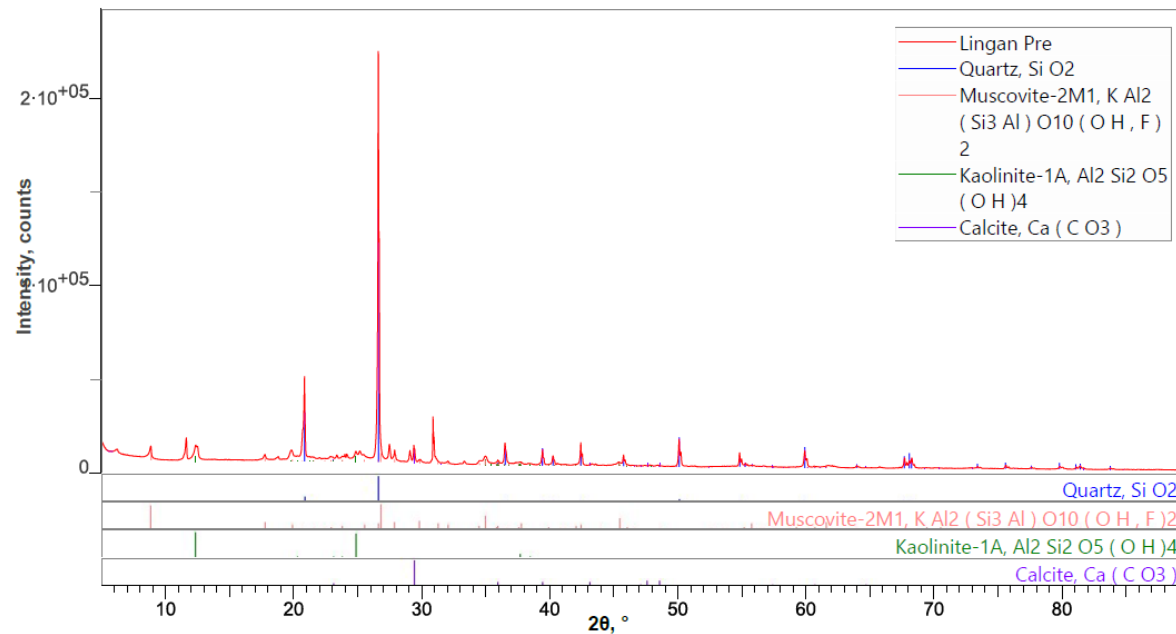
Path: C:\2022Academic\30-29622.ACA.CEE (Difan Su)\Lingan  
Pre\_Solution.rmsIn

Solution

## Qualitative Analysis Results

Phase name	Chemical formula	FOM	Phase reg. detail	Space Group	DB Card Number
Quartz	Si O <sub>2</sub>	2.280	S/M:PDF-4+ 2022	154 : P3221	01-075-8322
Muscovite-2M1	K Al <sub>2</sub> ( Si <sub>3</sub> Al ) O <sub>10</sub> ( O H , F ) <sub>2</sub>	2.524	S/M:PDF-4+ 2022	15 : C12/c1	00-006-0263
Kaolinite-1A	Al <sub>2</sub> Si <sub>2</sub> O <sub>5</sub> ( O H ) <sub>4</sub>	2.854	S/M:PDF-4+ 2022	1 : C1	00-058-2004
Calcite	Ca ( C O <sub>3</sub> )	1.308	S/M:PDF-4+ 2022	167 : R-3cH	04-008-0198

## Phase Data View



Lingan Pre-Evaluation report (Solution)

Page 3 of 12

Figure E. 1 Lingan XRD result

Qualitative Analysis Results

Phase name	Chemical formula	FOM	Phase reg. detail	Space Group	DB Card Number
Amorphous		2.100	Amorphous		
Quartz low, syn	Si O2	0.586	S/M:PDF-4+ 2022	154 : P3221	03-065-0466
Muscovite-2M1	K ( Al2.9 Si3.1 O10 ) ( O H )2	1.041	S/M:PDF-4+ 2022	15 : C12/c1	01-084-1302

Phase Data View

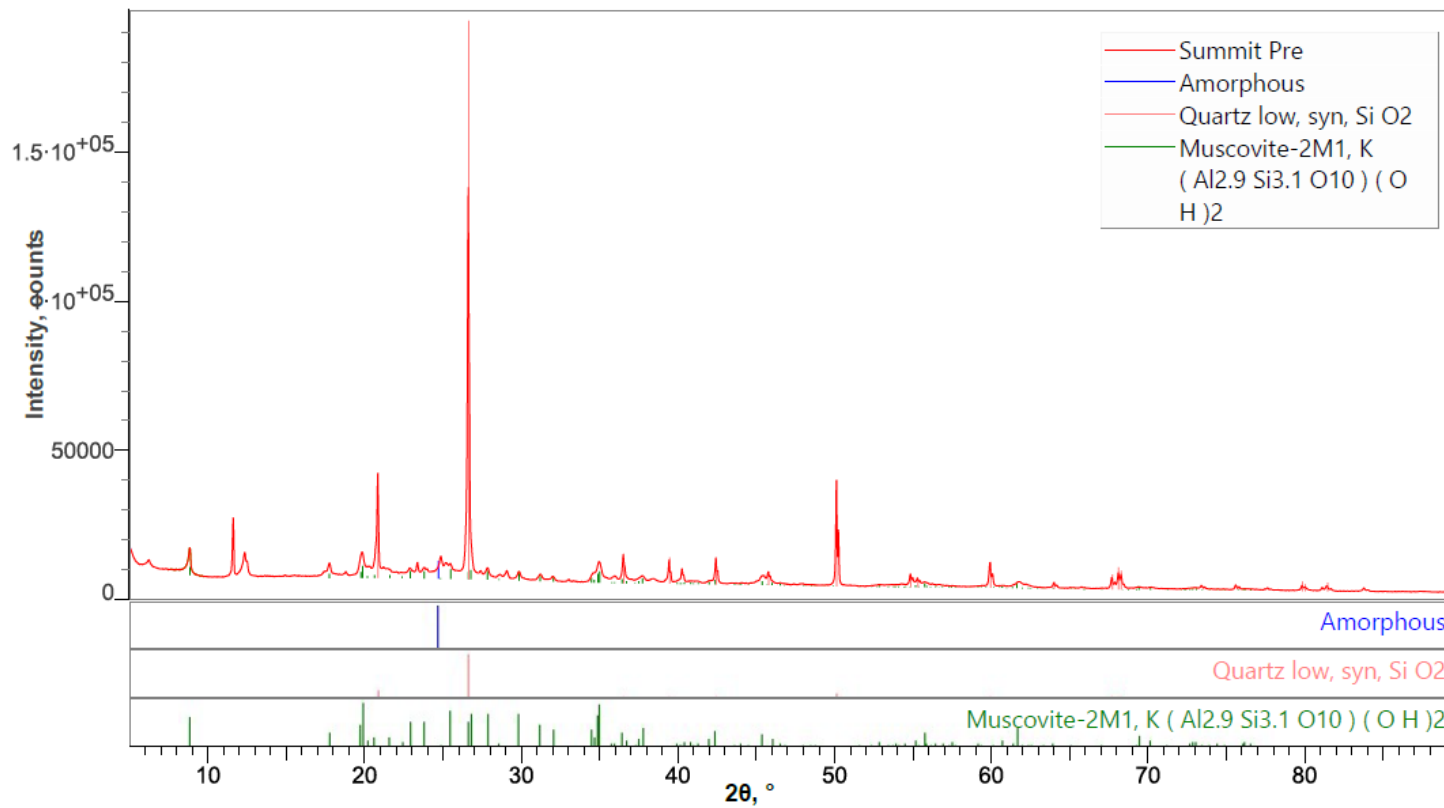


Figure E. 2 Summit XRD result

Qualitative Analysis Results

Phase name	Chemical formula	FOM	Phase reg. detail	Space Group	DB Card Number
Amorphous		2.259	Amorphous		
Quartz, syn	Si O2	1.070	S/M:PDF-4+ 2022	154 : P3221	00-046-1045

Phase Data View

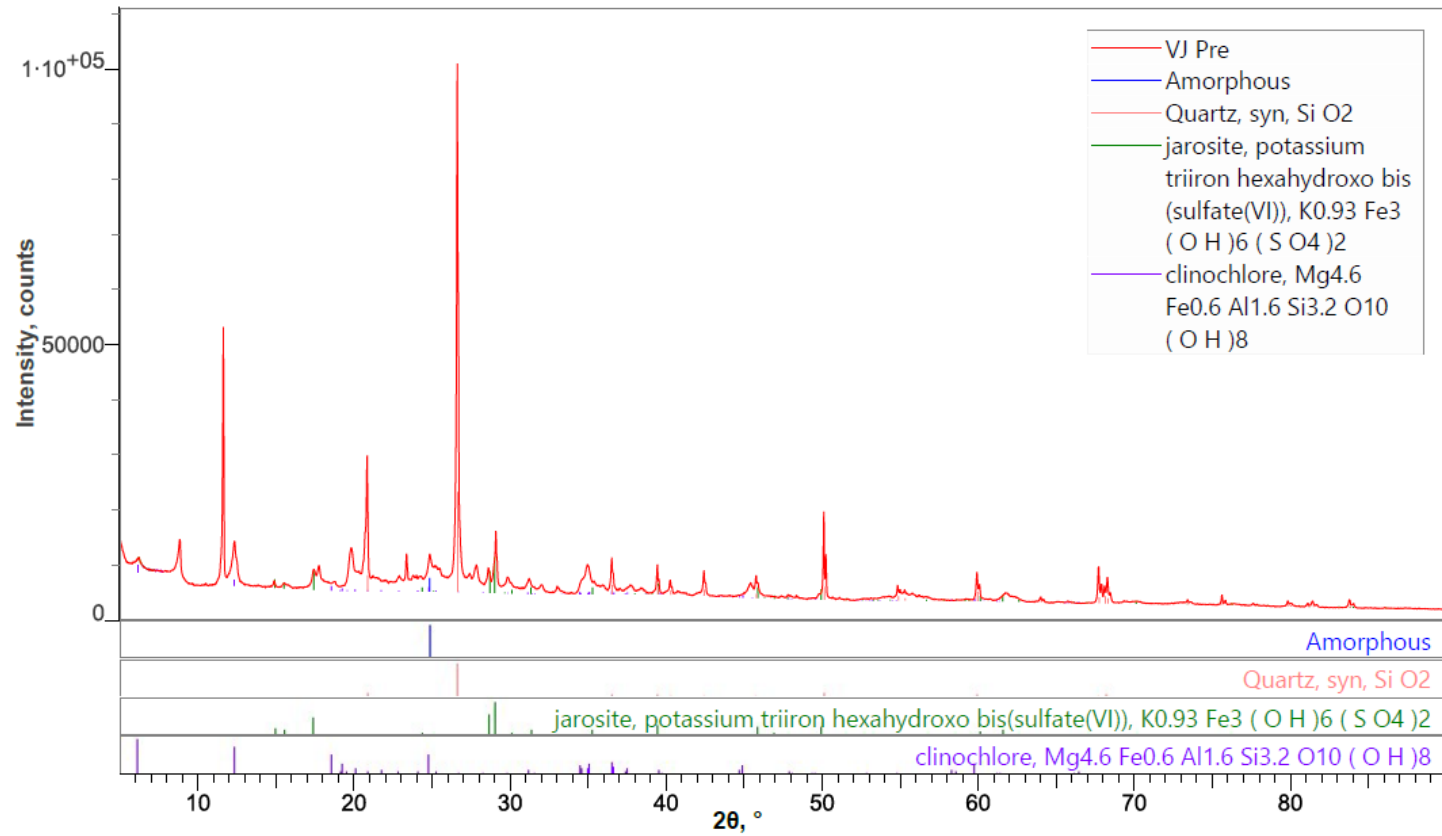
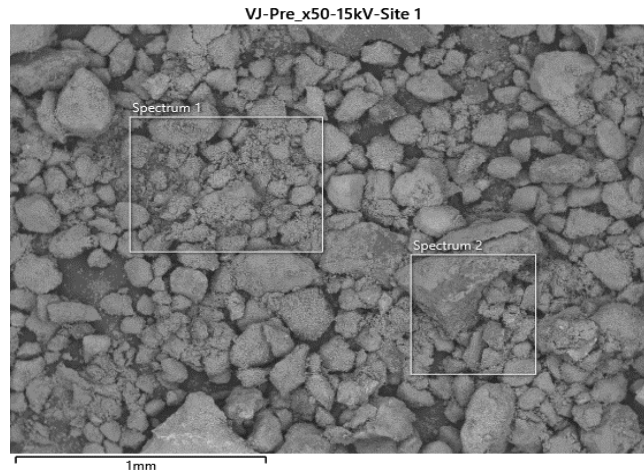
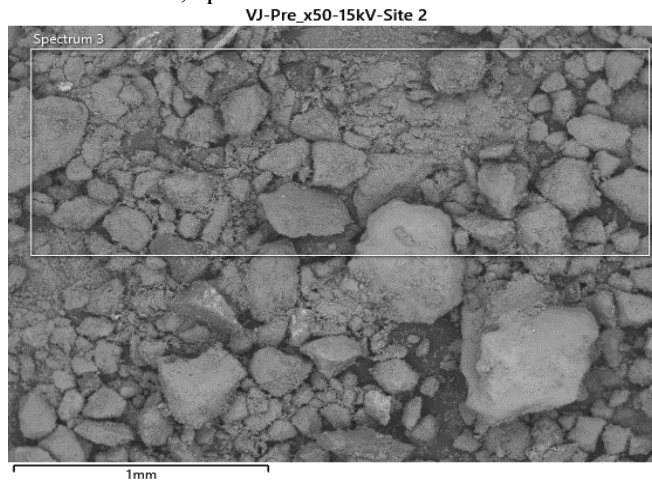


Figure E. 3 Victoria Junction XRD result

## Appendix F: SEM/EDX Results



**Figure F. 1** SEM Scan, spectrum 1 & 2 for the Victoria Junction sample



**Figure F. 2** SEM Scan, spectrum 3 for the Victoria Junction sample

**Table F. 1** Elemental composition of the pretreatment Victoria Junction Sample

<b>Spectrum Label</b>	<b>C</b>	<b>O</b>	<b>Na</b>	<b>Mg</b>	<b>Al</b>	<b>Si</b>	<b>S</b>	<b>K</b>	<b>Ca</b>	<b>Ti</b>	<b>Fe</b>	<b>Total</b>
1	20.2	47.3	0.3	0.6	8.7	14.0	1.1	2.3		0.4	5.3	100
2	29.4	43.2	0.2	0.4	7.2	11.1	0.9	2.0		0.3	5.3	100
3	25.4	45.8	0.2	0.5	7.6	12.2	1.1	2.0	0.2	0.4	4.8	100

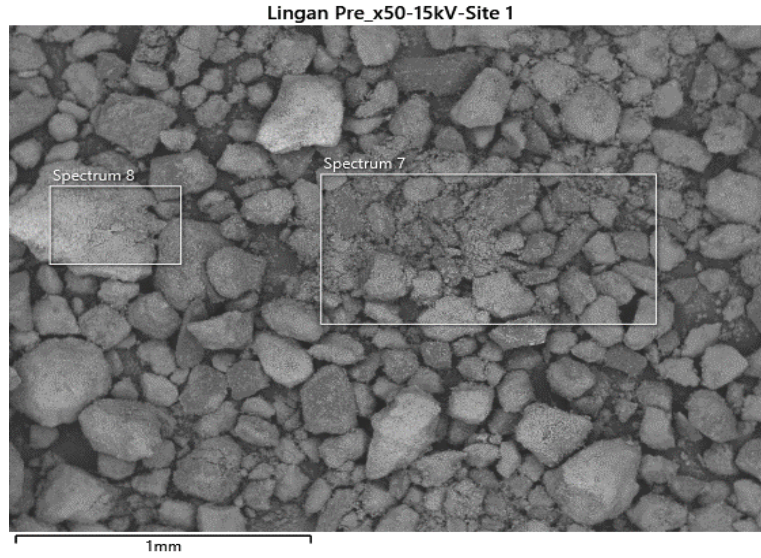


**Figure F. 3** SEM Scan, spectrum 7&8 for the Lingan sample  
Lingan Pre\_x50-15kV-Site 2

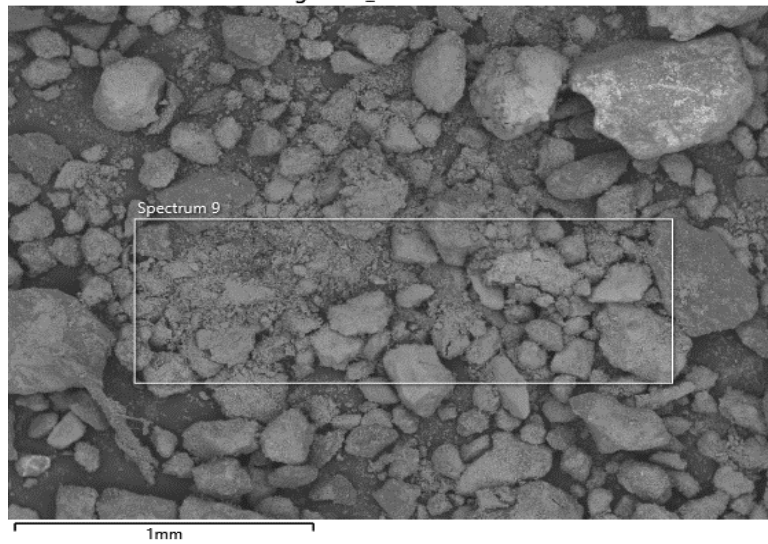


**Figure F. 4** SEM Scan, spectrum 9 for the Lingan sample

**Table F. 2** Elemental composition of the pretreatment Lingan Sample

Spectrum Label	C	O	Na	Mg	Al	Si	S	K	Ca	Ti	Fe	Total
7	38.3	39.9	0.2	0.4	5.0	9.2	0.7	1.4	1.1	0.3	3.7	100
8	31.8	44.2	0.2	0.6	6.4	10.0	.8	1.5	1.1	0.3	3.3	100
9	31.8	42.8	0.2	0.5	5.9	10.7	0.7	1.5	1.3	0.3	4.4	100

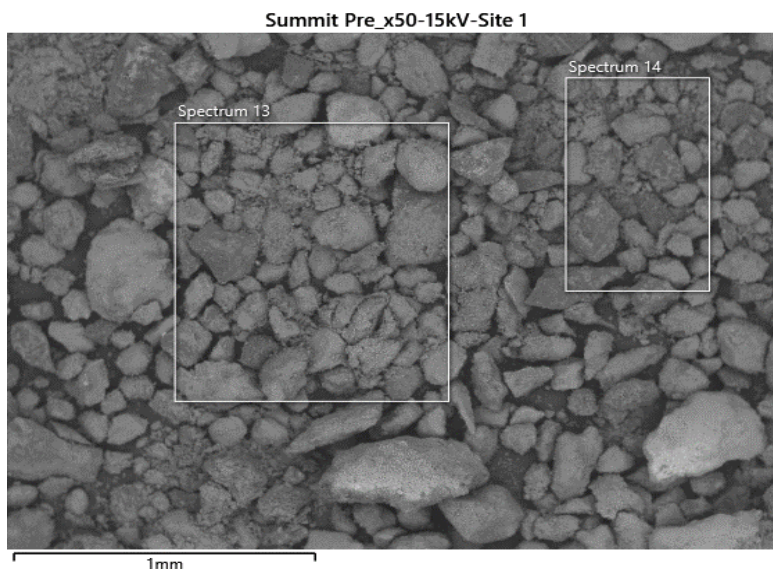


**Figure F. 5** SEM Scan, spectrum 13&14 for the Summit sample  
Summit Pre\_x50-15kV-Site 2

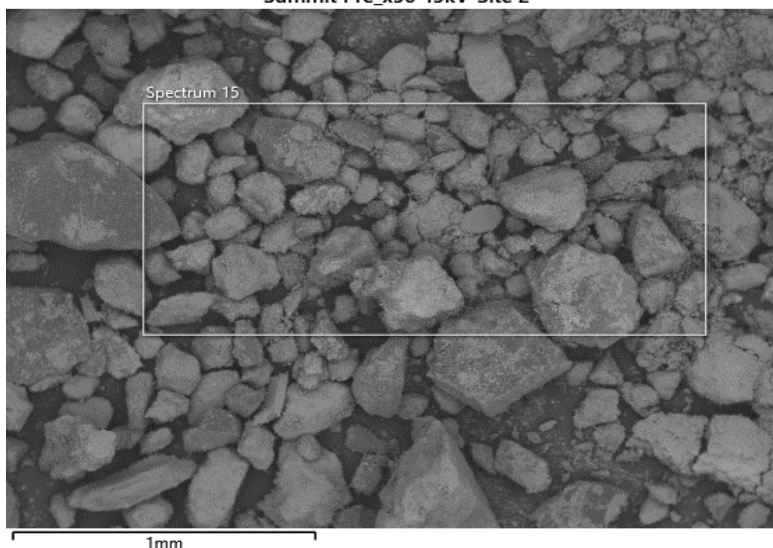


**Figure F. 6** SEM Scan, spectrum 15 for the Summit sample

**Table F. 3** Elemental composition of the pretreatment Summit Sample

Spectrum Label	C	O	Na	Mg	Al	Si	S	K	Ca	Ti	Fe	Total
13	29.5	43.7	0.2	0.5	6.9	10.9	0.7		1.8	0.4	5.5	100
14	35.4	41.6	0.2	0.4	5.8	9.7	0.7	0.1	1.6	0.2	4.4	100
15	30.5	44.1		0.5	6.4	10.5	0.7		1.6	0.3	5.6	100

## Appendix G: Supplementary SIP Results

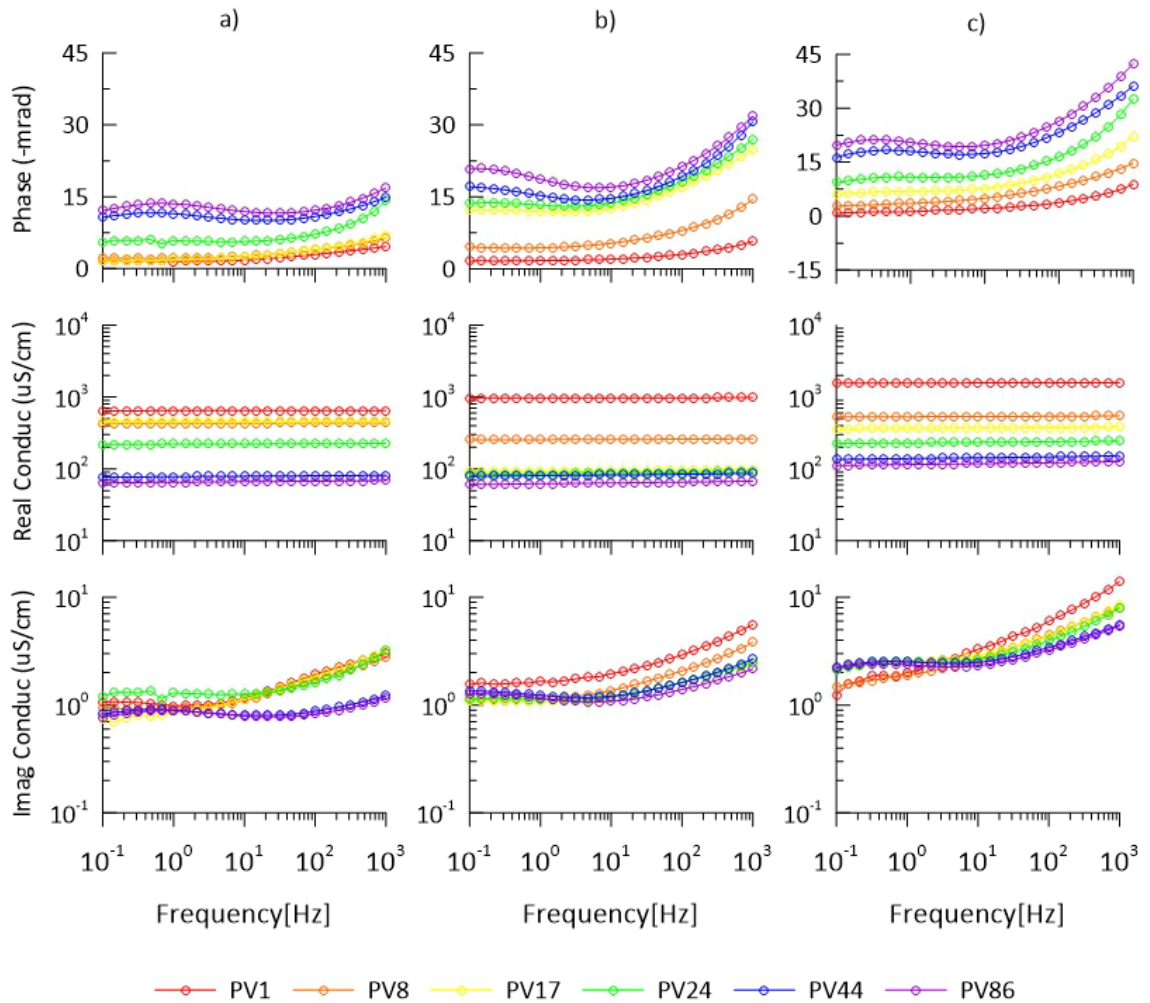


**Figure. G 1** Column leaching test SIP AB responses for: a) Langan; b) Summit; c) Victoria Junction

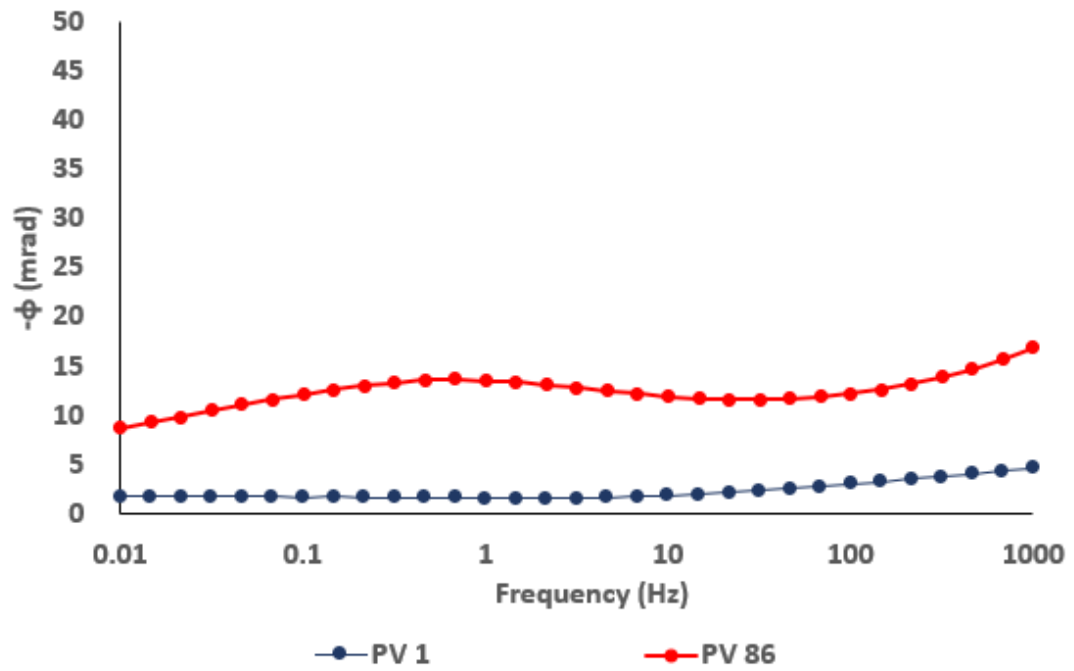


Figure. G 2 Lingan column leaching test potential pair AB PV1 & PV 86 Comparison (0.01 Hz to 1,000 Hz)

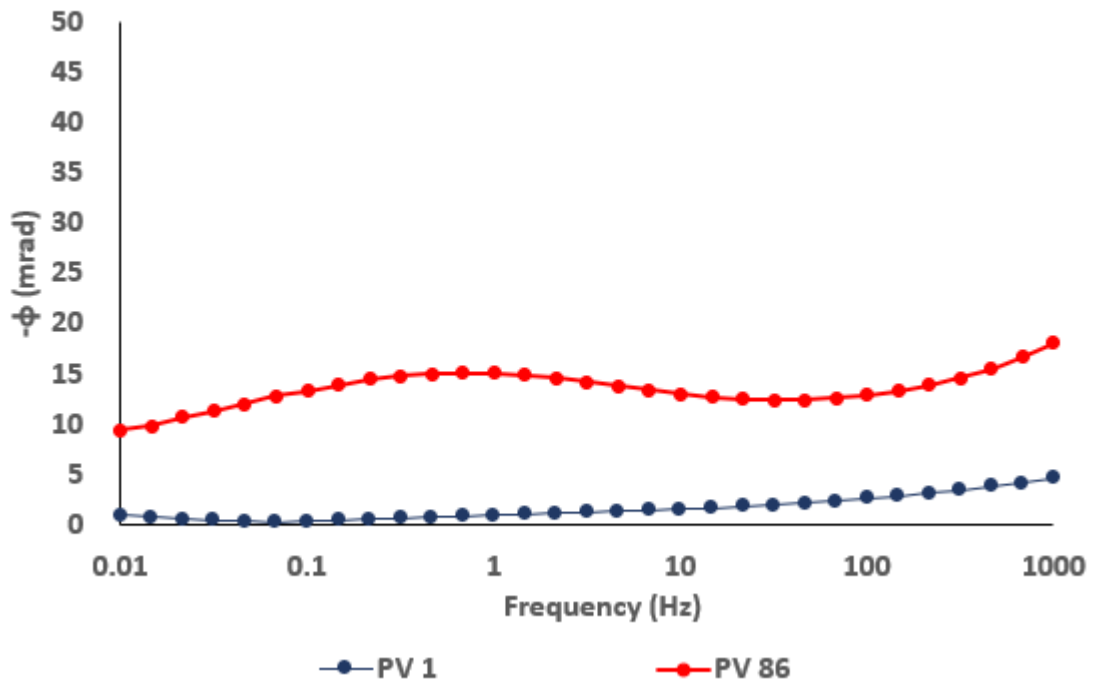


Figure. G 3 Lingan column leaching test potential pair BC PV1 & PV 86 Comparison (0.01 Hz to 1,000 Hz)

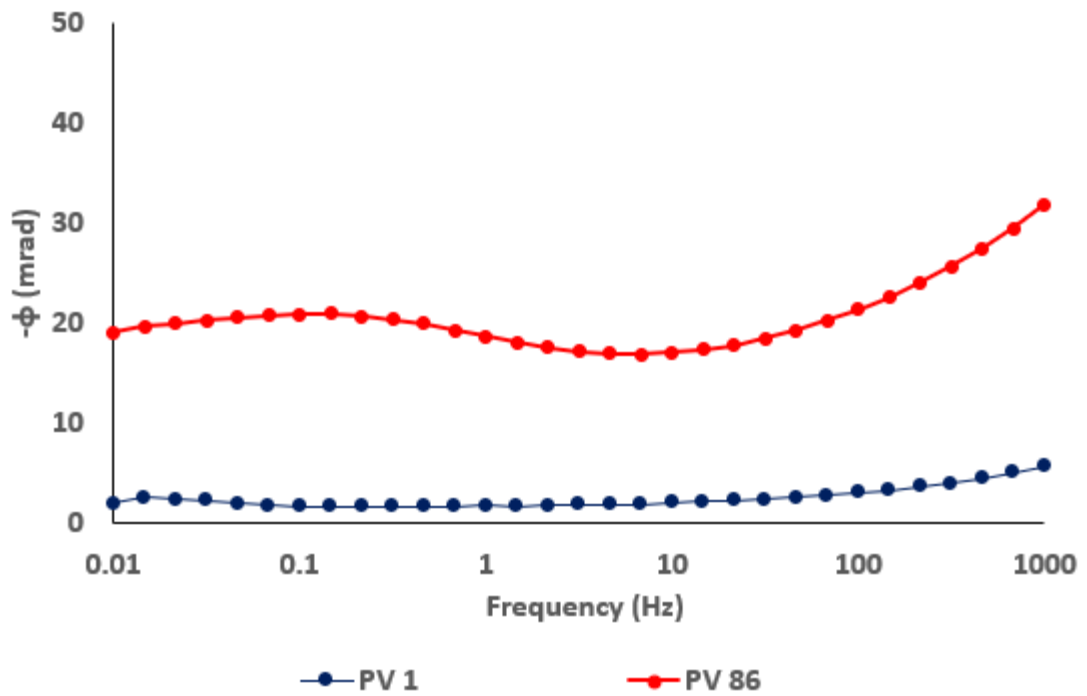


Figure. G 4 Summit column leaching test potential pair AB PV1 & PV 86 Comparison (0.01 Hz to 1,000 Hz)

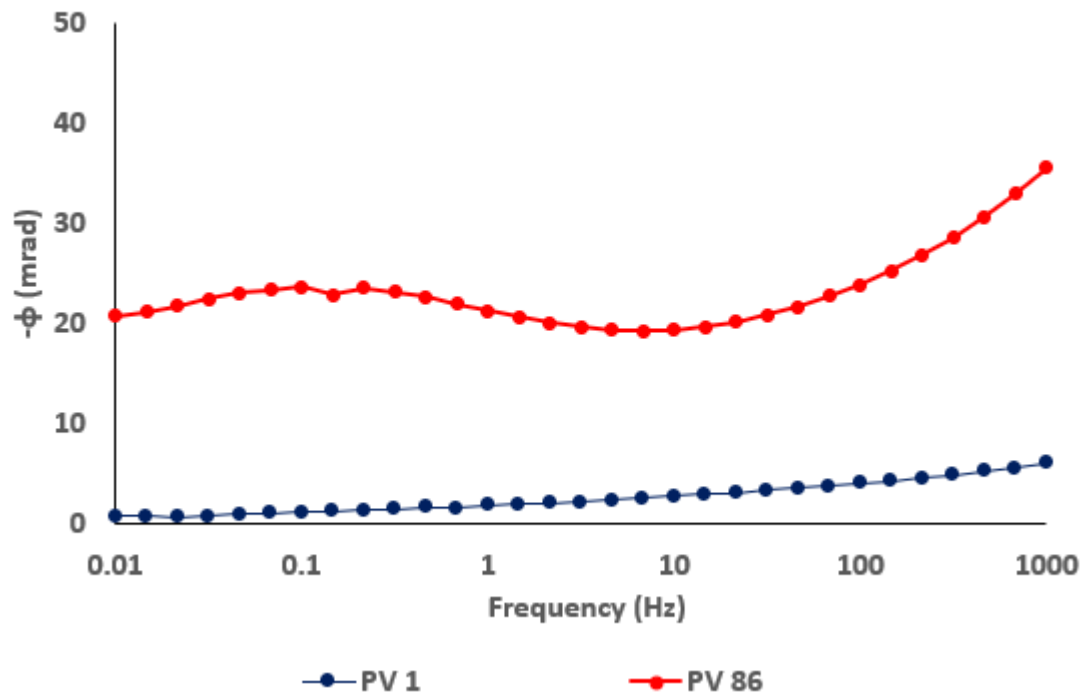
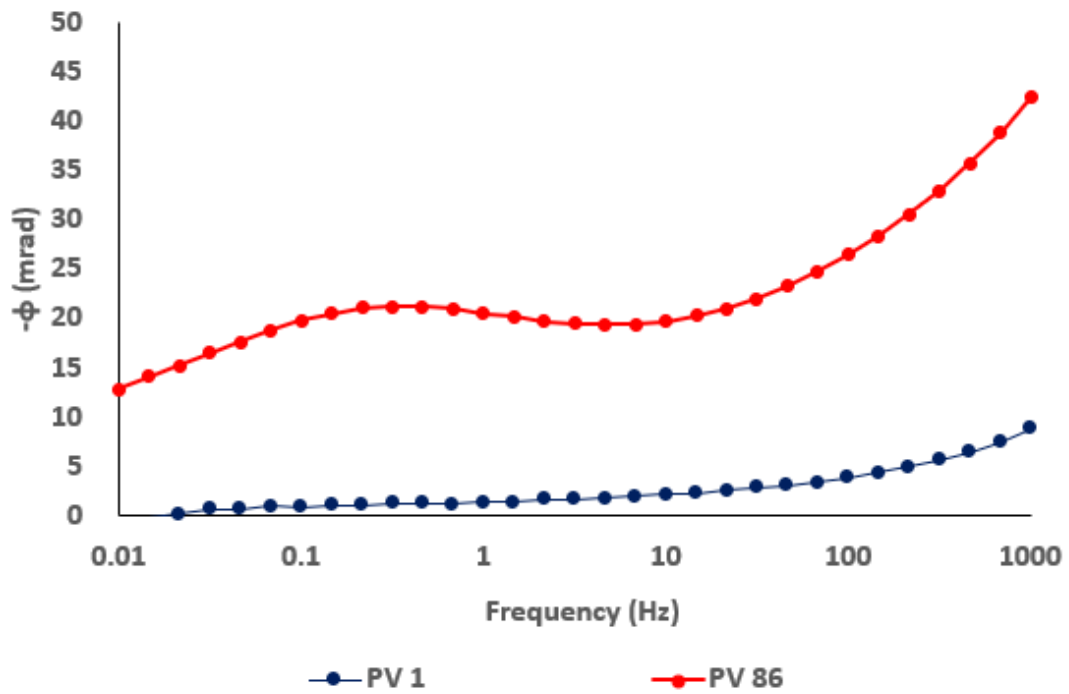
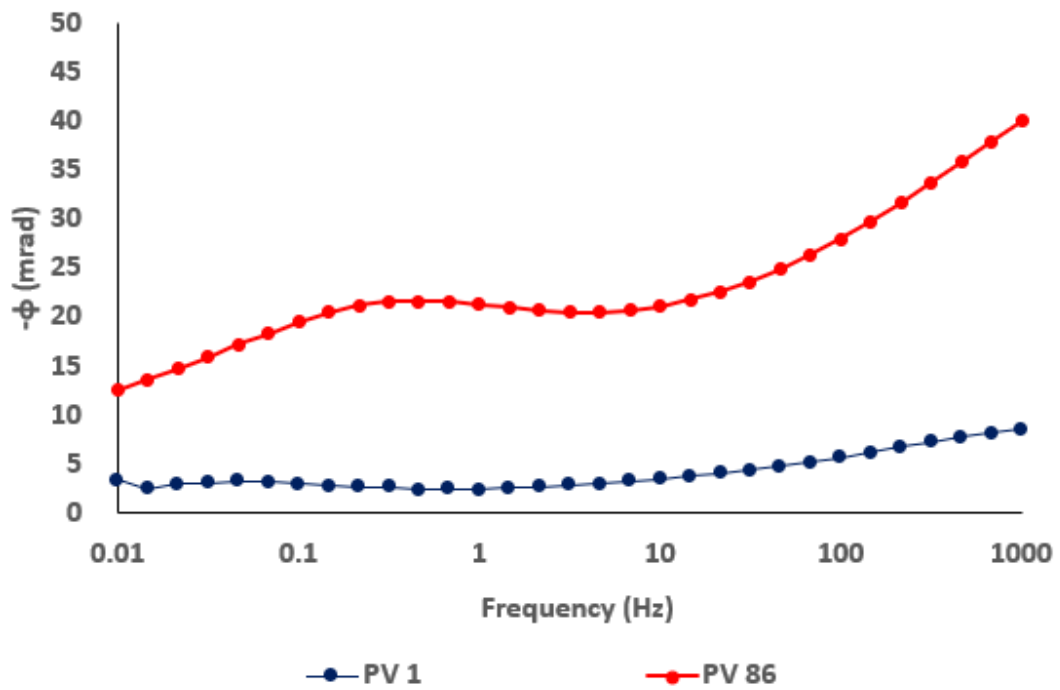


Figure. G 5 Summit column leaching test potential pair BC PV1 & PV 86 Comparison (0.01 Hz to 1,000 Hz)



**Figure. G 6** Victoria Junction column test potential pair AB PV1 & PV 86 Comparison (0.01 Hz to 1,000 Hz)



**Figure. G 7** Victoria Junction column test potential pair BC PV1 & PV 86 Comparison (0.01 Hz to 1,000 Hz)

## CURRICULUM VITAE

**Name:** Difan Su

**Post-secondary Education and Degrees:** University of Regina  
Regina, Saskatchewan, Canada  
2014 – 2019

**Honors and Awards:** 2022 R.M. Quigley Award Winner  
2022 Fall 3-minute thesis (3MT) competition – 2<sup>nd</sup> Place  
2021 ‘Rain it In’ student competition – 2<sup>nd</sup> place

**Related Work Experience:** Graduate Research Assistant  
Western University  
2021 – 2023  
Graduate Teaching Assistant  
Western University  
2021 – 2022